COMPUTER METHODS IN APPLIED MECHANICS AND ENGINEERING 52 (1985) 527–634
NORTH-HOLLAND

MODELS AND COMPUTATIONAL METHODS FOR DYNAMIC FRICTION PHENOMENA*

J.T. ODEN and J.A.C. MARTINS

Texas Institute for Computational Mechanics, The University of Texas at Austin, Austin, TX 70712, U.S.A.

Received 22 October 1984

This paper addresses the general problem of formulating continuum models of a large class of dynamic frictional phenomena and of developing computation methods for analyzing these phenomena. Of particular interest are theories which can adequately predict stick-slip motion, frictional damping in structural dynamics, and sliding resistance. This work is divided into three principal parts. In Part I, a large body of experimental and theoretical literature on friction is critically reviewed and interpreted as a basis for models of dynamic friction phenomena. In Part II, continuum models of interfaces are developed which simulate key interface properties identified in Part I. Variational principles for a class of dynamic friction problems are also established. In Part III, finite element models and numerical algorithms for analyzing dynamic friction are presented. Also, a dynamic stability analysis is presented in which it is established that stick-slip motion can be associated with dynamic instability of the governing nonlinear system for certain ranges of slip velocity and coefficient of friction. Numerical results suggest that the new models derived here can satisfactorily depict a large and important class of dynamic friction effects.

1. Introduction

The contact and rubbing of solid bodies: to many it must seem remarkable that an event so common, so intrinsic to the mechanics of everyday life, so important in a multitude of applications of mechanics to engineering problems, and so often the subject of experimental research, has not been satisfactorily depicted by a sound continuum model to date. However, to those who have taken more than a superficial look at the subject, the absence of a universal continuum model of friction may not be surprising. The nature of dynamic friction forces developed between bodies in contact is extremely complex and is affected by a long list of factors: the constitution of the interface, the time scales and frequency of the contact, the response of the interface to normal forces, inertia and thermal effects, roughness of the contacting surfaces, history of loadings, wear and general failure of the interface materials, the presence or absence of lubricants, and so on. Thus, dynamic friction is not a single phenomenon but is a collection of many complex mechanical and chemical phenomena

* This research was supported by the Air Force Office of Scientific Research (AFSC) under contract number F-49620-84-C-0024.

entwined in a mosaic whose features cannot be grasped through isolated simple experiments.

Successful computational methods in nonlinear mechanics are generally those based on a thorough familiarity with the natural phenomena being simulated and on a good understanding of the mathematical models available to describe it. A major issue in the computer simulation of many natural events is the absence of a physically and mathematically sound model of the phenomena. This may not be a critical issue in large areas of fluid and gas dynamics where the models characterized by the classical Navier–Stokes equations or the Euler equations are regarded as acceptable, but it is an especially important issue in many areas of nonlinear solid mechanics, where debates still rage over appropriate models of finite elastoplasticity, thermomechanical phenomena, etc. The study of friction effects in solid mechanics is particularly hampered by the absence of sound, generally accepted, models.

The recognition that it may not be reasonable to attempt to describe all dynamic friction effects by a single theory seems to be a major step forward. Just as a theory of linear elasticity may provide an appropriate model of the behavior of mild steel only for a limited range of deformations, so also can any single model of friction be expected to be valid only under a limited set of conditions. Thus, we shall focus here on a limited but very important class of friction problems: the dynamic contact and relative sliding of dry, metallic surfaces with engineering finishes (ground, abraded, scraped, polished, etc.) Still further restrictions are required. We choose to divide this general class of frictional effects into three general categories:

Type I. Quasi-static dry friction.

Type II. Dynamic, sliding friction.

Type III. Wear and plowing.

While these classifications are by no means sharp and exclusive, they are adequate for our present purposes.

By quasi-static dry friction (Type I friction), we mean frictional mechanisms present when two possibly polished, metallic surfaces are pressed slowly together and are in static equilibrium or are slowly displaced relative to one another, and for which normal loads are sufficiently small that no severe penetration and gouging of the contact interface occurs. Here the most conspicuous mechanisms contributing to friction are the plastic deformation of asperities, the formation of elastoplastic junctions on the contact surface, the strong coupling between normal and tangential plastic deformations, and the dissipative mechanisms afforded by the history-dependence of junction deformation and possible fracture of these junctions. The frictional forces may depend upon histories of micro-tangential displacements of particles on the contact surface. Theories describing such frictional effects are basically static in nature; inertia effects are generally not important and the modeling should capture the elastoplastic deformation of the interface in some way. Models and computational procedures for studying these classes of problems have been advanced by several investigators, and we mention as examples the papers of Fredrickson [40], Oden and Pires [70], Pires and Oden [73], Michalowski and Mroz [64], and Campos, Oden and Kikuchi [27].

By dynamic sliding friction (Type II friction), we refer to that large and important class of truly dynamic problems which include such effects as frictional damping, dynamic sliding, stick-slip motion, chattering, etc. The constitution of the material interface is essentially stable; there is no marked penetration or normal plastic deformation of the interface and, at least

from a global point of view, the frictional forces developed on the contact surface appear to depend on the sliding velocity of one surface relative to another. To obtain reproducible experimental data on these types of frictional effects, it is generally necessary to rub the contacting surfaces together for a period of time until a steady-state condition of the interface is reached. Such pre-conditioning may fracture and work-harden the surface asperities and result in a smoother contact surface for which, unlike category I, plastic deformations normal to the interface are not significant or do not occur at all.

A significant distinguishing feature between Type I and II friction is that of scales: In Type I, the local frictional forces on the interface depend upon surface micro-displacements which may be of an order of magnitude of ten microns; in Type II, much larger rigid relative motions can occur and frictional forces vary with sliding velocity.

The wear and plowing phenomena (Type III) encompasses cases in which substantial damage and penetration of the metallic interfaces occurs; there may be phase changes in the interface materials, and portions of the material may be removed or relocated during contact. These types of contact situations may involve the transfer of large normal forces across a small contact area. Wear may be experienced in all three of the categories mentioned, but in categories I and II it is either ignored or assumed to be negligible. We shall not consider these types of frictional phenomena in the present work. We also do not consider here problems of collision and impact, which differ from those mentioned earlier due to the occurrence of significant jumps in particle velocities at the contact surface, and instantaneous transfer of momentum from one body to another, and the propagation and reflection of stress waves. Moreover, while all contact problems with friction involve thermal effects to varying degrees, we shall ignore such effects in the present investigation.

The present paper is a study of models and computational procedures for analyzing contact and friction problems that fall into category II: sliding friction and stick-slip motions of dry, rough, metallic surfaces.

The first and perhaps most difficult step in the analysis of dynamic friction is the development of an acceptable model of the contact interface. It is well known that the interface through which bodies contact is a mechanically-complicated media, the constitution of which is different from that of the parent material of either contacting body. The interface may be a rough irregular pair of surfaces composed of impurities, oxides, work-hardened or crushed materials, gases and lubricants. *Therefore, it is natural in developing phenomenological models of friction, to assign to the interface a separate structure characterized by constitutive equations independent of those characterizing the parent metals.*

Toward assessing what features these interface models should exhibit, we devote the first part of this study to a review and critique of a substantial body of experimental literature on this subject. Then, on the basis of our interpretations of this data, we propose forms of constitutive equations for the contact interface, particularly its response to normal stress.

In Part II, we incorporate these dynamic friction effects into a nonlinear continuum model of contact and sliding friction of elastic bodies. The contacting bodies are assumed to be linearly elastic, but the overall theory is highly nonlinear, owing to nonlinearities in the contact constraints, frictional behaviors and interface response. We derive new variational principles governing these dynamic problems.

Part III of the study is devoted to the numerical analysis of the dynamic friction models

developed in Part II. There we describe several numerical algorithms for studying dynamic friction. Dynamic stability and other qualitative features of sliding friction phenomena are studied numerically using a simple mechanical model and finite element discretizations of our continuum model. Several representative problems are solved numerically.

There are several results of this study which we feel are particularly significant:

(1) *Contrary to a widely accepted belief that has prevailed since the time of Coulomb, the coefficient of friction may not necessarily change with increasing relative sliding velocity. Our results confirm the experimentally-based conjectures of Tolstoi* [103] *and some other researchers. This apparent change is traditionally interpreted as a decrease from a static to a kinetic coefficient. It is, however, only the average value of the friction force that may decrease after the initiation of sliding and not necessarily instantaneous ratios tangential to normal stress components on the contact surface. Of course, if the sliding body is modeled as a single (tangential) degree-of-freedom system, as is so often the case, then the reduction of the coefficient of friction upon sliding is the only possible device for incorporating these experimentally observed phenomena. Such crude models, experimental and/or analytical, cannot take into account normal force oscillations, and thus omit a critically important property of dynamic friction.*

(2) *A key feature of acceptable interface models for dynamic friction is the characterization of the response of the interface to normal forces. This mechanical response for most metal-on-metal interfaces is highly nonlinear.*

(3) *Stick-slip motion may be a manifestation of dynamic instabilities inherent in the coupling of normal and tangential relative motions of contacting bodies. This phenomenon is not necessarily the result of a decrease in the coefficient of friction with changes in sliding velocity, and can in fact be observed when the coefficient of friction is constant and equal to its so-called static value.*

(4) *It is possible to develop and to incorporate simple nonlinear interface models into a continuum model of elastodynamics which captures many fundamental features of dynamic friction. In particular, frictional damping can be depicted in such models in a natural and straightforward way.*

(5) *Finite element approximations of the continuum models can be developed which feature consistently-derived frictional damping/stiffness matrices. These finite element methods, together with numerical schemes for solving associated systems of nonlinear ordinary differential equations, are capable of modeling stick-slip motion, dynamic sliding, friction damping, and related phenomena in a significant range of practical problems.*

Part I. Physical aspects of dynamic friction

This portion of our study is devoted to a review of a selected body of literature, mostly experimental in nature, that deals with the subject of dry friction on metallic surfaces. It is necessarily an incomplete review, since this subject is an old and active one in which a large volume of literature exists; but we have attempted to focus on a selected sample of results that collectively provide some basis for friction-interface models to be proposed later.

2. Some properties of metallic surfaces

2.1. Preliminaries

We begin with a quotation from Whitehouse and Archard [110]:

> "All surfaces are rough. This is the starting point from which current ideas about friction, wear, and other aspects of surfaces in contact have evolved."

It is well known that the most polished metallic surfaces are not perfectly flat. Under magnification, one observes that these surfaces have undulations that form hills and valleys the dimensions of which are large in comparison with molecular dimensions. These deviations from the plane are called *asperities*.

Many experimental techniques have been used to observe and measure the roughness of the surfaces. Summary accounts of these techniques and references for more detailed descriptions can be found, e.g., in [22, 67, 99]. Recent developments can be found in [91]. A popular instrument to measure surface roughness is the Taylor–Hobson Talysurf, with which the vertical movement of a stylus moving over a representative length of the surface under examination is amplified electrically and recorded on a moving paper chart. Since the length traversed by the stylus is very large compared with the height of the asperities, a different scale is used for the horizontal and vertical magnifications (see Fig. 1).

Depending on the method of production of the surface, the height of the peaks may vary between 0.05 μm to 50 μm while the spacings between them range from 0.5 μm to 5 mm [86]. The average slope of the asperities is usually very small, of the order of 5° to 10° [98].

Various quantities have been proposed as measures of surface roughness. For example, let

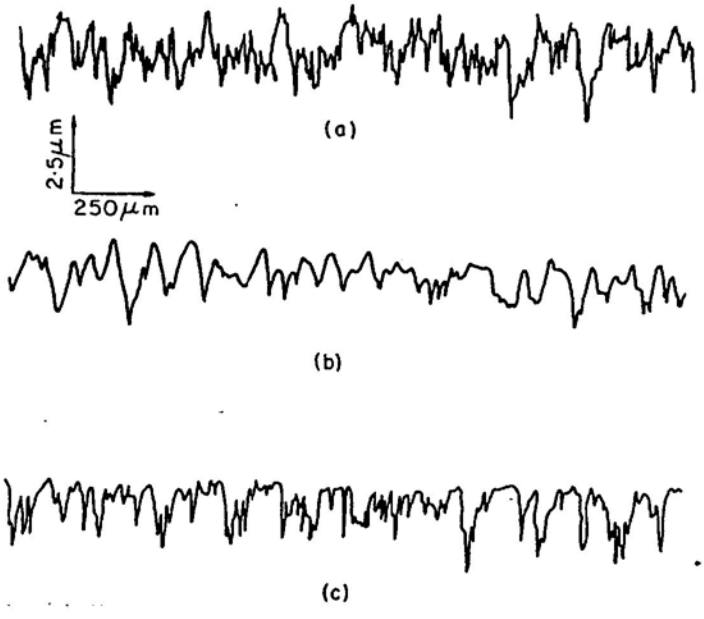

Fig. 1. Profiles of mild steel specimen after three surface treatments. (a) Surface ground only; (b) Surface ground and then lightly polished; (c) Surface ground and then lightly abraded on 600 paper (reproduced from [42]).

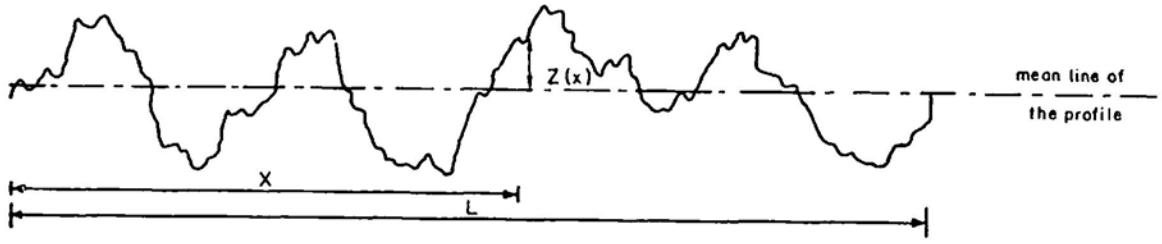

Fig. 2. Geometry of a profile.

$z(x)$ denote the actual height of particles on a material surface about a fixed datum plane at a point x on the plane (indicated in one dimension in Fig. 2). The center-line, average of asperity-heights over a test length L, is obviously

$$\frac{1}{L}\int_0^L |z(x)|\,\mathrm{d}x\,.$$

We can relocate this datum on the mean profile plane, and compute as roughness measures the r.m.s. ('root-mean-square') deviation σ, the r.m.s. of derivatives σ', r.m.s. of second derivatives σ'', the autocorrelation C or the power spectral density P,

$$\sigma = \left[\frac{1}{L}\int_0^L z^2\,\mathrm{d}x\right]^{1/2}, \qquad \sigma' = \left[\frac{1}{L}\int_0^L z'^2\,\mathrm{d}x\right]^{1/2}, \qquad \sigma'' = \left[\frac{1}{L}\int_0^L z''^2\,\mathrm{d}x\right]^{1/2},$$

$$C(\Delta) = \frac{1}{L}\int_0^L z(x)z(x+\Delta)\,\mathrm{d}x = \frac{1}{2\pi}\int_{-\infty}^{\infty} P(\lambda)\exp(\mathrm{i}\lambda\Delta)\,\mathrm{d}\lambda\,,$$

$$P(\lambda) = \int_{-\infty}^{\infty} C(\Delta)\exp(-\mathrm{i}\lambda\Delta)\,\mathrm{d}\Delta\,.$$

Here Δ is the delay interval and λ is the angular frequency of asperities. The parameters σ' and σ'' are regarded as sensitive indicators of the slope of the asperities and of the degree of sharpness at asperity peaks, respectively.

The *autocorrelation function of a profile* $C(\Delta)$ describes the extent to which (on an average) the height at any point on the profile is correlated with the height at another point downstream. For a random signal, $C(\Delta)$ declines from σ^2 at $\Delta = 0$ to zero, as Δ becomes large. *The power spectral density function* $P(\lambda)$ is the Fourier transform of $C(\Delta)$ and represents the rate of change of mean square value with frequency, where the mean square value is taken in a narrow frequency band at various center frequencies. For this reason $P(\lambda)$ is also known as the *mean square spectral density.*

2.2. Constitution of metallic surfaces

The frictional properties of unlubricated metals are greatly affected by the presence of surface films. Fig. 3 illustrates schematically the surface layers encountered on metallic surfaces in industrial environments [77]. According to Rabinowicz, the *contaminant layer* may

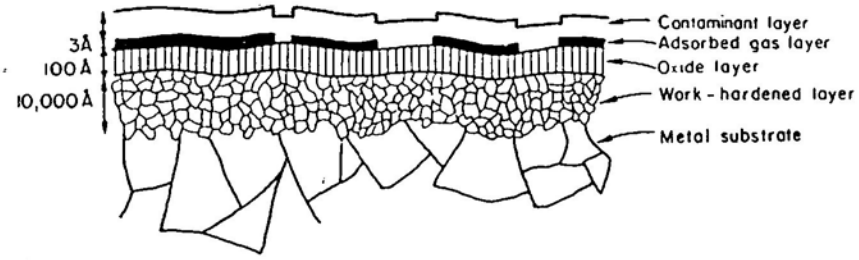

Fig. 3. Schematic illustration of films on a metal surface (not to scale) (reproduced from [77]).

be derived from a variety of sources, among them the oil drops found in industrial environments and the lubricants applied during the preparation of the surface. When in contact with the air, the main constituents of the *adsorbed layer* are generally molecules of water vapor and oxygen. The *oxide layer* is produced by reaction of oxygen from the air with all metals (except with the noble metals, such as gold and platinum, which are generally free of oxide or other surface films). The *work-hardened layer* results from the heavy deformation of the metal due to the mechanical preparation of the surface.

According to Bowden and Tabor [23], if the preparation of the surface involved polishing at high speeds, the surface layer may consist of a smeared 'fudge' of metal, metal oxide, and polishing powder. Below the severely deformed layers, the metal usually shows vestigial traces of deformation produced in earlier stages of abrasion. A schematic representation of this is shown in Fig. 4.

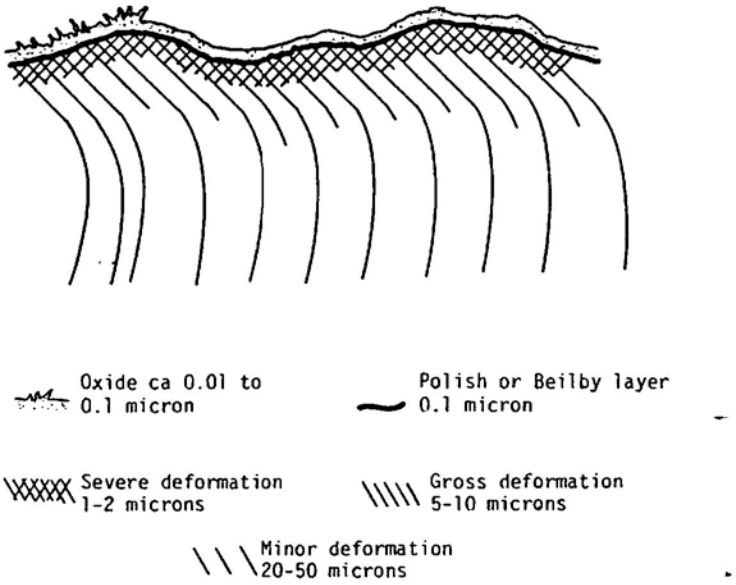

Fig. 4. Schematic diagram showing topography and structure of a typical polished metal specimen (reproduced from [23]).

3. The normal contact of metallic bodies

3.1. Static contact of rough surfaces

In this section we summarize several theoretical and experimental results on the static normal contact of rough surfaces. For the theoretical developments we follow, essentially, the survey papers of Archard [6], Thomas [99] and Whitehouse [109]. For the experimental work we follow, essentially, the survey papers of Back, Burdekin and Cowley [9] and Woo and Thomas [113]. We are especially interested in answers to the following questions: *What is the stiffness of two asperity-covered surfaces when pressed against each other? What is the corresponding true area of contact?*

3.1.1. Various models of contacting rough surfaces

Because surfaces are rough, the true area of contact is much smaller than the apparent area of contact. As a result, the true contact surfaces may often support pressures so large that they are comparable with the strengths of the materials of the contacting bodies. Bowden and Tabor [22] suggested that these pressures would be always high enough to produce plastic flow. The contacting regions would deform plastically until the true area of contact would be just large enough to support the load. The true area of contact A_r would be then proportional to the applied load N. With this proportionality, $A_r \propto N$, it is possible to provide a simple and elegant explanation of Amontons' laws of friction (see Sections 4.1 and 4.2).

Objections to the concept of plastic deformation of the asperities were put forward by Archard [5]. According to this author, when materials of comparable hardness rub together, a protuberance may be plastically deformed at its first encounter with the other surface, but its relaxation would be elastic. At its many subsequent encounters with the other surface the protuberance would bear the same load by elastic deformation. Archard shows then that although the simple Hertzian theory does not predict the proportionality between A_r and N, a generalized model in which each asperity is covered with microasperities, and each microasperity with micro-microasperities, gives successively closer approximations to the law $A_r \propto N$ as more stages are considered (Fig. 5). Archard explained that the essential part of the argument was not the choice of asperity model: it was whether an increase in load creates new contact areas or increases the size of existing ones. For physically plausible surfaces any elastic model in which the number of contacts remains constant, we find that $A_r \propto N^{2/3}$; but if the average size of contacts remains constant (and its number increases) then $A_r \propto N$. Although admittedly artificial, Archard's models were thus very important in showing the admissibility of elastic deformation of the asperities and the effect of the superposition upon the surfaces of asperities of widely differing scales of sizes.

The next step came with the development of surface models based on knowledge gained from the examination of the actual surface topography. Greenwood and Williamson [42], and others, have shown that, for many surfaces, the distribution of heights is very close to Gaussian. These authors also investigated the distribution of peak heights and concluded that it was also close to Gaussian (see Fig. 6). The model developed by Greenwood and Williamson thus assumed a Gaussian distribution of peak heights (asperity heights). They also assumed that the asperities, at least near their summits, were spherical with a constant radius of curvature. The topography of the surface was described in terms of three parameters: σ^*, the

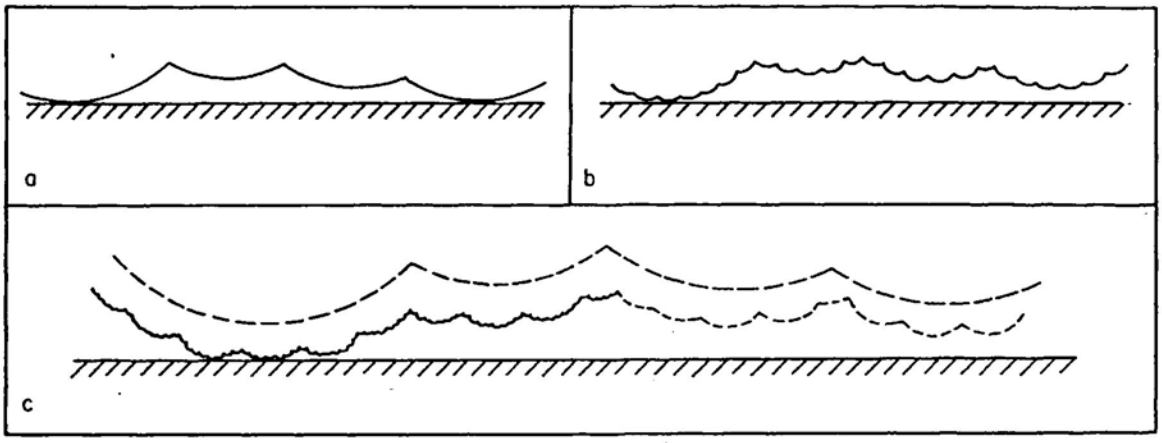

Fig. 5. Models of surfaces containing asperities of differing scales of sizes. The relationships between the true area of contact (A_r) and the normal load (N) are: (a) $A_r \propto N^{4/5}$; (b) $A_r \propto N^{14/15}$; (c) $A_r \propto N^{44/45}$. (Reproduced from [6].)

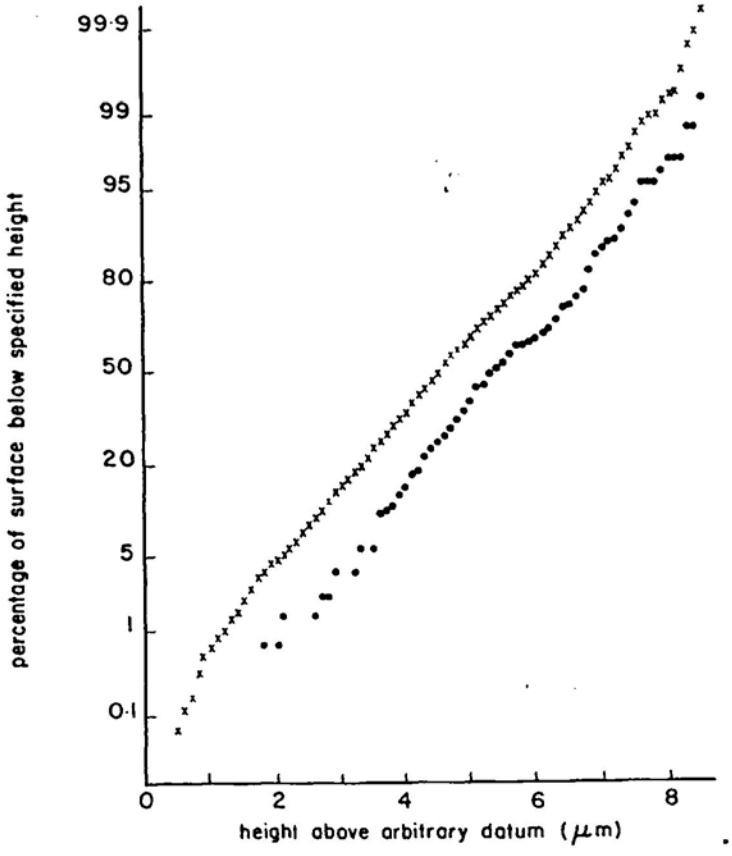

Fig. 6. Cumulative height distribution of bead-blasted aluminum. (×) Distribution of all heights; (●) Distribution of peak heights. A perfect Gaussian distribution would give, with the vertical scale used, a straight line. (Reproduced from [42].)

standard deviation of the distribution of asperity heights, R, the mean radius of curvature of the asperity tips (assumed constant in the model), and η, the surface density of asperities (later, Whitehouse and Archard [110] showed that these parameters are not independent).

The deformation of the asperities was assumed to be elastic (Hertzian). The material property required was thus the equivalent elasticity modulus of the two surfaces E', defined as

$$\frac{1}{E'} = \frac{1-\nu_1^2}{E_1} + \frac{1-\nu_2^2}{E_2}, \tag{3.1}$$

where E_1 and E_2 are the moduli of elasticity of each of the contacting bodies and ν_1 and ν_2 are the corresponding Poisson's ratios.

The results obtained using this theory, for typical values of σ^*, R, η and E' are shown in Figs. 7 and 8. In Fig. 7, the separation h^* is the distance between the mean planes of the distributions of peak heights of the two surfaces. It is clear that *the separation decreases approximately proportionally to the increase of the logarithm of the normal load and that the real area of contact is, approximately proportional to the normal load.* Greenwood and Williamson observed that the above proportionalities hold exactly if the distribution of asperity heights is assumed exponential rather than Gaussian. For such a distribution, which is a fair approximation to the uppermost 25 percent of the asperities of most surfaces, it is possible to obtain closed form expressions for the relation: load-separation, area of contact-separation and, consequently, area of contact-load. These relations are the following:

$$\frac{p}{E'} = \sqrt{\pi}(\eta R\sigma^*)\sqrt{\sigma^*/R}\exp(-h^*/\sigma^*),$$
$$\frac{A_r}{A} = \pi(\eta R\sigma^*)\exp(-h^*/\sigma^*), \qquad \frac{A_r}{A} = \sqrt{\pi}\sqrt{R/\sigma^*}\,\frac{p}{E'}, \tag{3.2}$$

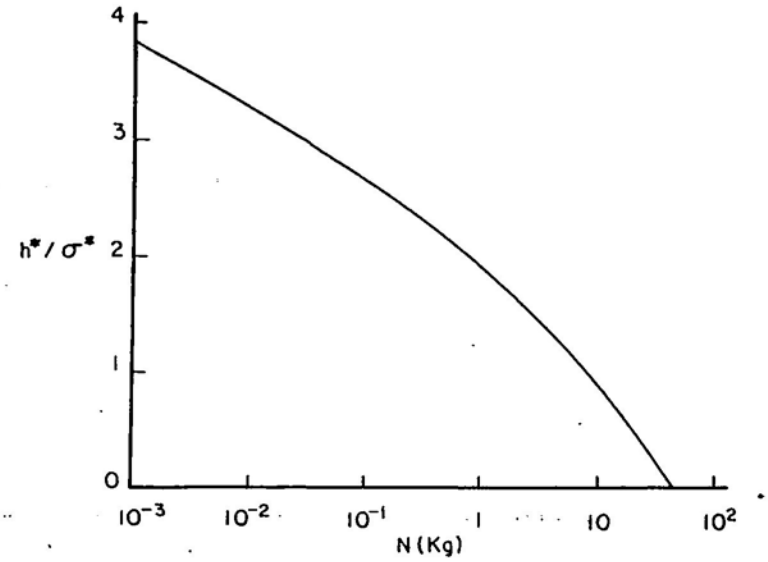

Fig. 7. Relation between separation and load (reproduced from [42]).

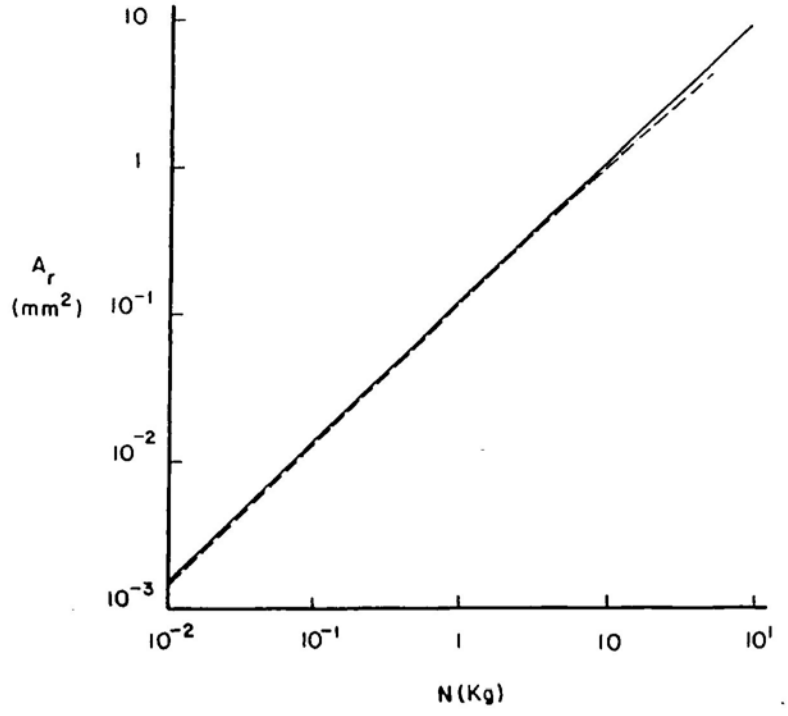

Fig. 8. Relation between true area of contact and load (reproduced from [42]). ———— nominal area $A = 10\,\text{cm}^2$; ---------- nominal area $A = 1\,\text{cm}^2$.

where p is the nominal contact pressure, A is the nominal area of contact and A_r is the real area of contact.

Tsukizoe and Hisakado [105, 106] developed a statistical model for the contact of rough surfaces under the assumption of plastic deformation of the asperities. They further assumed a Gaussian distribution of surface heights and that the material displaced due to plastic deformation could be neglected. This approach, which works well for light to moderate loads, leads to the following relations involving load, area of contact and separation:

$$\frac{p}{H} = \tfrac{1}{2}\operatorname{erfc}\left(\frac{1}{\sqrt{2}}\frac{h}{\sigma}\right), \qquad \frac{A_r}{A} = \tfrac{1}{2}\operatorname{erfc}\left(\frac{1}{\sqrt{2}}\frac{h}{\sigma}\right), \qquad \frac{A_r}{A} = \frac{p}{H}. \tag{3.3}$$

Here the separation h is the distance between the mean planes of the distributions of surface heights (see Fig. 9), and H is the indentation hardness. (H = applied load/permanent indentation area when a hard indenter is pressed into a 'flat' surface.)

Some of the limitations of these early statistical models of elastic or plastic contact have been successively overcome by more sophisticated models proposed by other authors.

Whitehouse and Archard [110] used the fact that, if a surface profile is of a random type, then it can be defined completely (in a statistical sense) by two characteristics: the probability

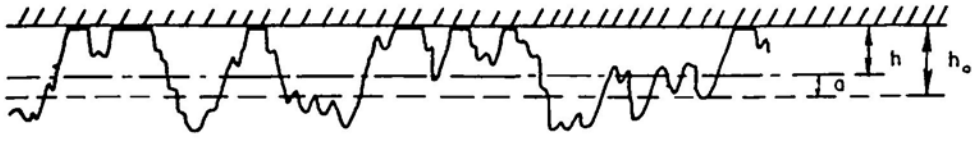

Fig. 9. Separation and penetrating approach between a rough and a flat surface. ------- current mean line of the rough surface; ------- mean line of the rough surface at the beginning of contact; h current separation; h_0 separation at the beginning of contact; $a = h_0 - h$ penetrating approach.

density of the height distribution and the autocorrelation function. More recently, Whitehouse and Phillips [111, 112] have generalized the previous model in order to incorporate a general autocorrelation function $C(\Delta)$ and in order to have a fully 2D surface model (rather than a 1D profile model).

An alternative model was developed by Nayak [68]. In his model, the height of a rough surface $z = z(x, y)$ is considered to be a two dimensional random variable, the cartesian coordinates x and y being the independent variables. The essential differences between this model and those of Whitehouse et al. are the following: this model is based on continuous (rather than discrete) properties of random waveforms and uses the power spectral density function (rather than the autocorrelation function). In this paper Nayak also emphasized the distinction between the statistics of the surface and the statistics of a profile of the surface. This author then shows how the higher-order surface statistics of interest can be correctly obtained from the parameters σ, σ' and σ'' (r.m.s. values of z and its first and second derivatives, respectively) of a single profile, for Gaussian isotropic surfaces.

Bush, Gibson and Thomas [26] developed a model based on Nayak's random surface theory with the additional assumption that the cap of each asperity is replaced by a paraboloid having the same height and principal curvatures as the summit of the asperity. The asperity deformation was assumed to be elastic (Hertzian). The authors conclude that *for large separation the contact area is proportional to the load and for smaller separation the proportionality is only approximate. The normal stiffness becomes vanishingly small at large separations and, at constant separation, the stiffness is proportional to the load.* Also *the stiffness is inversely proportional to the square of the r.m.s. roughness.* The explicit relations obtained, for large separation, h, are the following:

$$\frac{p}{E'} = \frac{\sigma'}{2\sqrt{2}\pi}\frac{1}{(h/\sigma)}\exp\left[-\tfrac{1}{2}\left(\frac{h}{\sigma}\right)^2\right],$$

$$\frac{A_r}{A} = \frac{1}{2\sqrt{2}\pi}\frac{1}{(h/\sigma)}\exp\left[-\tfrac{1}{2}\left(\frac{h}{\sigma}\right)^2\right], \qquad \frac{A_r}{A} = \frac{\sqrt{\pi}}{\sigma'}\frac{p}{E'}, \tag{3.4}$$

$$S = -\frac{dp}{dh} = \frac{E'\sigma'}{2\sqrt{2}\pi\sigma}\exp\left[-\tfrac{1}{2}\left(\frac{h}{\sigma}\right)^2\right] = \frac{ph}{\sigma^2},$$

where S is the normal stiffness per unit area of contact.

O'Callaghan and Cameron [69], using a model with some features in common with the previous one, obtained results (also for elastic contact) that are qualitatively analogous to those of previous authors: *approximate proportionality between real area of contact and*

normal load and also approximate proportionality between separation and minus the logarithm of the load.

Other authors have also modeled conditions on the contact that are more complex than a simple elastic *or* plastic deformation of the asperities. Mikic [65] modeled *elasto-plastic* conditions. He assumed that the real contact pressure is equal to the lower hardness of the contacting materials and that the total deformation of each asperity is the sum of elastic and plastic deformations produced by that pressure. Analogous assumptions were later used by Ishigaki et al. [48] to model *loading-unloading* situations. *Work-hardening* of the asperities was first considered by Halling and Nuri [44]. *Work-hardening* and the mechanics of *unloading-reloading* were incorporated in the model of Francis [39].

3.1.2. The mode of deformation-plasticity indices

While many elastic and elasto-plastic models of surface response to normal loads have been proposed, the question of what circumstances dictate the use of an elastic or a plastic representation remains central. In particular, when can plastic deformations be expected to be sufficiently large to be a necessary ingredient in a reasonable model of surface behavior? In an attempt to resolve this question, several authors have proposed parameters to indicate which mode of surface deformation may be dominant in various situations.

Greenwood and Williamson [42] used their model of the surface topography to study the limits of the elastic deformation of rough surfaces. Although their model assumed elastic contact, they used it to study the early stages of growth of plastic contact areas with increasing load. The criterion for the initiation of plastic flow at the asperity level was based on the analysis of ball indentation tests. The criterion for the limit of elastic behavior of the contacting surfaces was based on the ratio: plastic area of contact/total area of contact. For values of this ratio greater than around 0.02, the surfaces can no longer be considered to behave elastically.

These authors found that a nondimensional parameter could be defined which predicts the mode of deformation of the surface over very wide ranges of loads. This parameter is the so-called *plasticity index,*

$$\psi = \frac{E'}{H}\sqrt{\frac{\sigma^*}{R}}.$$

When ψ is less than 0.6, plastic contact could be caused only if the surfaces were forced together under very large nominal pressures; when ψ is greater than 1.0 plastic flow will occur even at trivial nominal pressures. *The load has thus little effect on the mode of deformation of the surface. The essential factors are the material properties* (E/H) *and the surface finish* $(\sigma^*/R)^{1/2}$. For most engineering materials and surface finishes $\psi > 1$. We can conclude that *during the initial contact of these surfaces the deformation will be mainly plastic even at the lightest loads.*

The repeated loading-unloading-loading of the metal surfaces, as in normal sliding or in metallographic polishing, will produce changes in the shape of the asperities (decrease of σ^*/R) *and the deformation will become elastic.* It turns out that over a wide range of experimental conditions the real contact pressure on the asperities becomes of the order of $0.1H$ to $0.3H$ [96]. However, Greenwood and Williamson [42] observed that the wear debris procedure in

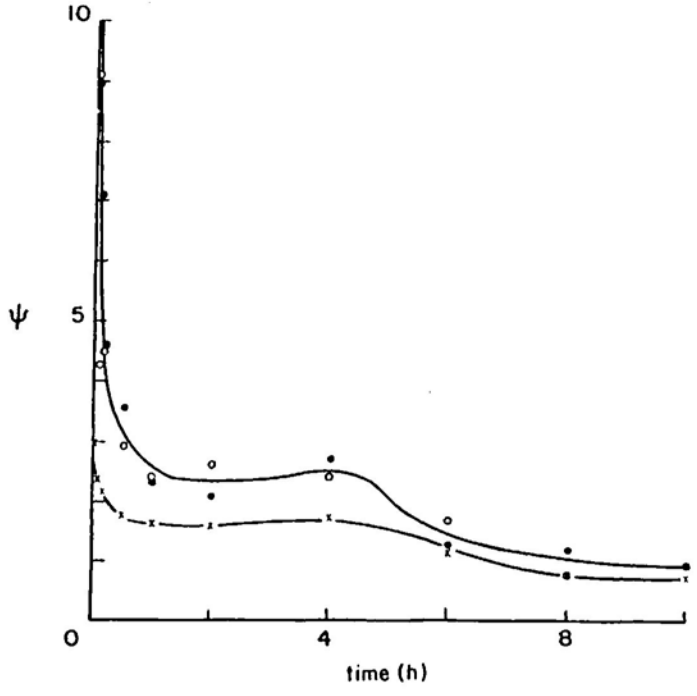

Fig. 10. Effect of continued sliding on the plasticity index. The behavior of three mild steel specimens slid against a stainless steel woven grid at 100 cm/s under loads of 1.5 kg. (Reproduced from [42].)

sliding can reverse this trend and, by damaging the surface, can prevent ψ from reaching the elastic range.

The effect on the plasticity index ψ of the continued sliding of two metal surfaces, under conditions which prevented severe wear damage of the surfaces, is shown in Fig. 10, which is due to Greenwood and Williamson [42]. In this figure the decrease of ψ down to values which correspond to an elastic normal deformation of the asperities is easily observed. Several other such indices have been proposed by other authors, and we mention as typical those in the papers of Whitehouse and Archard [110], Onions and Archard [71], and Mikic [65].

A simplified analysis of Tabor [95] based on the indices proposed by Greenwood and Williamson [42] and Whitehouse and Archard [110], showed that a critical geometrical factor in the transition from elastic to plastic deformation of a rough surface is the average slope of the asperities.

3.1.3. Some experimental results

Early experimental results on the stiffness of contacting surfaces and their real area of contact can be found in [55]. Kragelskii [55] refers to the work of Sokolovskii [88], Bobrik [17] and Votinov [108] who proposed a relationship between the approach (a) and the nominal pressure (p) of the form

$$a = Cp^m + K, \tag{3.5}$$

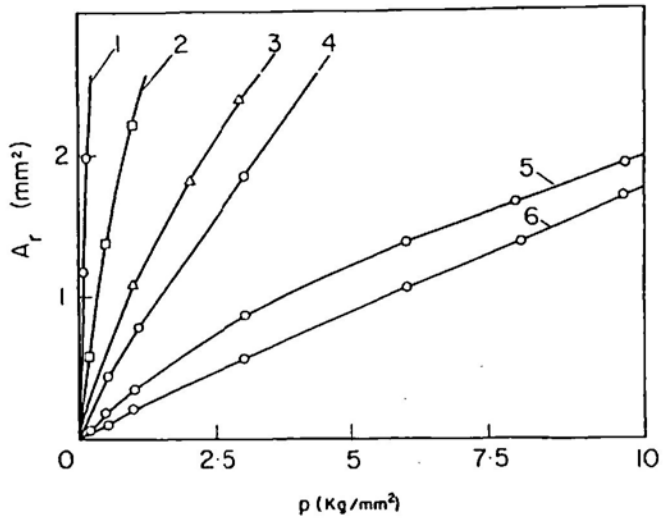

Fig. 11. Real area of contact vs. pressure for different metals in contact with a glass prism. (1) lead; (2) cadmium; (3) magnesium; (4) aluminum; (5) copper; (6) steel 10. Maximum height of surface asperities: 40 μ. (Reproduced from [55].)

where C, m and K are constants determined experimentally. According to Sokolovskii, these constants are usually $m = 0.3$–0.5 and $K = 0$. Fig. 11, also from [55], illustrates the experimental relationship between the real area of contact (A_r) and the nominal pressure (p) for different metals in contact with a glass prism. It can be seen that some of the curves obtained depart appreciably from linearity. According to Kragelskii, the relationship may only be considered linear at low pressures or for materials which do no work harden appreciably.

Important sources of experimental results on the contact of metallic surfaces can be found in the literature devoted to the design of machine tools. The research of several workers who studied the stiffness, damping, friction and wear characteristics of fixed and sliding joints has been summarized in a paper by Back, Burdekin and Cowley [9]. The essential conclusions related with the stiffness of contacting surfaces are the following:

(1) *For low nominal pressures,* characteristic of sliding connections, no plastic deformation was observed and *the approach-normal load relationship is of the form of* (3.5) with $K = 0$ and with m having values in the range $m = 0.32$–0.5, in perfect agreement with the observations of Sokolovskii mentioned above.

While these authors' reference to 'no plastic deformation' represents a mild contradiction to those results described earlier, a study of available discussions of the experimental set-up indicates that some rubbing of the surfaces may have been done prior to the experiments in order to obtain reproducible results (e.g. [34]).

(2) *For higher nominal pressures,* characteristic of fixed or bolted connections, the general behavior to be expected when successive loadings and unloadings of the surfaces are performed, is shown in Fig. 12. It is clear that *the total approach of the surface has an elastic and a plastic component* and that (if the joint orientation is not disturbed) *the unloading and reloading paths, are practically coincident.* For these elastic paths, Connolly and Thornley [28]

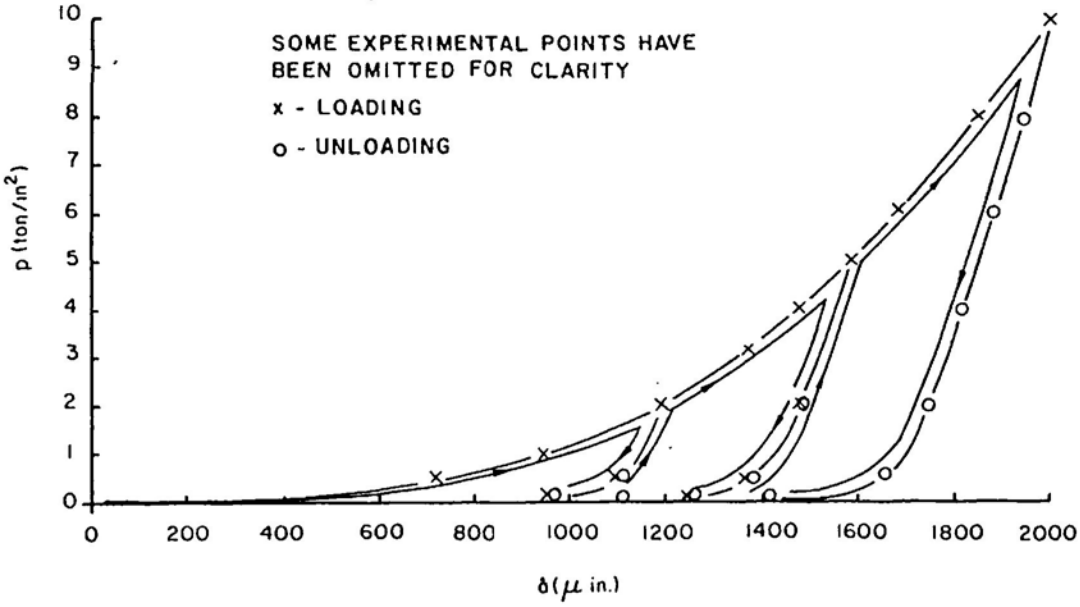

Fig. 12. Penetrating approach due to successive loadings and unloadings of a metal surface (reproduced from [29]). The experimental values $\hat{a}$ contain the deformation of the surface asperities (penetrating approach) and some deformation of the solid material in the neighborhood of the interface.

proposed the following relationship between the approach and the normal load:

$$a = \frac{1}{B} \ln p + Q, \tag{3.6}$$

where B and Q are constants.

Tables with experimental values of the constants C and m in (3.5) and B in (3.6) can also be found in [9] together with the corresponding ranges of validity.

The elastic stiffness of the surface per unit area (S) is thus given by

$$S = \frac{\mathrm{d}p}{\mathrm{d}a} = \frac{p^{(1-m)}}{mC} \tag{3.7}$$

when (3.5) is used, and by

$$S = Bp \tag{3.8}$$

when (3.6) is used. It was also found experimentally that for mild steel specimens with shaped or turned surfaces the constant B is inversely proportional to the surface roughness in c.l.a. Consequently, *the stiffness* (3.8) *is inversely proportional to the surface roughness.*

In recent years, much experimental work has been done to test the statistical models of the surface geometry and contact. The essential conclusions of a survey paper of Woo and Thomas [113] are the following:

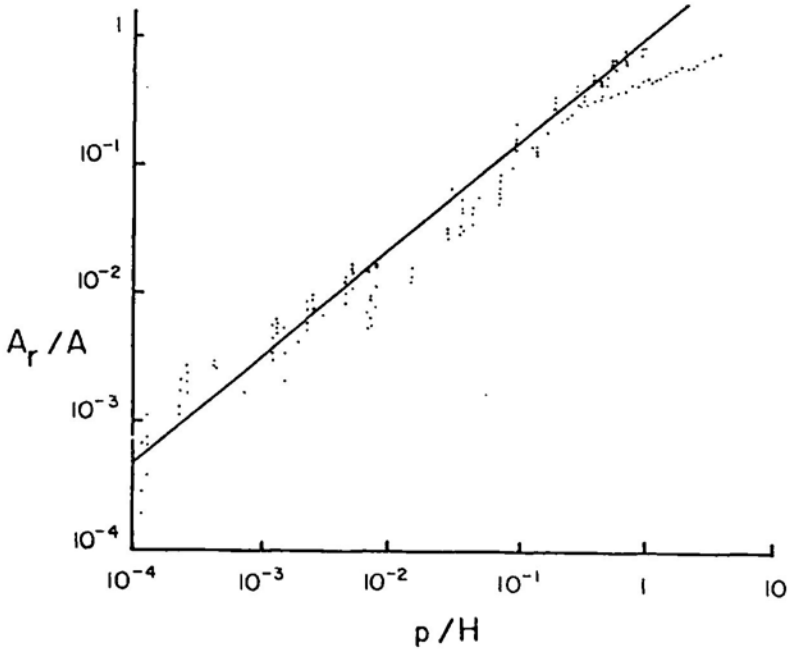

Fig. 13. Bearing area ratio vs. dimensionless load. Least squares straight line obtained on the basis of the experimental results of 6 different papers by various authors. (Reproduced from [113].)

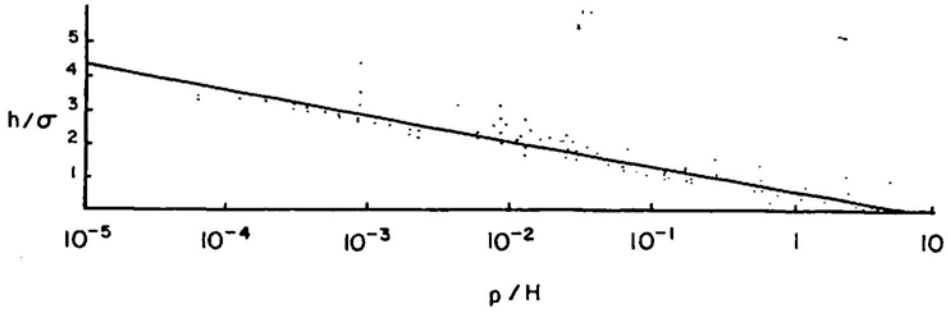

Fig. 14. Dimensionless separation vs. dimensionless load. Regression line obtained on the basis of the experimental results of 7 different papers by various authors. (Reproduced from [113].)

(i) The bearing area ratio (A_r/A) increases as the 0.8 power of the dimensionless load (p/H) up to values of p/H of the order of 0.1 (see Fig. 13).

(ii) The dimensionless separation (h/σ) decreases proportionally to the increase of the logarithm of the dimensionless load (p/H) (see Fig. 14).

3.1.4. Conclusions

Since the assumptions on the roughness of the surfaces and their mechanical behavior are different, the relationships involving area of contact, load and separation derived from the models described earlier are also different and, in some cases, difficult to compare. However, comparing the theoretical predictions of those models with the experimental results presented above, some broad conclusions can be drawn. We summarize them as follows:

On the mode of deformation of metal surfaces:

(i) The essential factors affecting the mode of deformation of a rough surface are the material properties (E', H) and the surface finish. The normal load is expected to have little effect on the mode of deformation of the surface.

(ii) For most engineering materials and surface finishes the initial contact of the surfaces is expected to be plastic even at light loads.

(iii) The repeated loading-unloading-reloading of the metal surfaces, as in normal sliding or in metallurgical polishing, produces changes in the shape of the asperities, which lead to a subsequent elastic deformation, provided that severe wear is prevented during the process of sliding.

On the stiffness of compressed rough surfaces:

(iv) At small penetrating approaches (large separations) the stiffness of rough surfaces becomes vanishingly small.

(v) The stiffness of a surface is inversely proportional to its roughness.

(vi) The normal load increases roughly as an exponential function of the penetrating approach (the separation decreases proportionally to the increase of the logarithm of the load).

(vii) For light loads, because of (iv), the normal load is closely proportional to a power, in the range 1/0.5 to 1/0.3, of the penetrating approach.

(viii) For the same normal load the stiffness during the first loading is smaller than the stiffness during unloading or reloading, due to the plastic deformation which occurs during the first loading.

On the real area of contact:

(ix) Most of the statistical models developed predict, for both elastic and plastic contact, an exact or an approximate proportionality between real area of contact and normal load.

(x) Experimental results show that, often, the real area of contact increases with a power of the normal load which is slightly smaller than one, even for light loads.

A definitive precise conclusion seems difficult due to the absence of a really satisfactory method for the experimental determination of the real area of contact – a fundamental difficulty pointed out by Tabor [98].

3.2. Dynamic contact of rough surfaces

In Section 3.1 we presented a review of theoretical models and experimental results on the static contact of rough surfaces. Our purpose in this section is to determine whether or not the conclusions drawn for the static deformation of rough surfaces can be expected to hold for dynamic situations. We are only interested in dynamic situations for which no bulk plastic deformation of the metallic bodies occurs. In the following we describe experimental observations of two phenomena for which the above criterion is satisfied: the low velocity impact of metallic bodies and the dynamic response (to a sinusoidal excitation) of metallic bodies compressed together with some preload.

The problem of the impact of two elastic bodies (two spheres or a sphere and a massive body) with relative velocity before impact smaller than the critical velocity required to initiate plastic deformation, has been studied by several authors on the basis of the Hertz theory of impact (see [60]). It has been observed [59] that the predictions of this theory for the time of contact of a steel sphere with a polished face of a mild steel block is given, with good accuracy,

by the Hertz solution (even up to velocities of impact that are eight times larger than the critical velocity corresponding to the onset of plastic deformation in the block). On the other hand, the Hertz theory does not predict any energy dissipation and, consequently, for velocities of impact smaller than the critical velocity mentioned above the velocity of rebound would be expected to equal the velocity of impact, i.e., the coefficient of restitution

$$e = V_r / V_0 \tag{3.9}$$

would be expected to equal unity (in (3.9) V_0 and V_r are the absolute values of the velocities of impact and rebound of the sphere, respectively).

However, the above predictions are not confirmed experimentally. Coefficients of restitution of the order 0.90–0.95 (energy losses of the order 10–20 percent) are reported by Hunter [47] for collisions between ball bearings and steel blocks and coefficients of restitution of the order 0.985 (energy losses of the order 3 percent) are reported by Tillet [102] for steel balls on glass blocks. These discrepancies between the theory and the experimental observations prompted several authors to study the possible sources of energy dissipation. Hunter [47] estimated the energy lost by the impacting ball due to the excitation of elastic vibrations on the massive body subsequently to the impact. Jenckel and Klein [49], and Tillet [102] correlated the energy lost by the impacting ball with the energy dissipated in the block due to internal friction.

It was concluded that the effects considered above, together with surface friction, air damping, etc., were sufficient to explain the small losses observed in the impact of the steel balls on glass blocks. However, the same was not true for the case of steel blocks. Lifshitz and Kolsky [59] then investigated the possibility of those losses being the result of local plastic deformation of the steel block – flattening of microscopic protuberances (asperities). To investigate this, measurements of coefficients of restitution of steel balls impacting on mild steel blocks with different surface finishes were carried out. Those authors found that with blocks with finely ground surface finishes the coefficients of restitution were very scattered and never exceeded 0.82; for surfaces polished with very fine emery paper the results were much less scattered and a maximum value of 0.87 was obtained; for a highly polished surface (highly reflecting mirror finish) the coefficient of restitution was found quite consistent at 0.95. Lifshitz and Kolsky thus conclude that *the coefficient of restitution is very sensitive to the surface finish* and that, probably, further polishing would produce higher values of e, closer to the theoretical predictions.

We note that these observations on the effect of the surface roughness on the rebound of metallic bodies can be easily predicted, at least qualitatively, from the models discussed in Section 3.1. We recall that for most engineering surface finishes and materials the plasticity index assumes values which correspond to a plastic deformation of the asperities, upon first loading, for a wide range of normal loads. This obviously leads to important energy dissipation which contributes, in the manner experimentally observed, for the low values of coefficient of restitution. In particular, for mild steel (the material of the blocks used by Lifshitz and Kolsky) the model of Greenwood and Williamson [42] predicts that only for a highly polished surface and small loads, can the deformation of the asperities be essentially elastic (see Fig. 15, due to Tabor [96]). We can thus conclude that *Greenwood and Williamson's model allows for an interpretation of the experimental results which corroborates the conclusions of Lifshitz and Kolsky.*

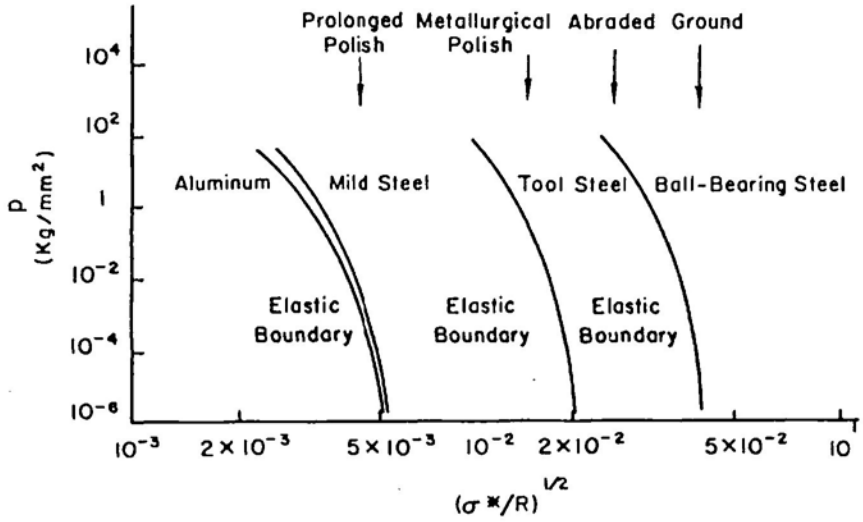

Fig. 15. Nominal pressure at which the transition from elastic to plastic deformation occurs for a flat metal of specified roughness pressed on to a flat ideally smooth hard surface. The model used for the calculations is the model of Greenwood and Williamson [42]. Material properties used: Aluminum $H = 40\ \text{Kg mm}^{-2}$; Mild Steel $H = 120\ \text{Kg mm}^{-2}$; Tool Steel $H = 400\ \text{Kg mm}^{-2}$; Ball-bearing Steel $H = 900\ \text{Kg mm}^{-2}$. For each material below the 'elastic boundary' the deformation is elastic. The onset of plastic deformation of the asperities occurs on the 'elastic boundary'. (Reproduced from [96].)

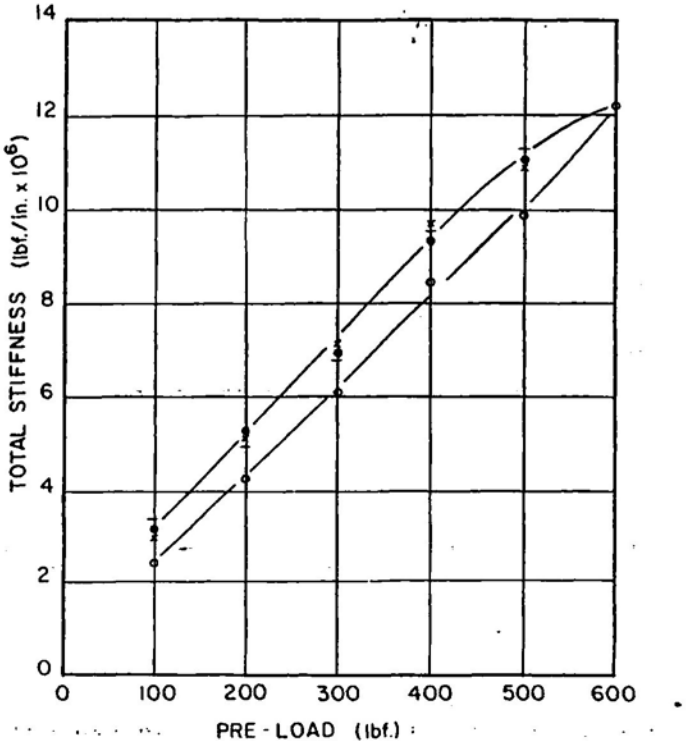

Fig. 16. Variation of dynamic stiffness with pre-load (reproduced from [2]). Test frequency 90 Hz. O First loading; ● First unloading; + Second loading; × Second unloading.

Experimental results of more quantitative nature on the dynamic characteristics of metallic surfaces were provided by Andrew, Cockburn and Waring [2]. In their experiments the annular interfaces of several mild steel discs compressed together with some preload were subjected to a normal harmonic force. From their dynamic response, the stiffness and damping of the interfaces was evaluated for different dimensions of the apparent area of contact, surface finishes, and for various values of the normal preload. Although some of their experimental results (influence of apparent area of contact and roughness on the stiffness) cannot completely be interpreted from the static contact results, other results are clearly similar to those observed in the static case. *The linear dependence of the stiffness on the normal load and the (small) difference between the initial loading and unloading stiffnesses*, shown in Fig. 16, could be predicted from (3.8) and Fig. 12, respectively, obtained experimentally for static contact.

Although the experimental evidence available is not abundant, we think that the facts collected in this section suggest clearly that *the dynamic behavior of most rough surfaces is consistent with the stiffness characteristics analyzed in detail in the static case.*

4. Dry sliding friction of metallic bodies

4.1. Classic laws of friction

When two metallic bodies in contact are subjected to applied forces which tend to produce relative sliding motion, friction stresses develop on the interface that tend to oppose that motion.

In the following only the resultants of the stresses on the contact surface will be considered: N, the compressive normal force and F, the friction force. The metallic bodies are considered essentially as rigid bodies with a well defined tangential relative velocity $\dot{u}_T$.

According to Moore [67], the classic laws of friction, as they evolved from early studies in the past centuries, are the following:

(i) The friction force (at the onset of sliding and during sliding) is proportional to the normal contact force,

$$|F| = \mu N. \tag{4.1}$$

The coefficient of proportionality, μ, is known as the coefficient of friction. Often two values of μ are quoted: the coefficient of static friction, μ_s, which applies to the onset of sliding and the coefficient of kinetic friction, μ_k, which applies during sliding motion.

(ii) The coefficient of friction is independent of the apparent area of contact.

(iii) The static coefficient is greater than the kinetic coefficient.

(iv) The coefficient of kinetic friction is independent of the sliding velocity.

Another important characteristic of the friction force is the following [77]:

(v) When tangential motion occurs, the friction force acts in the same direction of the relative velocity but in opposite sense,

$$F = -\mu N \dot{u}_T / |\dot{u}_T| . \tag{4.2}$$

The first two laws, usually known as the Amontons' Laws of friction, are generally observed to hold for gross motions of effectively rigid bodies. However, we notice that deviations from the first law have been reported at various circumstances: an increase of the coefficient of friction for light loads [23], or an increase of friction for loads greater than a fairly well defined value which corresponds to the breaking of the oxide films on the surface [23] or yet a decrease of the friction coefficient for very high loads when the true area of contact approaches the magnitude of the apparent area of contact and bulk plastic deformation of the bodies in contact occurs [12].

The third law derives from classical experiments [38]: if a body rests in equilibrium on an inclined plane and the inclination of the plane is slowly increased up to the angle at which the sliding initiates (this angle is known as the angle of static friction $\theta_s = \tan^{-1} \mu_s$) it is often observed that, when the motion starts, it starts abruptly and the body acquires a large velocity in a short time. If the kinetic friction force were equal to the maximum static friction force, the slippage down the inclined plane, at the critical angle θ_s, would be infinitely slow, since no source for tangential acceleration would exist. The source for the observed acceleration is thus the difference between the maximum static friction force ($\mu_s N$) and the kinetic friction force ($\mu_k N$). The stick-slip phenomenon discussed in Section 5 is also intimately associated with this law.

The fourth law is now known to be invalid. A large volume of experimental data and empirical formulas for the variation of the friction coefficient with sliding velocity can be found, e.g., in [55, 67]. However, as noted by Rabinowicz [77], for many purposes in which only limited velocity ranges are of interest, the kinetic friction coefficient may be taken to be a constant independent of the sliding velocity.

Also according to Rabinowicz [77], the fifth law has been, essentially, confirmed by experiment: for surfaces without pronounced directional properties, the instantaneous friction force may fluctuate by a degree or so from its assigned direction, changing direction continuously and in random fashion as sliding proceeds.

4.2. The origins of friction – A brief review

In this section we present a summary account of the theories that have been proposed to explain the origins of the friction force. Detailed historical accounts and thorough discussions of these theories can be found in [23, 35, 55, 56].

4.2.1. The early theories of friction

Many of the early theories of friction, developed during the eighteenth and nineteenth centuries, attempted to explain the frictional behavior in terms of the surface roughness and the interlocking of the surface asperities. It was thought that the sliding of two contacting bodies involved the riding of rigid asperities of one surface over the other. If the average asperity angle is θ the coefficient of friction would be equal to $\tan \theta$ and consequently it would be independent of the load or the size of the contacting surfaces. This provided an explanation for the Amontons' laws. The assumption that the asperities on one surface could traverse the gap between asperities on the other provided an explanation for the fact that often the kinetic friction is smaller than the static one. According to Tabor [98], the main weakness of this early

work on friction [1, 30, 38] is that basically *the models proposed are non-dissipative and friction is certainly a dissipative process* – a critique which was first expressed by Leslie [58].

4.2.2. The adhesion-plowing theory

A substantially different explanation for the friction phenomena was provided by Bowden and Tabor. Their theory (reviewed in [22, 23, 94, 96, 98] has been the most widely accepted in recent decades among the researchers of solid contact phenomena. The interfacial friction between metallic bodies is attributed essentially to two causes: the formation and shearing of metallic junctions between the surface asperities and the plastic deformation of the softer surface by hard asperities. As a consequence, the friction coefficient can be given as the sum of two components resulting from each of the above effects,

$$\mu = \mu_a + \mu_p . \tag{4.3}$$

where μ_a results from the adhesion (welding) and μ_p results from the plastic deformation (plowing).

The adhesion component of friction. As noted earlier, Bowden and Tabor [23] assume that when *two clean metal bodies* are put in contact, plastic flow at the tips of the asperities and local welding between opposing asperities occur. The true area of contact is then proportional to the normal load,

$$A_r = N/H . \tag{4.4}$$

Here H is the hardness of the softer of the contacting materials.

Neglecting the contribution of plowing, the friction force is then equal to the force F_a required to shear the junctions formed in the manner described above. If τ_j is the average shear strength of the junctions, then

$$F_a = A_r \tau_j = (\tau_j/H)N ,$$

or, dividing by N,

$$\mu_a = \tau_j/H .$$

Due to plastic yielding and work-hardening, the interface between welded asperities is as strong or probably stronger than the undeformed material in the hinterland. For this reason, the average shear strength of the junctions (τ_j) can be assumed to be equal to the shear strength of the softer of the contacting materials (τ). Consequently,

$$\mu_a = \tau/H . \tag{4.5}$$

The Amontons's laws of friction are then verified: the friction force is proportional to the normal load and independent of the apparent area of contact.

For most materials, τ is of the order of $0.2H$ so that, for this simplified model,

$$\mu_a \approx 0.2 .$$

However, for clean metals enormous values of μ may be obtained and even for metals in air μ may be of the order unity.

According to the same authors, this discrepancy can be overcome if the plastic *junction growth* due to combined normal and tangential loading of the asperities is considered. The yield criterion assumed for this situation is of the form

$$p_r^2 + \alpha s_r^2 = H^2 = \alpha\tau^2 , \tag{4.6}$$

where p_r and s_r are the normal and tangential stresses at each asperity, i.e., the average true stresses on the true area of contact and α is a constant of the order 10.

The above criterion predicts that when an asperity, initially in pure normal contact, has its tip plastically deformed,

$$p_r = H .$$

When a small tangential stress s_r is applied, further plastic flow will occur. However, although the newly added stress is tangential, the normality rule dictates that the initial plastic movement will be a normal approach and, because of the shape of the asperity, it will lead to an increase in the area of contact. As s_r is increased, the plastic displacements will become more nearly tangential.

If $A_0 = N/H$ is the initial true area of contact, due to the normal load alone it can be shown from (4.6) that the equation governing the increase of the true contact area with the tangential load is

$$1 + \alpha\left(\frac{F_a}{N}\right)^2 = \left(\frac{A_r}{A_0}\right)^2 . \tag{4.7}$$

With *real surfaces in air* this process of junction growth is terminated due to the presence of the contaminant layers which are weaker than the bulk material. If $\tau_i = K\tau$ (with $K < 1$) is the critical shear stress of these interface films, the junction growth terminates when the tangential stress on the interface reaches the value τ_i; then gross sliding occurs. From (4.6) sliding occurs when

$$p_r^2 + \alpha\tau_i^2 = \alpha\tau^2 .$$

The adhesion component of the coefficient of friction is then

$$\mu_a = \frac{A_r\tau_i}{A_r p_r} = \frac{1}{\alpha^{1/2}(K^{-2} - 1)^{1/2}} . \tag{4.8}$$

Fig. 17 correlates the tangential force coefficient $\phi_a = F_a/N$ with the growth of the true contact area A_r/A_0 for different values of K. It can be seen that:

(i) For $K \to 1$ $\mu_a \to \infty$; this corresponds to perfectly clean surfaces of very ductile metals, where junction growth goes on indefinitely.

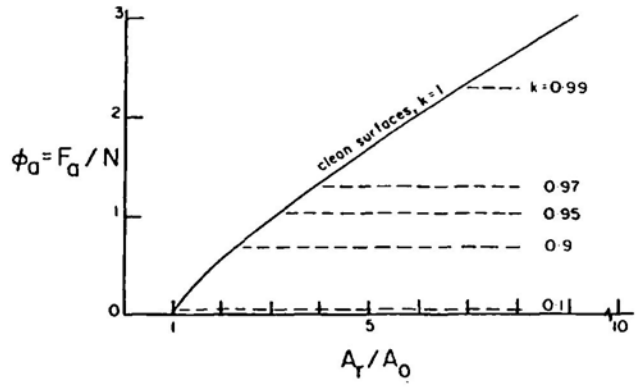

Fig. 17. Growth in area of contact for different values of K (reproduced from [23]).

(ii) A very small amount of weakening of the interface (say, $K = 0.95$) reduces the coefficient of friction to reasonable values (of the order unity).

(iii) For a very weak interface (say, $K < 0.2$) the junction growth is very small; this situation corresponds to the presence of a good boundary lubricant or a thin film of a softer metal; for this case μ_a can be written with sufficient accuracy as

$$\mu_a = K/\sqrt{\alpha}\,,$$

and using (4.6),

$$\mu_a = \tau_i / H\,, \tag{4.9}$$

which is formally analogous to (4.5).

We wish to point out that the theory described above not only gives an explanation for the Amontons' laws of friction, but also allows for interpretations of the other classic laws (Section 4.1). Following arguments of Rabinowicz [74, 77], the static friction is often greater than the kinetic one because the strength of the junctions would increase with the time of stationary contact (we will discuss this point in Section 5.1); the weak dependence of the friction force on the sliding velocity would be a consequence of the small rate dependence of the strengths of most solids; the opposite directions of friction and sliding velocity would be a consequence of the plastic deformation of the isotropic material on the contact.

We also point out that all the theory is based on the proportionality $A_r \propto N$ (cf. (4.4)). We recall, from Section 3.1., that the assumption of plastic deformation of the asperities is not essential to obtain this proportionality. Consequently, arguments similar to those presented earlier can also be used to explain Amonton's laws in the case of elastic deformation of the asperities. On the other hand, deviations from the proportionality $A_r \propto N$, would lead to deviations from the Amontons' laws.

Finally, we note that in recent years an extensive effort has been devoted to the understanding of the physical nature of the interfacial bonds between metallic bodies and the factors that may influence the existence, strength and persistence upon unloading of these bonds

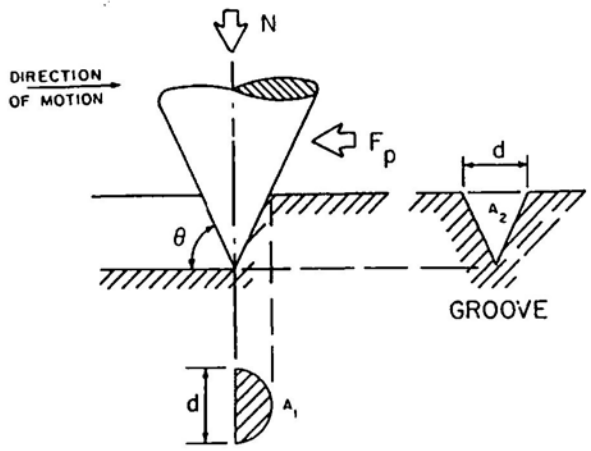

Fig. 18. Plowing component of friction for a cone sliding on a softer metal,

$$\mu_p = \frac{F_p}{N} = \frac{A_2}{A_1} = \frac{\frac{1}{4}d^2 \tan\theta}{\frac{1}{8}\pi d^2} = \frac{2}{\pi}\tan\theta .$$

(mutual solubility of the metals, ductility, roughness, surface films, etc.). Reviews of these developments can be found in [63, 97, 98].

The plowing component of friction. The plowing component of the friction can be estimated using the simplified model of a hard conical asperity grooving on a softer surface, as shown in Fig. 18. Assuming that the plastic-yielding metal is isotropic, the plowing component of the coefficient of friction, μ_p, can be shown to be

$$\mu_p = \frac{2}{\pi}\tan\theta . \tag{4.10}$$

Due to the small slopes of the asperities, this expression leads to values of the order of 0.07 (for $\theta = 5°$) to 0.14 (for $\theta = 10°$). As a consequence of these small values, the contribution of the plowing component of friction will be negligible unless the adhesion is small.

4.2.3. Recent theories

Despite the wide acceptance of the theory described above and its effectiveness in explaining the basic laws of friction, several serious criticisms have been offered and some alternative theories have been proposed, especially in recent years.

Some of the criticisms [14] result from the fact that, in the air, most of the solids are covered with various films which prevent atomic contact between the bulk materials of two contacting bodies. As a consequence, the force required to pull apart two contacting bodies is, in daily life, zero (if gravity is compensated). Furthermore, according to Bikerman, the formation of adsorbed layers in the air is so fast that all the effects associated with sliding are comparatively slow. From these facts and the critical review of several experimental observations on adhesion and friction, Bikerman [14] concludes that the importance of the adhesion in frictional phenomena is negligible, as long as the term friction is used in the sense of a force which, for a given path, is reproducible and is a definite function of the normal load.

Other alternative theories have been developed by authors who are especially concerned with the *evolution of the friction force during prolonged sliding* and with the *interaction between friction and the wear damage of the surfaces.* In the following we summarize some of the more elaborate theories that have been proposed. Our purpose is only to exemplify the type of ideas which have been advanced: a renewed interest on the *interlocking effects of the roughness, now associated with plastic deformation – plowing by hard asperities and entrapped wear particles and deformation of the asperities and of the subsurface layers.*

Rigney and Hirth [80] developed a new model to explain the origin of friction during the steady-state sliding of metals. This steady-state sliding is the advanced stage of sliding during which a near surface micro-structure of the type indicated in Fig. 19 (developed during the initial break-in stage) remains constant. In particular, the average thickness of the highly deformed region with cell structure, remains constant during the steady-state sliding. With the assumptions that the frictional force arises from plastic deformation in the near-surface region and that most of the deformation work is confined to the cell region, those authors equate the work of the friction force to the work of deforming plastically the subsurface volume and obtain an expression for the friction coefficient.

Kuhlmann-Wilsdorf [57] proposes the modification of the adhesion theory of friction to include the interlocking effect due to the micro-roughness superimposed on the hills and tops of the asperities. This micro-roughness is thought to be due to inhomogeneities in the near surface deformations and its importance during sliding is suggested by its persistence during the sliding process and by the observation of micro-grooves on the wear tracks. The same author analyzes the importance of the adhesion during sliding and concludes that only for very smooth surfaces (average slopes $\leqslant 0.9°$) the adhesion will be strong. A detailed analysis of the plastic deformations in the subsurface material, using concepts of the theory of dislocations, is then presented and quantitative expressions for friction and wear are proposed.

Suh and Sin [92] offered the following explanation of the genesis of friction: "The coefficient of friction between sliding surfaces is due to the various combined effects of an asperity deformation component μ_d, a component μ_p from plowing by wear particles and hard surface asperities and a component μ_a from adhesion between the flat surfaces. The relative contribution of these components depends on the condition of the sliding interface, which is

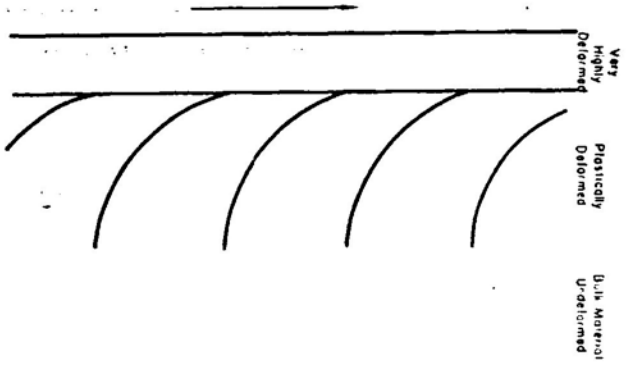

Fig. 19. Longitudinal section of a wear specimen. The curved lines indicate strain and the arrow indicates the sliding direction (reproduced from [80]).

affected by the history of sliding, the specific materials used, the surface topography and the environment."

The asperity deformation coefficient μ_d is expected to be very important at the onset of sliding (static coefficient of friction) and is also expected to contribute for the steady-state sliding if new asperities are continuously generated as a consequence of wear; μ_d is not expected to contribute significatively in early stages of sliding. High values for the plowing component μ_p are associated with two identical metals sliding against each other with deep penetration by wear particles while low values are obtained either when wear particles are totally absent from the interface or when a soft surface is slid against a hard surface with a mirror finish. The component μ_p is expected to contribute continuously during the sliding process and its contribution is expected to increase when, due to wear, the number of particles entrapped between the two surfaces increases. The low values for the adhesion component μ_a are associated with the sliding of well lubricated surfaces and high values with identical metals sliding against each other without any contaminants or oxide layer; μ_a is expected to be zero (or negligible) at the onset of sliding due to the presence of contaminants. With the deformation of the asperities and the exposure of fresh new surfaces, the adhesion is expected to increase.

The history dependence of the friction force is then the consequence of the evolution of the variables that, respectively, affect the components μ_d, μ_p and μ_a of the friction force: the roughness, expressed by the average slope of the contacting asperities, θ; the ratio of the width of asperity penetration to the diameter of the particle, $\omega/2R$; and the interface shear strength factor τ_i/τ which is the ratio of the interface shear strength to the shear flow strength of the softer contacting material,

$$\mu = \mu(\theta, \omega/2R, \tau_i/\tau)\,. \tag{4.11}$$

4.3. Some remarks on friction and plasticity theory

Although specific details may differ (significatively . . .), most current theories of the origin of friction single out plastic deformation on the contact neighborhood as a major phenomenon associated with the frictional sliding of metallic bodies. On the other hand, the model of a particle sliding with friction on a surface is often presented as a prototype of plastic behavior. A question which then arises is why classical plasticity theory has not been applied successfully to friction problems (viewed as boundary plasticity problems).

One reason for this has been pointed out by several authors (e.g. Drucker [36], Klarbring [54], Michalowski and Mroz [64], Sanchez-Palencia and Suquet [85]): The sliding rule dictated by the Coulomb's law of friction is *not* an associated flow rule as defined in the Classical Theory of Plasticity. In particular, a pointwise version of Coulomb friction is encompassed in the relations (see [73])

$$\begin{aligned}
&|\boldsymbol{\sigma}_T| \leq \mu|\sigma_n|, \qquad \sigma_n \leq 0\,,\\
&\dot{\boldsymbol{u}}_T = \mathbf{0} \qquad \text{if } |\boldsymbol{\sigma}_T| < \mu|\sigma_n|\,,\\
&-\dot{\boldsymbol{u}}_T = \lambda\boldsymbol{\sigma}_T \quad \text{if } |\boldsymbol{\sigma}_T| = \mu|\sigma_n|, \quad \lambda \geq 0\,.
\end{aligned}$$

Here $\dot{u}_T$ is the tangential sliding velocity at a point on the contact surface, σ_n is the normal stress (the 'contact pressure'), λ is a real number, and σ_T is the tangential stress vector (the frictional stresses). (Thus, σ_n corresponds to N and σ_T to F in the classical rigid-body case.) Thus, one can define a slip surface, such as that shown in Fig. 20, in the spirit of a yield surface in plasticity, such that contact stress states on the surface correspond to states at which sliding occurs. Since $-\dot{u}_T = \lambda \sigma_T$ on this surface, classical friction does not satisfy the classical normality rule. And, therefore, most of the standard arguments of classical plasticity do not have a straightforward extension to frictional phenomena (unless the normal forces on the contact boundary are known a priori, in which case the frictional forces are essentially derivable from a convex dissipation functional (see [37])).

We observe that the theory of Bowden and Tabor [23] suggests a way to analyze friction contact problems in terms of the classical (associated) plasticity theory. The yield criterion (4.6) can be rewritten in terms of the nominal normal and tangential stresses in the following way:

$$f(p, s, \delta) = p^2 + \alpha s^2 - \delta^2 H^2 = 0\,,$$

where $\delta = A_r/A \in [0, 1]$ is the bearing area ratio. In the above equation δ plays the role of a hardening (softening) parameter, which can make the yield surface shrink to the point $p = 0$, $s = 0$ if there is loss of contact ($\delta = 0$).

Similar ideas were also proposed by Michalowski and Mroz [64] who included an additional hardening parameter to describe the contact hardening due to tangential sliding. However,

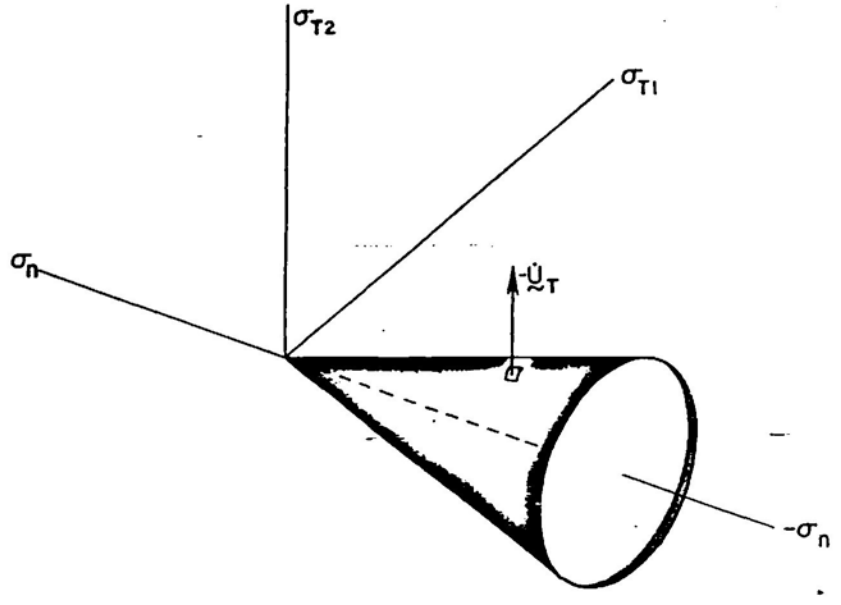

Fig. 20. The slip-surface corresponding to Coulomb's law for which the normality rule is clearly violated.

these authors assume that the elastic part of the contact deformation is linear which, as seen earlier, does not apply to rough metallic surfaces.

Independently of the difficulties that might be encountered in trying to use the theories of Bowden and Tabor [23] or of Michalowski and Mroz [64] in continuum models for quantitative purposes (and Bowden and Tabor [23] advise readers not to try to push their theory too far), *it seems that their essential applicability would be to quasistatic friction problems* (which we called Type I in Section 1).

The recent theories mentioned in the end of the previous section are not of much use for us here either, since it is not our final goal to analyze the effects of prolonged sliding and wear on the friction phenomena.

We still have to look for further experimental evidence on the transition between static and kinetic friction before we can try to develop a model for computational mechanics.

5. Static and kinetic friction. Stick-slip motion

5.1. The initiation of sliding

5.1.1. Preliminary micro-displacements

The classic laws of friction described in Section 4.1. dictate that, at the onset of sliding, the friction force is equal to the (static) coefficient of friction times the normal force. However, this law is valid only in a macroscopic sense, since, before macroscopic sliding is observed, some preliminary micro-displacements occur at lower force levels. Several experimentors have studied the evolution of these microdisplacements when the bodies are subjected to increasing tangential forces. References for these works can be found in [23].

Typical experimental curves of the tangential force coefficient $\phi = F/N$ versus the tangential displacement u_T, obtained by Courtney-Pratt and Eisner [31], are shown in Fig. 21. Courtney-Pratt and Eisner [31] also measured the electrical conductance of the contacting surfaces during their experiments. Neglecting the conductance of surface films, the increase in conductance c/c_0 is related with the increase in the true area of contact A_r/A_0 according to

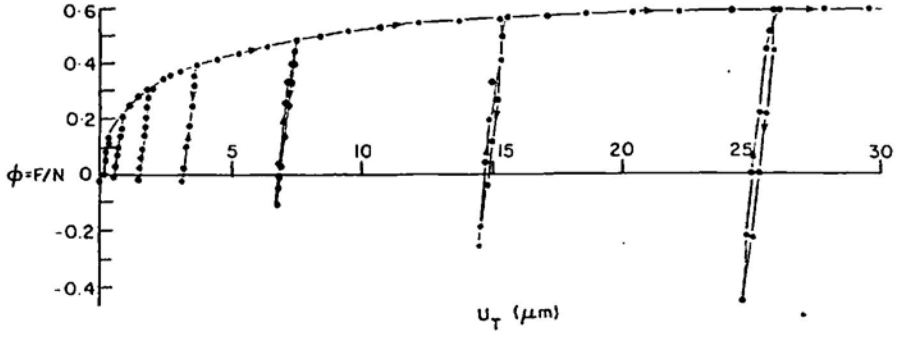

Fig. 21. Tangential microdisplacements due to successive loadings – unloadings. Platinum surfaces. Normal load $N = 920$ g. (Reproduced from [31].)

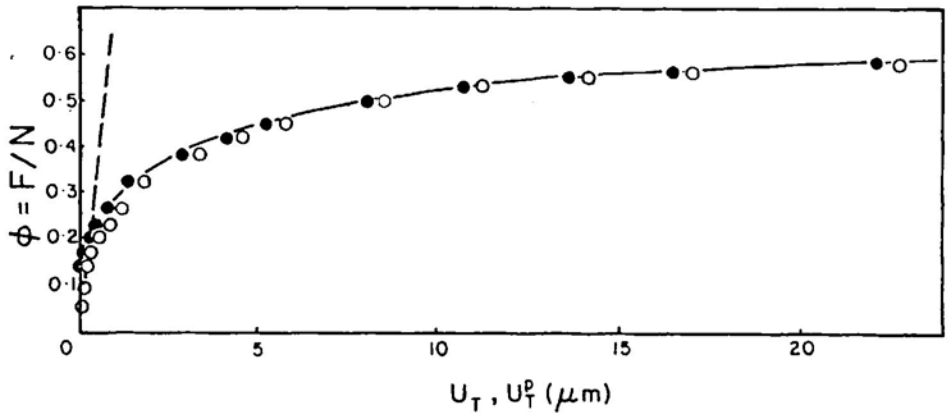

Fig. 22. The irreversible part of the tangential displacement. Platinum surfaces. Normal load $N = 920$ g. ○ Observed displacements u_T whilst the tangential force is applied. ● Residual displacements u_T^p obtained by subtracting from the observed displacements u_T the elastic displacements (deduced from the experimental results of Fig. 21). — Theoretical elastic displacements computed assuming that they result from elastic distortion of the slider according to the equation $u_T = [(2-\nu)/4Gr]F$ due to Mindlin [66] where G = modulus of rigidity and ν = Poisson's ratio. (Reproduced from [23], after experimental results of [31].)

$$\frac{c}{c_0} = \left(\frac{A_r}{A_0}\right)^{1/2}.$$

Using this expression, a comparison of the experimental results with the predictions of (4.7) is given in Fig. 23.

An important point made clear by the experiments of these authors was the nature of the preliminary displacements. As shown in Figs. 21, 22, *these displacements are essentially irreversible* (*plastic*). The origin of the elastic component was not clear for the authors who were not able to separate it into the elastic deformation of the specimen and that of the

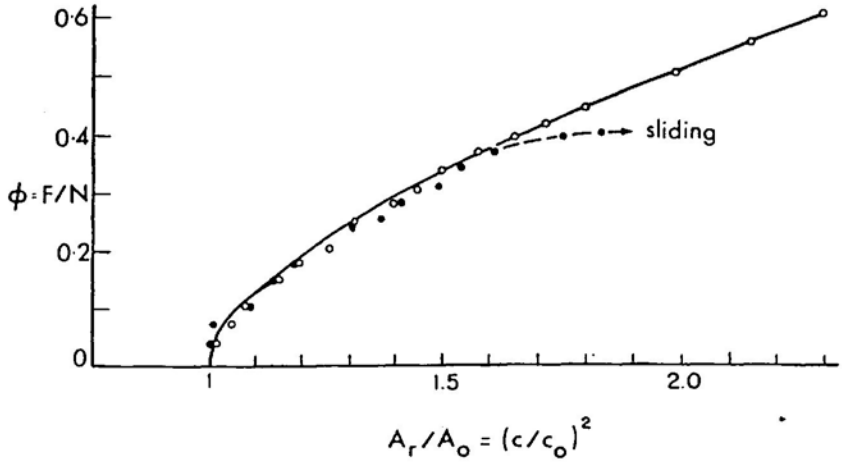

Fig. 23. Tangential force coefficient versus real area of contact. Platinum surfaces: ○ clean; ● lubricated. The full line is the theoretical curve plotted according to (4.7) with $\alpha = 12$. (Reproduced from [31].)

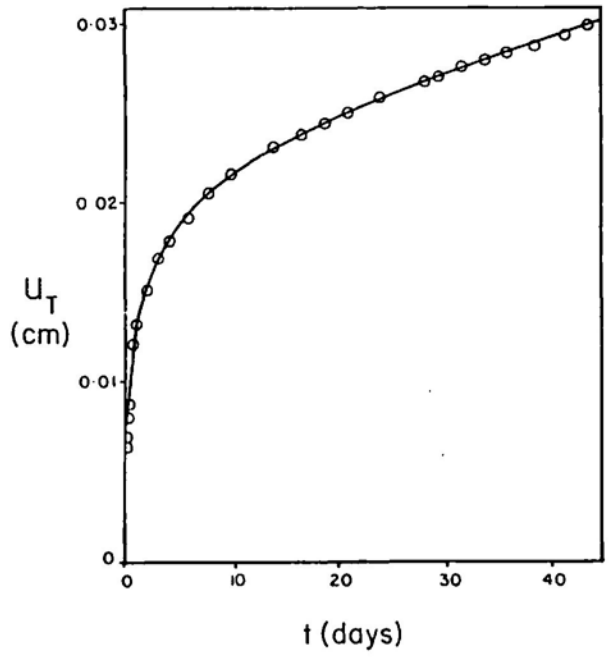

(a)

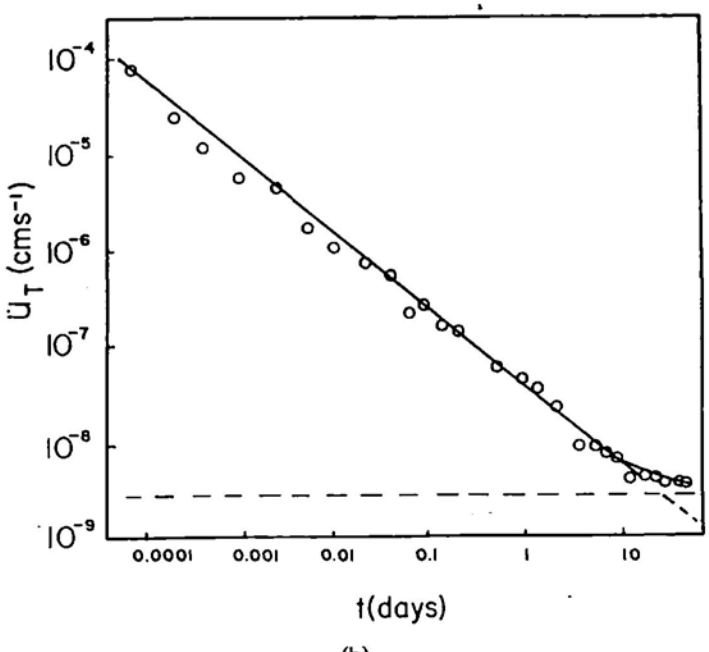

(b)

Fig. 24. Creep sliding. Steel on indium, clean; normal load $N = 300$ g; tangential force $F = 200$ g (constant). (a) Displacement as a function of time; (b) Sliding velocity as a function of time. (Reproduced from [25].)

apparatus. Bowden and Tabor [23], analyzing the same experimental results of Courtney-Pratt and Eisner, attribute that elastic component to bulk elastic distortion of the slider. On the other hand, the fact that the plastic component of the displacement (u_T^p) satisfies $du_T^p/d\phi \approx 0$ at $\phi = 0$ strongly suggests that when the tangential force begins to be applied the plastic deformation of the asperities is normal (rather than tangential) *exactly as predicted by the junction growth theory of Bowden and Tabor.*

5.1.2. Creep sliding

In all the experiments mentioned above, whether with hard or with soft metals, Courtney-Pratt and Eisner observed that the micro-sliding of the specimens continued for long periods of time after each increment of tangential force was applied. For example, with the soft metal indium, at the end of half an hour the rate of movement could be 2×10^{-6} cms^{-1}. For harder metals, after a few minutes, the movement was imperceptible.

Burwell and Rabinowicz [25] also observed the creep sliding on low melting point metals at low velocities (see Figs. 24, 25). In Fig. 25 each point on the initial increasing branch of the $\mu - \dot{u}_T$ curve corresponds to the final steady state sliding (constant velocity $\dot{u}_T$) attained by a slider acted upon by a constant tangential force, which (divided by the normal force) corresponds to a friction coefficient μ. The same authors point out that, for harder metals, such as aluminium, copper, steel, etc., it is probable that an initial increasing branch of the $\mu - \dot{u}_T$ curve also exists. The difficulty to provide additional experimental evidence of this, at velocities of the order 10^{-9} cm/s, is obviously extraordinary. In any case, since those velocities

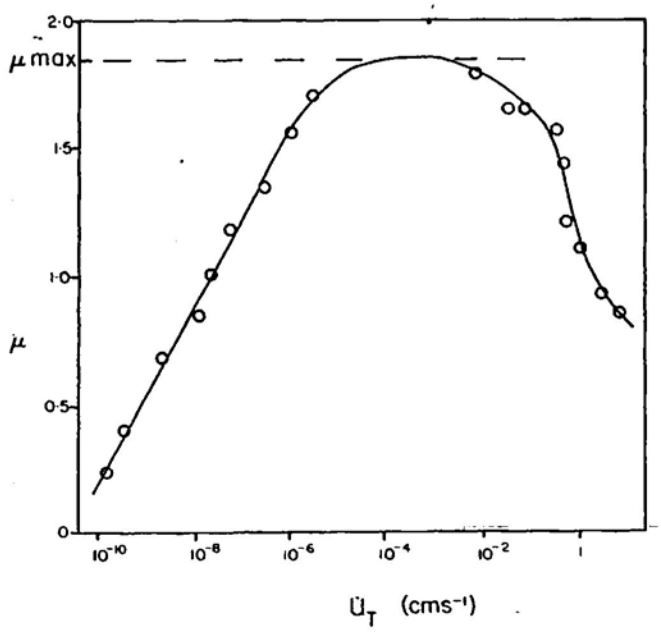

Fig. 25. Coefficient of friction as a function of final sliding velocity. Clean steel on indium; normal load $N = 300$ g. Each point on the increasing branch of the $\mu - \dot{u}_T$ curve corresponds to the final steady state sliding obtained by imposing a constant tangential force. For tangential forces corresponding to $\mu > \mu_{max}$ no steady state sliding was obtained. The points on the decreasing branch of the $\mu - \dot{u}_T$ curve were obtained, using conventional experimental techniques by imposing a much higher sliding velocity. (Reproduced from [25].)

are so small, it can be concluded, following Bowden and Tabor [23], that *the frictional behavior of ordinary engineering metals at room temperature is reasonably well explained in terms of their plastic properties without introducing the part played by creep.*

5.1.3. Rate dependence of the static coefficient of friction

A more important time dependent effect on the static friction has been observed by several authors who have studied the stick-slip motion (see Section 5.2).

Consider a slider resting on a surface with no macroscopic sliding motion relative to the surface and a tangential force F, applied to the slider, being increased at constant rate $\dot{\phi} = \dot{F}/N$ until gross sliding occurs. Under these conditions, it can be observed that the value μ_s of $\phi = F/N$ at which the macroscopic sliding occurs depends on the rate $\dot{\phi}$ of increase of the tangential force. As shown in Fig. 26, *μ_s decreases with the increase of the rate of application of the tangential force.*

The interpretation given by early researchers for this phenomenon was essentially the same used to explain the difference between static and kinetic friction (recall Section 4.2). The strength of the contact junctions would increase with the time of stationary contact. Consequently, the smaller the time of stationary contact, t_s, the smaller the coefficient of static friction would be (see Fig. 26). Expressions proposed by several authors for this time dependence of the coefficient of static friction can be found in a survey paper by Richardson and Nolle [78] and are reproduced in Table 1. Sketches of the corresponding behaviors are shown in Fig. 27.

However, the experimental work of several authors has made clear that this interpretation was not correct.

Simkins [87] carried out experiments similar to those of Courtney-Pratt and Eisner [31] to observe the micro-displacements before gross-sliding. He found that higher rates of loading inevitably led to macroscopic sliding at lower force levels. However, in other experiments

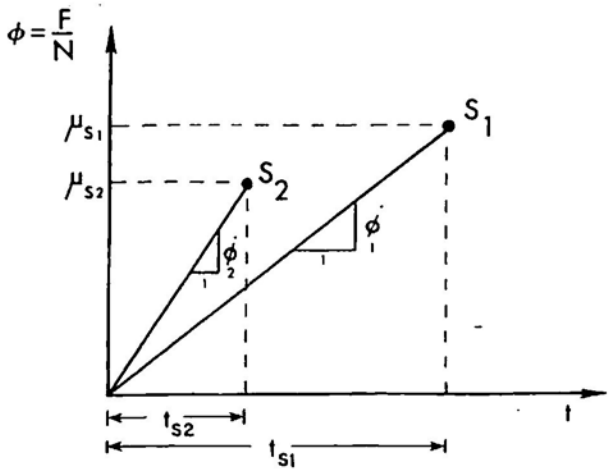

Fig. 26. Rate dependence of the static coefficient of friction. S_1 and S_2 are the points at which gross sliding initiates; $\dot{\phi}_1$ and $\dot{\phi}_2$ are the rates of increase of the tangential force coefficients ϕ_1 and ϕ_2; t_{s1} and t_{s2} are the times of stationary contact; μ_{s1} and μ_{s2} are the static coefficients of friction. $\dot{\phi}_1 < \dot{\phi}_2 \Rightarrow \mu_{s1} > \mu_{s2}$.

Table 1
Variation of μ_s with time of stationary contact (t_s) (reproduced from [78])

Equation	Expression	References	Year where first used	Basis for derivation	Experimental support
1	$\mu_s = \mu_k + c_1 t_s^{c_2}$	[19, 33, 75]	1958 (with 1946 data)	Empirical and idealised model of metallic junction	Stick-slip oscillation between lubricated metals
2	$\mu_s = \mu_0 + (\theta_{s\infty} - \mu_0)(1 - e^{-\alpha t_s})$	[18, 45]	1955	Theoretical consideration of Van der Waals' forces	Oscillation of glass surfaces
3	$\mu_s - \mu_k = (\mu_{s\infty} - \mu_k) t_s/(t_s + \tau)$	[32]	1957	Empirical, on the basis of observed behavior	Self excited stick-slip oscillations
4	$\mu_s = \mu_{s\infty} - (\mu_{s\infty} - \mu_0) \exp(-\gamma t_s^m)$	[51, 52]	1970	Initially empirical, later shown to be in qualitative agreement with theory	Stick-slip oscillation between lubricated metals

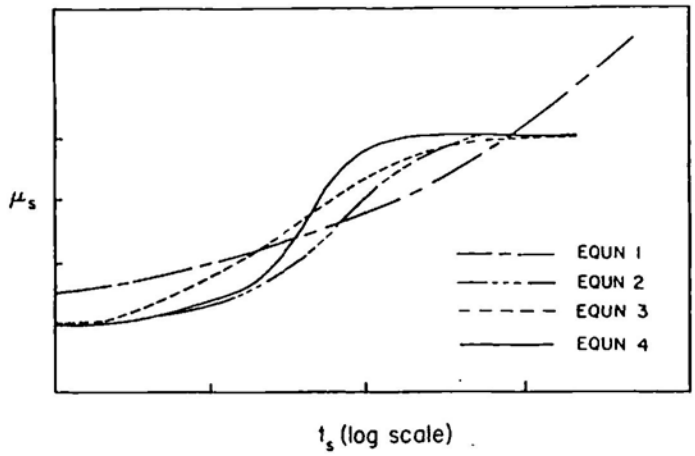

Fig. 27. Coefficient of static friction vs. time of stationary contact; equations from the literature (see Table 1). (Reproduced from [78].)

designed to assess the influence of the time of stationary contact on the value of the static coefficient of friction, he could not find any correlation between the time of stationary contact and the value obtained for that coefficient.

Johannes, Green and Brockley [50] and Richardson and Nolle [78] carried out experiments in such a manner that they could vary independently the rate of application of the tangential force and the time of stationary contact. This was achieved by interrupting the increase of the tangential force or delaying its application (see Fig. 28). Richardson et al. found that, if no delay was introduced (Fig. 28(a)) the best fit to the experimental data (expressing μ_s as a function of t_s, which in this case is not independent of $\dot{\phi}$) was obtained with Equation 4 of Table 1. However, if the time of stationary contact was made independent of the rate of application of the tangential load (Figs. 28(b), 28(c)) Johannes et al. and Richardson et al. found that the governing variable was the rate of increase of the tangential force and not the time of stationary contact. The dependence of μ_s on $\dot{\phi}$ obtained by Richardson and Nolle [78] is shown in Fig. 29. It can be seen that, *for sufficiently small load rates, the coefficient of static friction is constant and equal to a value which is the usually quoted coefficient of static friction.*

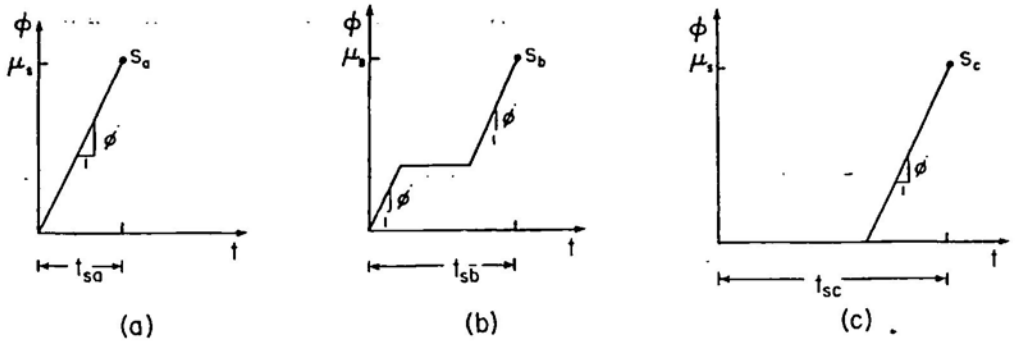

Fig. 28. Dependent (a) and independent (b), (c) rates of loading and times of stationary contact. Since the load rate $\dot{\phi}$ is the same for the three experiments μ_s would be the same regardless of the differences in the times of stationary contact. S_a, S_b, S_c are the points at which gross sliding initiates.

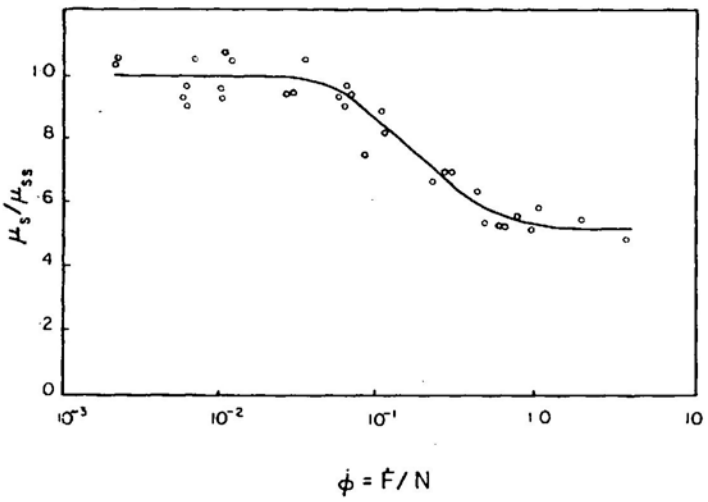

Fig. 29. Static friction vs. loading rate. Logarithmic $\dot{\phi}$ scale and static coefficient of friction normalized by dividing by μ_{ss} the coefficient of static friction at low loading rates. (Reproduced from [78].)

For large loading rates the coefficient of static friction tends to be constant and equal to a value which is usually interpreted as the coefficient of kinetic friction, although comparative measurements have rarely been made. As a consequence of these observations, those authors conclude that empirical expressions of the type shown in Table 1 should be recast with loading rate as the independent variable.

5.2. Stick-slip motion

5.2.1. Introduction

When two surfaces in contact slide relative to each other (Fig. 30), intermittent vibration of

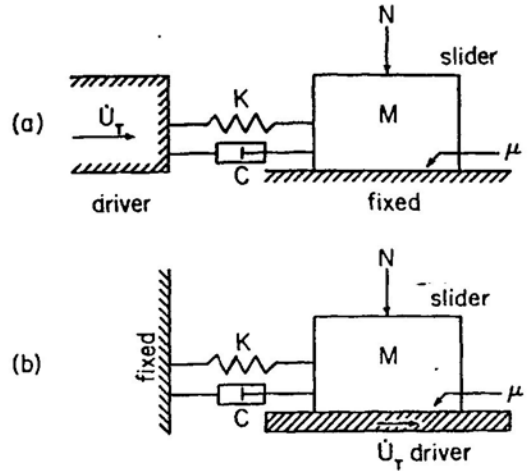

Fig. 30. Models of two (equivalent) sliding systems which may have stick-slip oscillations. K = linear stiffness; C = linear damping; M = mass of the slider; N = normal load; $\dot{U}_T$ = driving velocity; μ = friction coefficient.

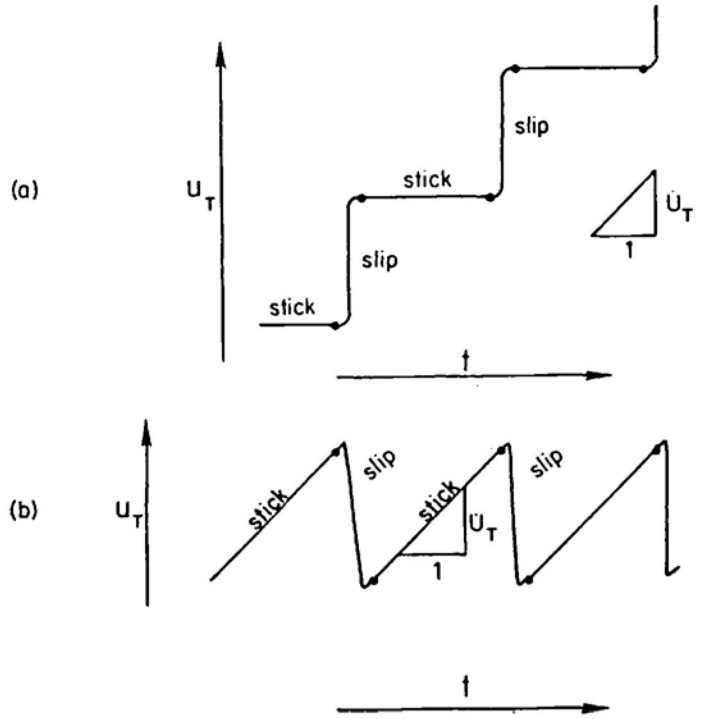

Fig. 31. Typical traces of stick-slip motion for systems (a) and (b) in Fig. 30. u_T = displacement of the slider; t = time; $\dot{U}_T$ = driving velocity.

the relaxation type can often be observed, especially at low driving velocities (Fig. 31). This phenomenon, usually known as stick-slip motion (after Bowden and Leben [20]) is highly undesirable in tables of machine tools, the precise positioning of which is fundamental for the accuracy of the work performed. In other applications, violent oscillations may lead to surface damage and failure of machine components.

Many authors have studied the stick-slip phenomenon. We shall describe here some of the more fundamental experimental observations on stick-slip motion and the most common interpretations for the phenomenon. For more complete lists of references see, e.g., [4, 13].

Blok [15], analyzing experimental results of Bowden and Leben [20] (obtained with metallic bodies) and of Papenhuyzen [72] (obtained with a rubber specimen on glass and road materials) concluded that *the essential condition for the occurrence of stick-slip motion is a decrease of the frictional force with increasing sliding speeds.* In the same paper, Blok provided also the first systematic study of frictional vibrations and established a quantitative criterion for their appearance.

In experiments carried out, using either especially designed apparati or slightly modified machine tool tables and slideways, it has been observed that the amplitude of the stick-slip motion decreases when:

(a) the driving velocity $\dot{U}_T$ increases (see Figs. 32–34);
(b) the damping coefficient C increases (see Fig. 32);
(c) the spring stiffness K increases (see Fig. 33);
(d) the mass M of the slider decreases (see Fig. 34).

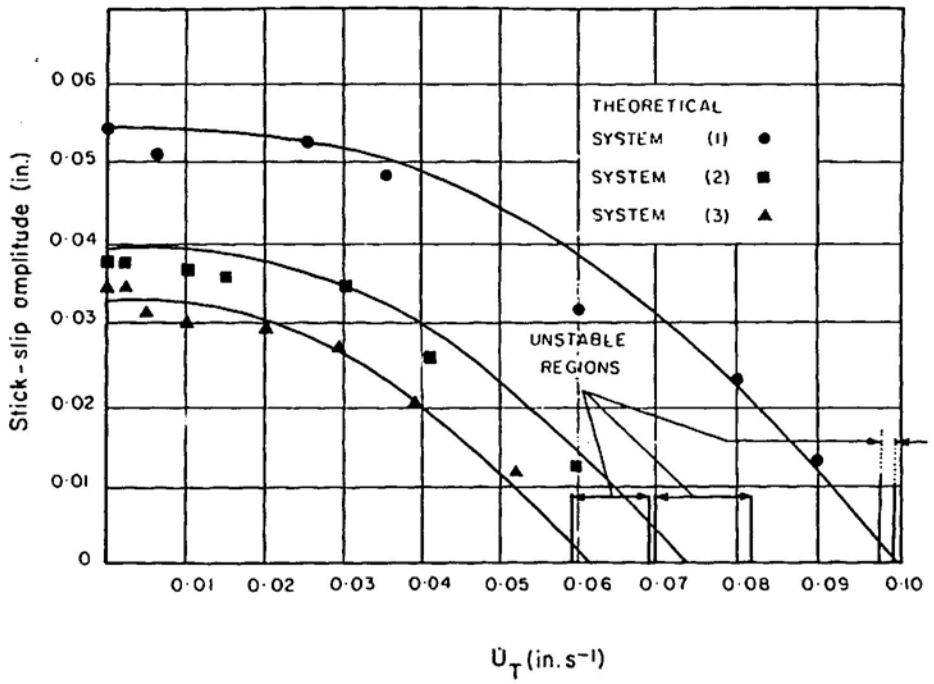

Fig. 32. Relation between amplitude of the stick-slip motion and velocity for various damping coefficients. (Reproduced from [18].) Theoretical: Model (I), (IIc) of Fig. 38. System (1) $C = 0.01$ lb.sec.in^{-1}. System (2) $C = 0.32$ lb.sec.in^{-1}. System (3) $C = 0.59$ lb.sec.in^{-1}.

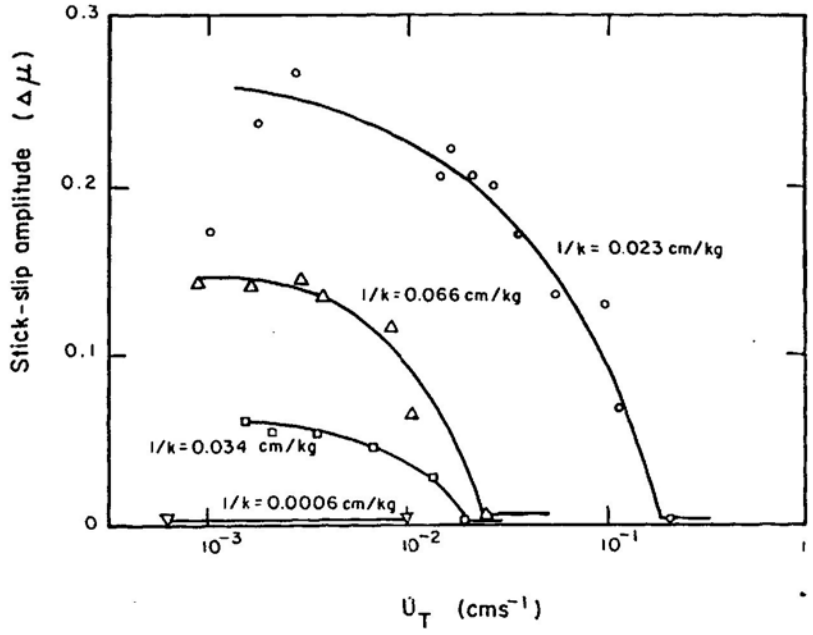

Fig. 33. Relation between amplitude of the stick-slip motion and driving velocity for various spring stiffnesses (K). Steel on steel unlubricated. Normal load $N = 1750$ g. (Reproduced from [77].)

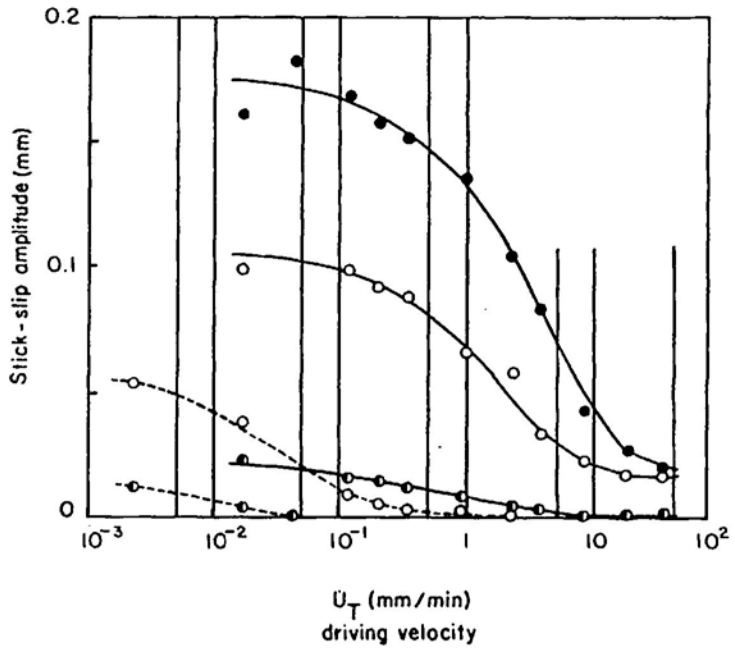

Fig. 34. Relation between amplitude of the stick-slip motion and driving velocity for various masses of the slider. (Reproduced from [51].) $K = 86.9$ Kg/mm. ———— Lubricant A; - - - - - - - - Lubricant C. ● $M = 53.2$ Kg; ○ $M = 36.0$ Kg; ◐ $M = 11.3$ Kg.

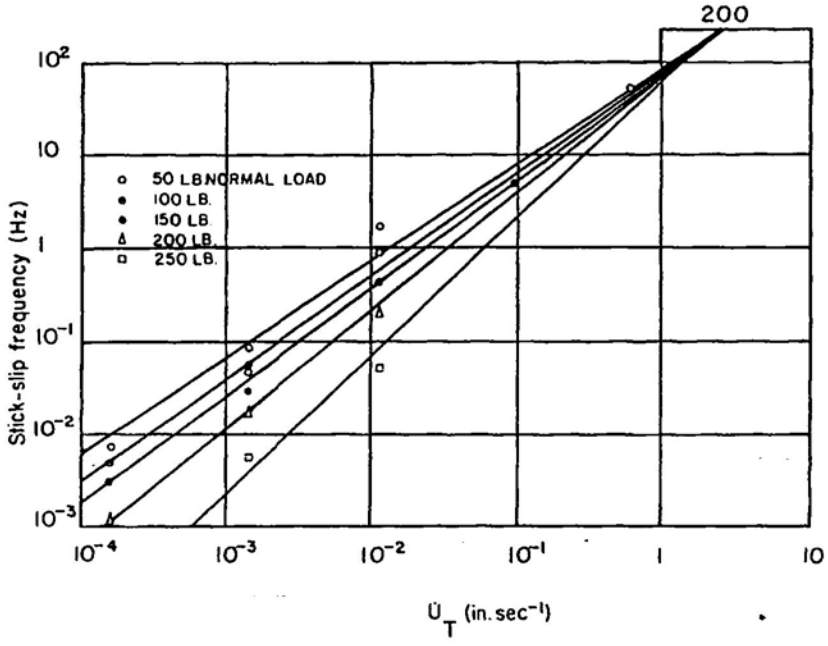

Fig. 35. Variation of stick-slip frequency with driving velocity for various normal loads. (Reproduced from [33].) Natural frequencies of the system: tangential mode ~150 Hz; normal mode ~200 Hz. Unlubricated.

It has also been observed that *the frequency of the stick-slip motion increases with the increase of the driving velocity* and that *the maximum value of this frequency approaches the undamped natural frequency of the system* (Figs. 35–37) although in some cases the oscillation stops at a level below that natural frequency.

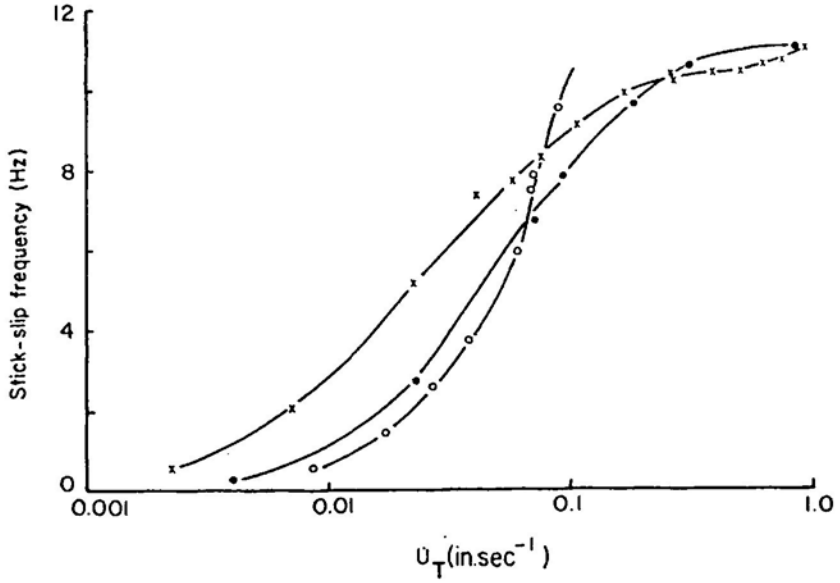

Fig. 36. Variation of stick-slip frequency with driving velocity for various lubrication conditions. (Reproduced from [13].) Natural frequencies of the systems (tangential motion) at 11.6 Hz. Lubrication conditions: ● Unlubricated; × Lubricant 1; O Lubricant 2.

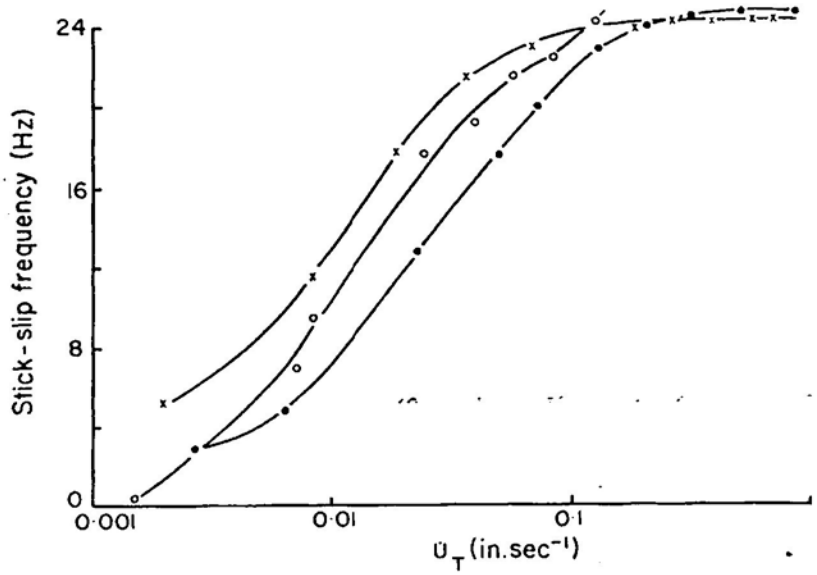

Fig. 37. Variation of stick-slip frequency with driving velocity for various lubrication conditions. (Reproduced from [13].) Natural frequencies of the systems (tangential motion) at 25 Hz. Lubrication conditions: ● Unlubricated; × Lubricant 1; O Lubricant 2.

The frictional properties of the contacting surfaces and the dynamic characteristic of the bodies involved (mass, stiffness, damping) are thus required to study the stick-slip motion.

The equation that governs the tangential movement of the slider in the model of Fig. 30(b) is the following (note that appropriate choice of variables leads to analogous equation for the model of Fig. 30(a):

$$M\ddot{u}_T + C\dot{u}_T + Ku_T = F, \tag{5.1}$$

where F is the instantaneous friction force.

The difficulties obviously arise from the friction force F. The essential problems have not been mathematical, they have been mechanical and experimental. The question is: *how does the friction force vary when the sliding velocity is zero or in the neighborhood of zero*?

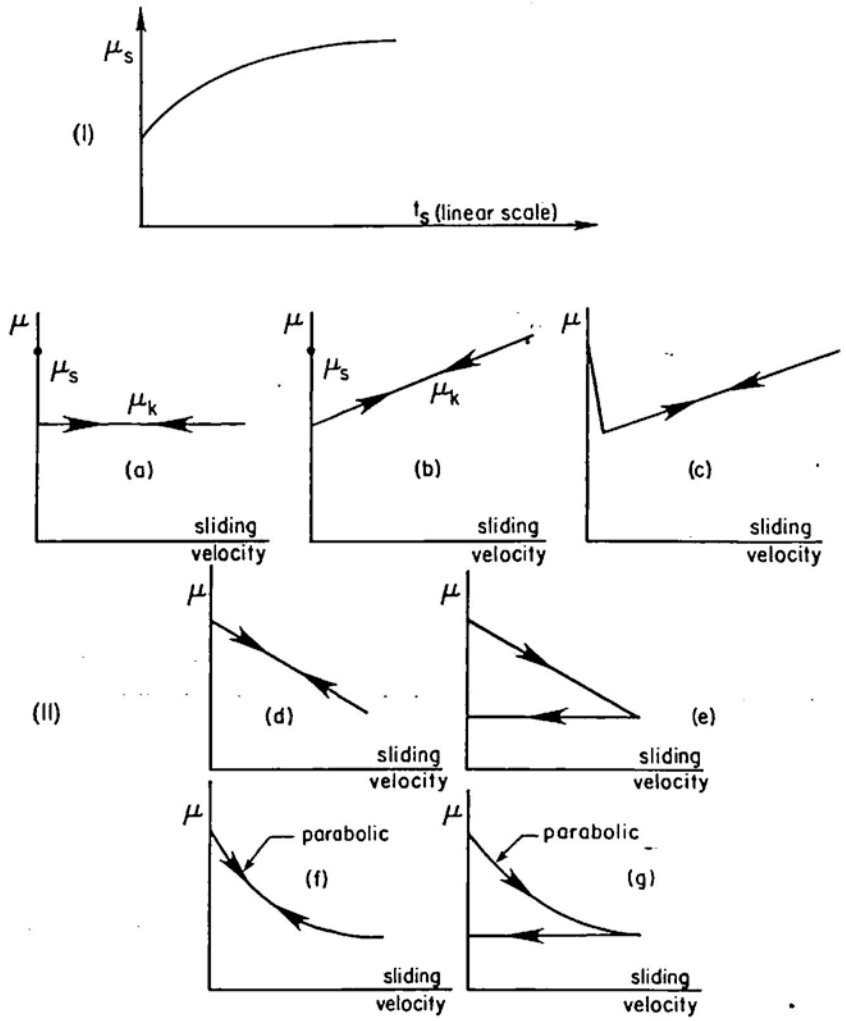

Fig. 38. Models of the variation of the friction force. (I) Variation of μ_s with time of stationary contact (t_s). (For analytical expressions used and discussion recall Section 5.1) (II) Variation of μ_k with sliding velocity. (IIa) is used in [15]; (I), (IIa) in [76]; (I), (IIb) in [32]; (I), (IIc) in [18]; (IId) and (IIe) in [13]; (IIf) in [11], and (IIg) in [16].

5.2.2. The assumed friction characteristics

Models with different assumptions on the dependence of the friction on time, displacement, velocity and acceleration have been used to characterize the occurrence of stick-slip motion. We summarize some of the most representative in Fig. 38.

These models, with the input of appropriate data will simulate stickslip motion. The accuracy of their predictions (e.g., the amplitude and frequency of the oscillation and the critical driving velocity $\dot{U}_T^{cr}$ above which no oscillation is observed) will depend on how close the assumed characteristic for the friction force is to the actual characteristic existing under the particular conditions involved. Another difficulty is the determination of unique data to incorporate in the above models.

5.2.3. The experimental friction characteristics

The limitations of the above models can be better appreciated by analyzing the characteristics obtained experimentally by several authors, as shown in Figs. 39–43. We wish to point out the following:

(i) In obtaining these characteristics some authors (e.g. Sampson et al. [84]) have smoothed and numerically differentiated the data available: traces of the displacement oscillations. Some irregularities inherent to friction processes plus effects assumed of secondary importance by the authors, may have been partially obscured by using these techniques.

(ii) Other authors (Bell et al. [13], Kato et al. [53]) have measured simultaneously displacements, velocities and accelerations using different transducers. As pointed out by Antoniou et al. [4] since each transducer has its own response, which does not coincide

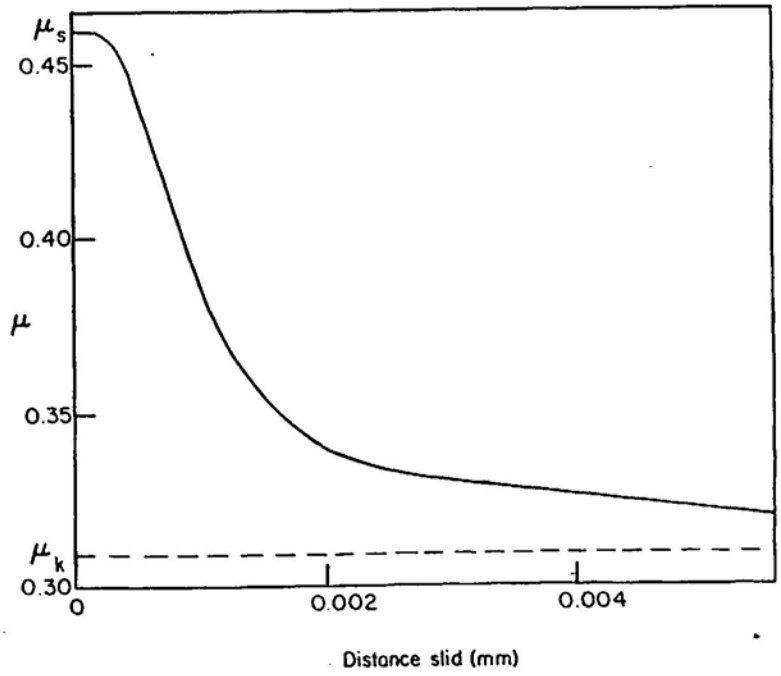

Fig. 39. Relation between coefficient of friction and distance slid in an impact experiment. Clean copper on mild steel. The sliding of a body on an inclined plane is initiated with the impact of another body. (Reproduced from [74].)

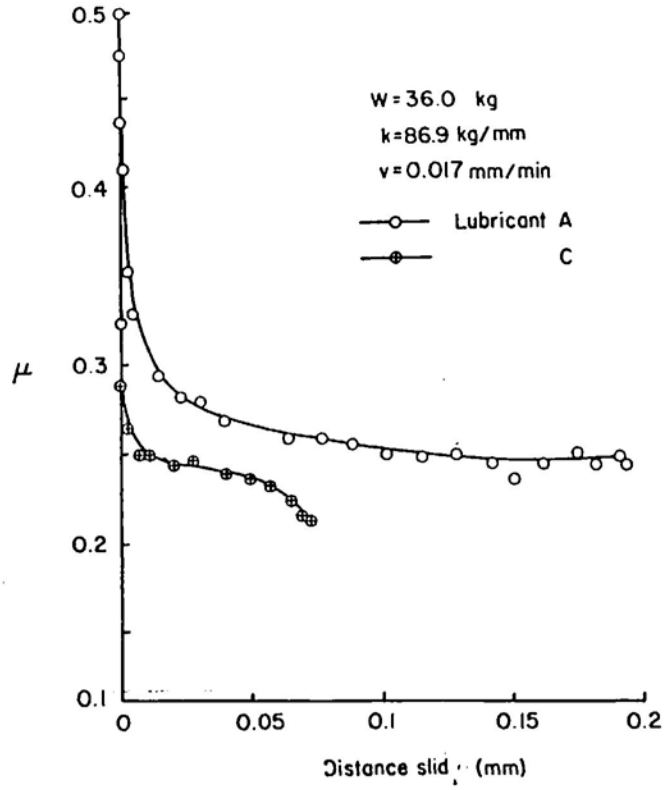

Fig. 40. Relation between coefficient of friction and distance slid in a stick-slip experiment. (Reproduced from [53].)

absolutely with the response of the other two transducers, the results obtained may contain the effects of calibration and hysteresis errors.

(iii) Most of the authors have studied only the tangential movement of the slider. Consequently, they have assumed the normal load on the contact to be constant and equal to the weight of the slider or to the force which produces the static deflection of their elastic normal loading system. Explicitly or implicitly, all variations observed on the friction force are thus assumed to be the consequence of corresponding variations in the friction coefficient. We note that Blok, in his early work, rightly emphasized that, in general, curves showing a decrease of frictional force with velocity do not imply a corresponding decrease of the coefficient of friction, as fluctuations of load might also occur.

Some comments and conclusions suggested by Figs. 38–42 are presented in the following:

(a) The change of friction force from the maximum static value to the minimum kinetic value occurs in a very short distance – of the order of 10^{-2} mm in the impact experiments of Rabinowicz, and of the order of 10^{-1} mm in the stick-slip experiments of Kato et al. (Figs. 39, 40).

(b) The existence of a second slip in the experiments of Sampson et al. (Fig. 41(b)) shows again the rate dependence of the maximum static friction force: in the second slip (large load rate, short time of stationary contact) the friction remains at a level close to the kinetic friction.

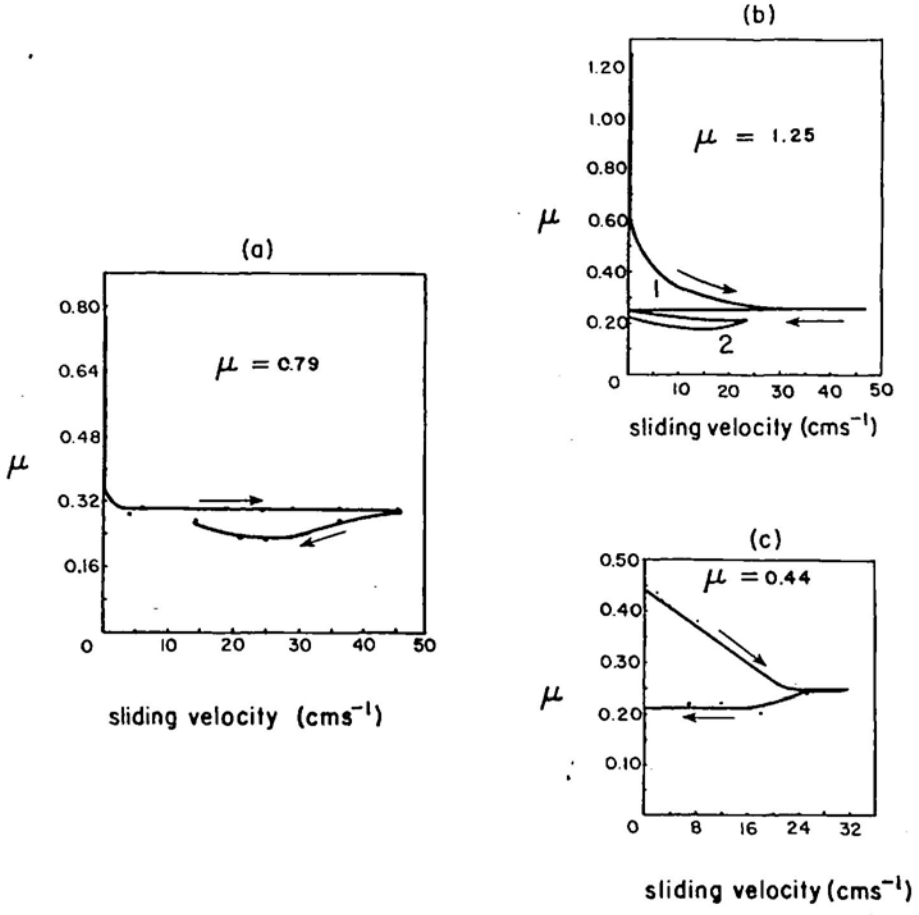

Fig. 41. Coefficient of friction vs. sliding velocity. (Reproduced from [84].) (a) Steel on Babbitt; (b) Wood's metal on Babbitt (1-first slip; 2-second slip); (c) Steel on steel.

(c) The friction force is *not* a reversible function of the sliding velocity. The accelerating and decelerating branches of the curves friction-velocity are usually distinct during stick-slip motion (Figs. 41–43).

(d) Different pairs of metals in contact and different lubrication conditions may produce characteristics with shapes clearly distinct (Fig. 41); according to Sampson et al. interchange of the metal on the slider and on the driving surface often makes a great difference.

(e) Even for the same combination of metals and lubrication, the shape and slope of the characteristic and the separation between the two branches will depend on the dynamic properties of the system (mass, stiffness) and on the driving velocity (see Fig. 42). This means that the experimental friction-sliding velocity curve is not defined uniquely by the nature of the surfaces in contact – it is a consequence of all the dynamic variables involved.

From the above observations, mainly from (e), we conclude that an acceptable theory of stick-slip motion will have to *explain* the complex relationship between the friction force and the sliding velocity, rather than *assume* a simplified relationship from which the experimental evidence will deviate often.

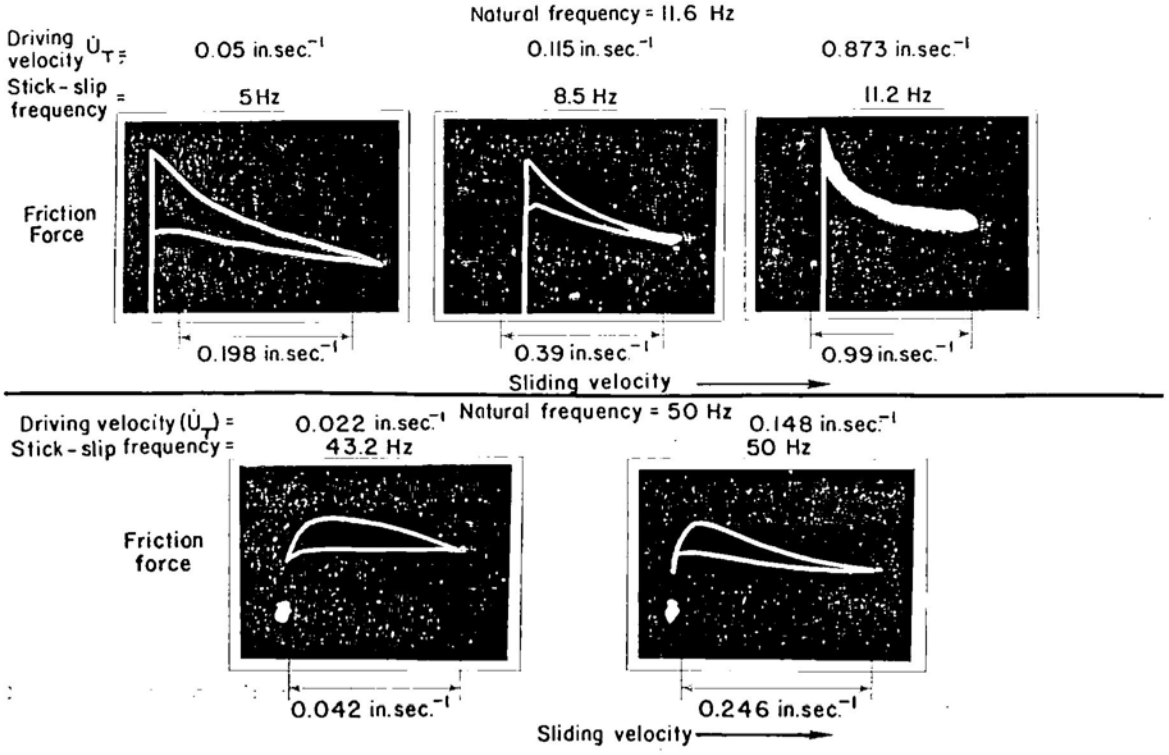

Fig. 42. Friction force vs. sliding velocity characteristics for various driving velocities and natural frequencies of the system. Unlubricated. (Reproduced from [13].)

5.3. *Memory-dependent friction*

Several authors have attempted to interpret the stick-slip oscillations on the basis of friction laws which allow for a dependence of the friction force on the previous sliding history. Early studies with metals suggesting friction laws of this type are due to Rabinowicz [75, 76]; more recent studies with rocks are due to Ruina [82, 83], Rice and Ruina [79], and Gu et al. [43].

Ruina [83] assumes that the frictional surface has at any instant in time, a state which can be characterized by a collection of variables α_i (internal variables). These variables represent the surface memory of previous sliding – in general they are weighted averages of some function of the recent sliding velocity. If only constant normal stress histories are considered and the friction stress is assumed to be proportional to the normal stress, then:

(i) the instantaneous coefficient of friction is assumed to be a function of the sliding velocity and the state;

(ii) the instantaneous rate of change of state is assumed to depend also on the sliding velocity and on the state.

These assumptions can be expressed in the form

$$\tau = pf(\dot{u}_T, \boldsymbol{\alpha}), \qquad \dot{\alpha}_i = g_i(\dot{u}_T, \boldsymbol{\alpha}) \quad (\boldsymbol{\alpha} = [\alpha_1, \alpha_2, \ldots]).$$

For each constant sliding velocity the functions g_i are such that the state variables evolve towards steady state values $\alpha_i^{ss}(\dot{u}_T)$ satisfying $g_i(\dot{u}_T, \boldsymbol{\alpha}^{ss}) = 0$, $i = 1, 2, \ldots$.

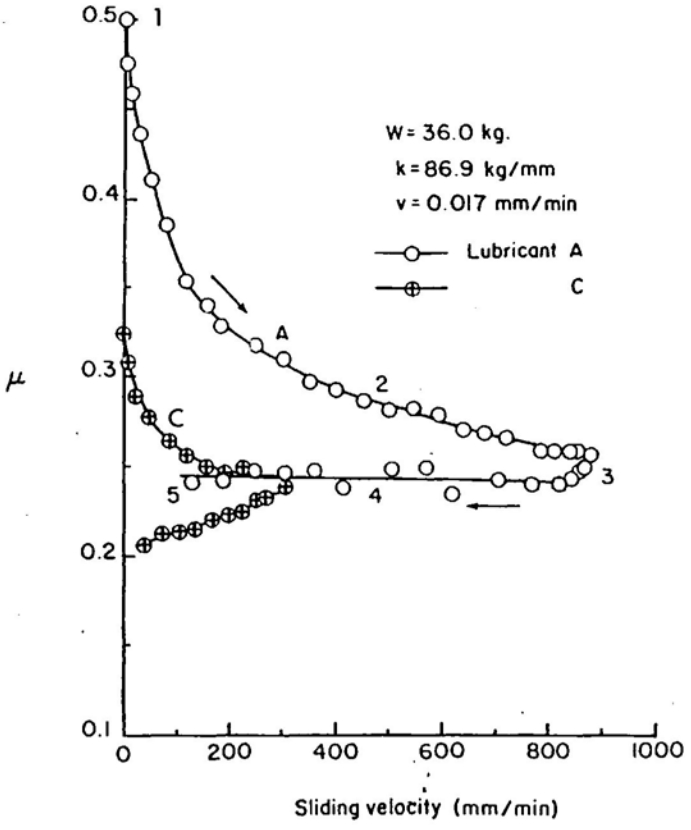

Fig. 43. Coefficient of friction versus sliding velocity. (Reproduced from [53].)

Several examples of state variables friction laws were provided by the same authors. The simplest one, involving only one state variable, is of the form

$$\tau = p[\mu^* + \alpha + A \ln(\dot{u}_T/\dot{u}_T^*)], \qquad \dot{\alpha} = -\frac{\dot{u}_T}{d_c}[\alpha + B \ln(\dot{u}_T/\dot{u}_T^*)], \tag{5.1a}$$

where $\dot{u}_T^*$ is an arbitrary positive constant and μ^*, A, B and d_c are positive empirical constants. According to this law, the frictional stress has a positive instantaneous rate dependence expressed by $A \ln(\dot{u}_T/\dot{u}_T^*)$ and the state variable α evolves towards the steady state value $\alpha^{ss} = -B \ln(\dot{u}_T/\dot{u}_T^*)$ with a characteristic slip distance d_c.

A dynamic stability analysis of the sliding with constant driving speed $\dot{U}_T$, leads to the following conclusion (for single state variable friction laws): for values of the spring stiffness K (Fig. 30(a)) greater than a critical value K_{cr} the steady motion is stable; for values of K smaller than K_{cr} the steady motion is unstable. The value of K_{cr} is found to be

$$K_{cr} = -\frac{\dot{u}_T \, d\tau^{ss}(\dot{u}_T)/d\dot{u}_T}{d_c}\left[1 + \frac{M\dot{u}_T}{d_c \partial\tau(\dot{u}_T, \alpha)/\partial\dot{u}_T}\right],$$

evaluated at $\dot{u}_T = \dot{U}_T$. A necessary condition for instability is then

$$\left.\frac{d\tau^{ss}(\dot{u}_T)}{d\dot{u}_T}\right|_{\dot{u}_T=\dot{U}_T} < 0 .$$

For the simple law (5.1a), K_{cr} reduces to

$$K_{cr} = \frac{(B-A)p}{d_c}\left[1+\frac{M\dot{U}_T^2}{d_c pA}\right].$$

This expression predicts the following experimental observation: an increase of the stiffness or a decrease of the mass increases the stability of the steady motion. However, this expression seems to contradict a known experimental fact (see the results of Rabinowicz in Fig. 33): the larger the driving velocity, the smaller the minimum stiffness required for a smooth sliding.

Finally, we note that a detailed study on the applicability of state variable friction laws to metal surfaces has not yet been done.

5.4. The importance of the normal degree of freedom in sliding friction

Here we follow essentially the fundamental paper of Tolstoi [103]. Other relevant contributions will also be mentioned.

It was seen in Section 5.2 that the stick-slip motion is a consequence of the decrease of the friction force with sliding velocity, i.e.,

$$\frac{dF}{d\dot{u}_T} < 0 . \tag{5.2}$$

As in Section 4.2, let F be equal to the product of the real area of contact by the average shear strength of the material being sheared,

$$F = A_r\tau .$$

As in Section 3.1, let A_r be a (differentiable) function of the separation between the contacting bodies,

$$A_r = A_r(h) .$$

Finally, assume that both τ and h are differentiable functions of the tangential velocity,

$$\tau = \tau(\dot{u}_T), \qquad h = h(\dot{u}_T) .$$

Then

$$\frac{dF}{d\dot{u}_T} = \tau\frac{dA_r}{dh}\frac{dh}{d\dot{u}_T} + A_r\frac{d\tau}{d\dot{u}_T} . \tag{5.3}$$

We shall analyze this relation in hopes of establishing conditions for the occurrence of stick-slip motion.

The second term in the second member ($A_r\, d\tau/d\dot{u}_T$) of (5.3) is always positive (or zero) at a constant temperature, because it represents the rate of increase of the rheological shear strength with the rate of shear. It is also clear that $dF/dh = \tau\, dA_r/dh$, in the first term of the second member, is always negative since, as h is increased, the true area of contact decreases. Furthermore, Tolstoi confirmed experimentally the $dF/dh < 0$ in static experiments, the results of which are shown in Fig. 44. In this figure it can be seen that, for the particular surfaces used in the experiment, friction is halved as the slider rises by only about 0.2 μm. *The friction force is thus very sensitive to the normal separation.*

In the same paper, Tolstoi presents, among others, the following argument to show that $dh/d\dot{u}_T > 0$: an increase in the speed of the slider increases the upward vertical components of the impulses exerted on the slider asperities as they collide with those of the underlying surface; this increases the amplitude of the normal natural vibrations of the slider, the frequency of which depends on the contact stiffness and mass of the slider; due to the

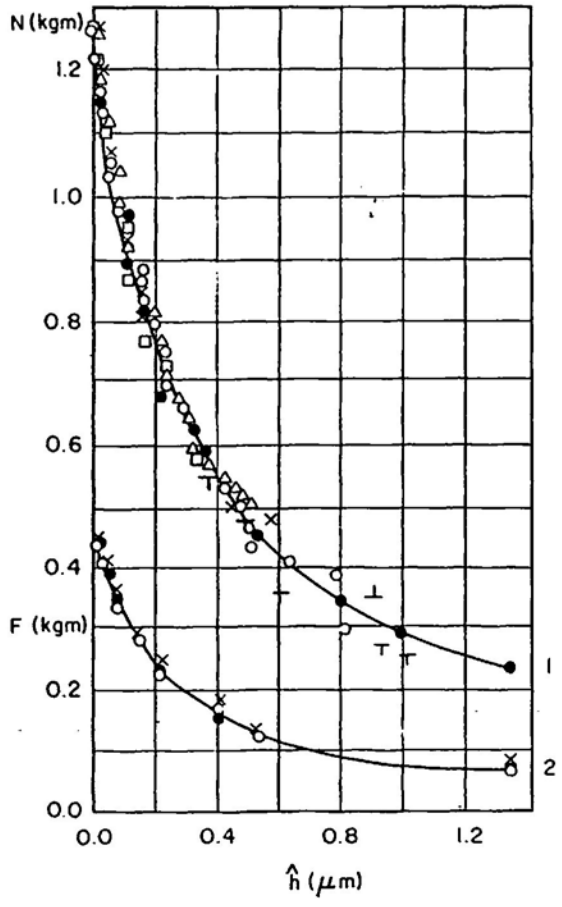

Fig. 44. Normal load (N, curve 1) and static friction force (F, curve 2) versus the separation $\hat{h}$ (arbitrarily $\hat{h}$ is taken to be zero for the maximum normal load used in the experiments). Dry steel surfaces. (Reproduced from [103].)

nonlinearity of the normal force-separation relationship (recall Section 3.1 and Fig. 44), the normal vibrations of the slider are highly asymmetric; consequently, an increase of the amplitude of those normal vibrations raises the mean level on which the slider moves. We note that, for steady state sliding of lubricated surfaces, Bell and Burdekin [13] obtained experimental results which confirm that $dh/d\dot{u}_T > 0$ under those conditions.

Having shown that $dF/dh = \tau\, dA_r/dh < 0$, $dh/d\dot{u}_T > 0$ and $A_r\, d\tau/d\dot{u}_T \geq 0$, it follows that condition (5.2) for occurrence of stick-slip motion may not be always fulfilled. For example, whenever h is kept constant, $dF/d\dot{u}_T$ is positive and the sliding must be smooth. To illustrate this point, Tolstoi shows two ways to keep h constant and obtaining a smooth sliding:

(1) By using an extremely small driving velocity.

(2) By using an external damping of the normal oscillations.

The author presents experimental results corresponding to both the above situations (see Fig. 45).

In case (1), a lower bound for the extremely small velocity required is estimated by the author in terms of the asperity height and spacing, the coefficient of friction, the normal yield stress and the creep viscidity. In fact, the small velocity obtained is that required for the creep deformation of the asperities without normal displacements (recall the information in Section 5.1.2 on creep sliding).

In case (2), the effect of the normal damping is such that no reduction on the friction force is

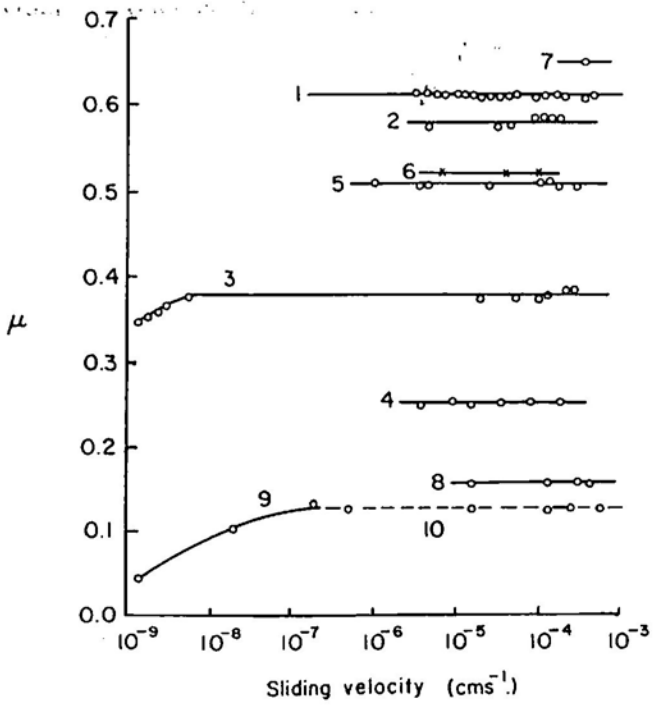

Fig. 45. Coefficient of friction as a function of sliding velocity under external normal damping (curves 1–8) or without normal damping (curves 9–10). 1, 2, 5, 6, 7: unlubricated steel; 3, 4, 9, 10: lubricated steel. ———— smooth sliding; - - - - - - stick-slip oscillations (the points plotted correspond to mean values of the friction coefficient during the oscillations). Note that only when no external normal damping is imposed, the stick-slip oscillations do appear (curve 10). (Reproduced from [103].)

observed when the sliding velocity is increased. There exists no quantitative difference between kinetic and static friction. Furthermore, if the normal damping is introduced, with no change on the driving velocity during a run which shows stick-slip oscillations, it is observed that these oscillations disappear and that the value of the coefficient of friction for the subsequent smooth sliding is even greater than the maximum values obtained at the end of the stick periods of the stick-slip motion.

The responsibility of the freedom of normal displacement for both the falling F-$\dot{u}_T$ relation and the stick-slip motion was corroborated in two ways:

(a) Sufficiently heavy external damping of the tangential vibrations alone could suppress these vibrations but failed to affect the negative slope of the $F - \dot{u}_T$ curve.

(b) Direct observations of the normal displacements of the slider carried out at low driving speeds showed that the forward movements of the undamped slider invariably occurred in strict synchronism with its upward jumps (see Fig. 46).

We note that several authors have also done observations analogous to (b). In their early study Bowden and Tabor [21] measured the electrical conductance during stick-slip motion and observed a marked fall of electrical conductance during the slip phase of the motion. This suggests the occurrence of normal jumps of the slider during the slip phase. Oscillograms of the normal contact oscillations which occur in stages of tangential jumps of the slider during stick-slip motion were obtained by Tolstoi, Borisova and Grigorova [104]. Study of those oscillations revealed a fundamental frequency consistent with the normal interface stiffness properties (see [24]). Direct measurements of the separation of unlubricated and lubricated surfaces during stick-slip motion were also done by Bo and Pavelescu [16] and by Tudor and Bo [107], respectively. Other experimental evidence of the influence of the normal oscillations on the stick-slip motion was presented by Antoniou, Cameron and Gentle [4].

In summary, Tolstoi [103] emphasized the fundamental role played by the normal stiffness of the contacting asperities in sliding friction. In particular, he concludes that *the decreasing friction-velocity characteristic at small velocities is not an intrinsic property of sliding friction: it is solely the consequence of the microvibrations in the direction normal to the sliding.*

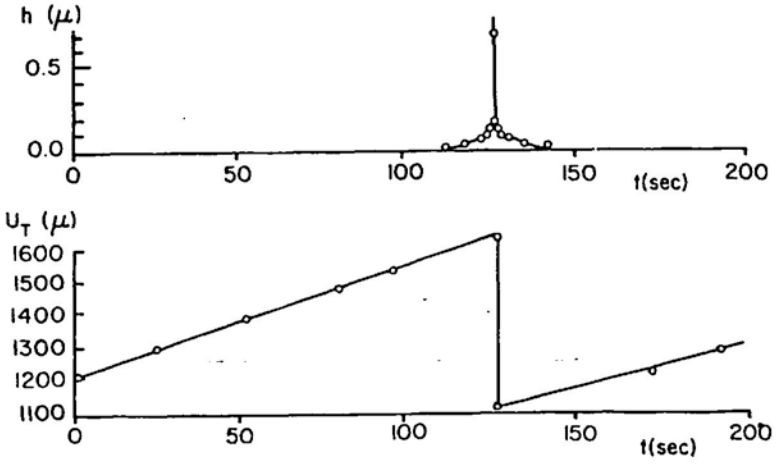

Fig. 46. Simultaneous tangential (u_T vs. t) and normal (h vs. t) jumps of the slider during stick-slip motion. Unlubricated. (Reproduced from [103].)

As might be expected, the influence of the normal contact vibration on the friction force is not exclusive of the stick-slip motion.

Tolstoi [103] and Godfrey [41] report, for both lubricated and unlubricated conditions, a resonance fall of the friction force when a normal forced oscillation of the slider (or of the surface on which it slides) is produced by an external vibrating source. Tolstoi [103] also reports a fall of friction force due to the normal oscillations produced by the normal impact of a small sphere on the slider.

Large normal and frictional force oscillations during smooth unlubricated sliding of two steel surfaces are reported by Soom and Kim [89, 90]. Again, synchronism between those two oscillations is observed experimentally and, except at very low speeds, those oscillations are dominated by frequencies in the vicinity of the normal contact resonance.

Aronov, D'Souza, Karpakjian and Shareef [7, 8] observed, with a pin-on-disk experimental apparatus, that an increase in normal load leads to the transition from a steady-sliding with small oscillations to high frequency self-excited oscillations (intermediate states were also observed). Strong coupling among the different degrees of freedom (tangential, normal, rotational) was observed in the course of those self-excited oscillations. Modelling the sliding system as a rigid body with plane motion and using experimentally determined modal frequencies and damping ratios, those authors provided an approximate solution for the oscillatory motion and showed its *dynamic instability.*

The experimental evidence collected in this section leads us to the conclusion that *an appropriate model for sliding friction must incorporate physically reasonable normal contact conditions. In addition, all the major sources of coupling between normal and tangential degrees of freedom should be taken into account in such a model.*

Part II. Continuum models and variational principles for dynamic friction

In this part of our study, we formulate continuum models of dynamic friction effects in elastodynamics which reflect some of the experimentally-observed properties discussed in Part I.

6. A simple model of normal interface response

6.1. Preliminary considerations

Before describing our formulation it is important to clarify what our major physical assumptions will be. In other words, we need to explain why, among so many experimental observations and theoretical interpretations, we will pick up only a few key features which we hope will provide the essential ingredients for modeling a large class of dynamic friction phenomena.

The first key ingredient of our model is a normal contact constitutive law which takes in account the normal deformability of the interface asperities. We will not introduce in our model a statistical description of the interface geometry and of the normal contact, which

would be a possible, defensible and interesting approach. Instead, we will introduce a mechanical law for normal contact which does not contradict the results of those statistical theories. As shown in Section 3.1, both theory and experiment seem to agree in an exponential type growth of the normal contact stresses with the penetrating approach for sufficiently high loads. For sufficiently small loads, which we will be working with, the vanishing normal stiffness for small penetrations predicted by the theory and the power laws obtained by experimentors are also not contradictory. We will thus assume that on the contact boundary each macroscopic point 'contains' a number of microscopic interface asperities sufficiently large that a power law of the type (3.5), (3.7) holds locally.

We incorporate this nonlinear boundary effect in our model instead of a classical non-penetration unilateral contact condition for the following reasons:

(i) For small linear elastic bodies with rough surfaces subjected to small loads the deformation of the contact interface may be of an order of magnitude comparable with the bulk linear elastic deformation of the contacting bodies.

(ii) The experimental results of Andrew, Cockburn and Waring [2] imply that such nonlinear contact behavior cannot be disregarded in dynamic situations even if no relative sliding occurs.

(iii) The high sensitivity of the friction force to the normal separation of the surface, the resonance drops in friction force due to normal deformation of the contacts and the striking observations of Tolstoi [103] and other authors described in Section 5.4 strongly suggest that a physically reasonable normal interface model has to be used.

Obviously, for highly polished surfaces it is physically reasonable to expect that the results obtained by including the effects of the normal interface deformability should approach those given by assuming a classical unilateral contact condition. Analytical solutions for frictionless static Hertz contact problems suggest that this is the case, although these questions have not been studied from a mathematical point of view.

The use of the power law (3.5) for the normal contact response corresponds to an assumption of an exclusively elastic normal response. Although this is the expected behavior after sufficient rubbing and smoothing of the interface it is questionable, and some experimental evidence contradicts that this is the case if the sliding is not smooth and severe oscillations (accompanied probably by small normal jumps) do occur. Possible physically consistent ways to incorporate in our model the dissipative effect of normal plastic deformation on the interface will be discussed in Part III of this paper.

The other key ingredient of our model is obviously the friction law.

We will not provide a model for the preliminary (plastic) microdisplacements which occur before gross-sliding. Essentially we will assume that these effects can be disregarded when compared with the much larger rigid-body type displacements which occur during sliding. The classic law of friction (i) in Section 4.1 will be thus assumed to hold locally on the contact boundary. Only a small generalization will be introduced in order to accommodate a possible dependence of the coefficient of friction on normal contact forces.

Following the ideas of Tolstoi [103], *we will not consider any distinction between static and kinetic coefficients of friction.* We will try to show, by analysis and by numerical results, that apparent decreases of measurable coefficients of friction are the result of dynamic instabilities which are a consequence of the inherent non-symmetry of friction problems. No other variations of the coefficient of friction with velocity will be considered either, although they could easily be

incorporated. We avoid here the potentially stabilizing or destabilizing effects that those variations would introduce.

Finally, we observe that creep sliding will not be modeled but the possibility of the experimental rate dependence of the static coefficient of friction being an inertia related phenomenon will be investigated in a forthcoming work.

6.2. *Interface models*

The interface between contacting bodies is a hypothetical medium of vanishing thickness, the mechanical response of which depends upon the various geometrical and physical properties of the surfaces in contact as discussed in Part I. For the class of problems addressed here, we wish to characterize the response of such an interface to normal deformations in a way that is consistent with the experimental, and statistical theoretic results summarized in Section 3.1.

Consider a continuous material body $\mathcal{B}$, in contact with another material body $\mathcal{B}_1$ over a contact surface $\Gamma_C \subset \partial\mathcal{B}$. We establish a fixed Cartesian coordinate system x_i, $i = 1, 2, 3$, and consider motions of $\mathcal{B}$ relative to this fixed spatial frame of reference. We denote by u the displacement of particles $X \in \mathcal{B}$ relative to a fixed reference configuration, the configuration occupied by the 'undeformed' body, and by u_i the Cartesian coordinates of u.

The notion of a contact surface Γ_C is worthy of some elaboration. This surface should represent the boundary of the parent bulk material of which the body is composed. One can regard it as parallel to a surface marking average surface heights. We suppose that Γ_C has a well-defined exterior normal vector n and that the actual interface (asperities, oxide film, gas, work-hardened material, etc.) is initially of thickness t_0, as shown. The initial gap between Γ_C and the other body that may come in contact with $\mathcal{B}$ is defined as the distance, measured along a line normal to Γ_C, between the highest asperities of the bodies in the reference configuration. The interface thickness after deformation is denoted t in Fig. 47 and the actual displacement of Γ_C in the direction of n is $u_n = u \cdot n$. Thus, the approach of the material contact surfaces is

$$a = t_0 - t = (u_n - g)_+ . \tag{6.1}$$

This definition is valid whenever the body $\mathcal{B}_1$ is rigid and bounded by a surface opposing Γ_C which is ideally flat, as indicated in the figure. This model is easily generalized to cases in which $\mathcal{B}_1$ is deformable and rough (see [114]).

Let σ_{ij} denote the Cartesian components of the Cauchy stress tensor at a particle X in $\mathcal{B}$. The normal stress developed in Γ_C is then

$$\sigma_n = \sigma_{ij} n_i n_j , \tag{6.2}$$

where the standard summation is used.

The constitutive properties of the interface are characterized by a relationship between σ_n and a. In Fig. 48 we have plotted the variation in the normal force N on a unit block of the material with the penetrating approach. Except for very large penetrations, where the response is essentially exponential, a large body of evidence points to a power-law relation between σ_n ($= N$/unit area) and a,

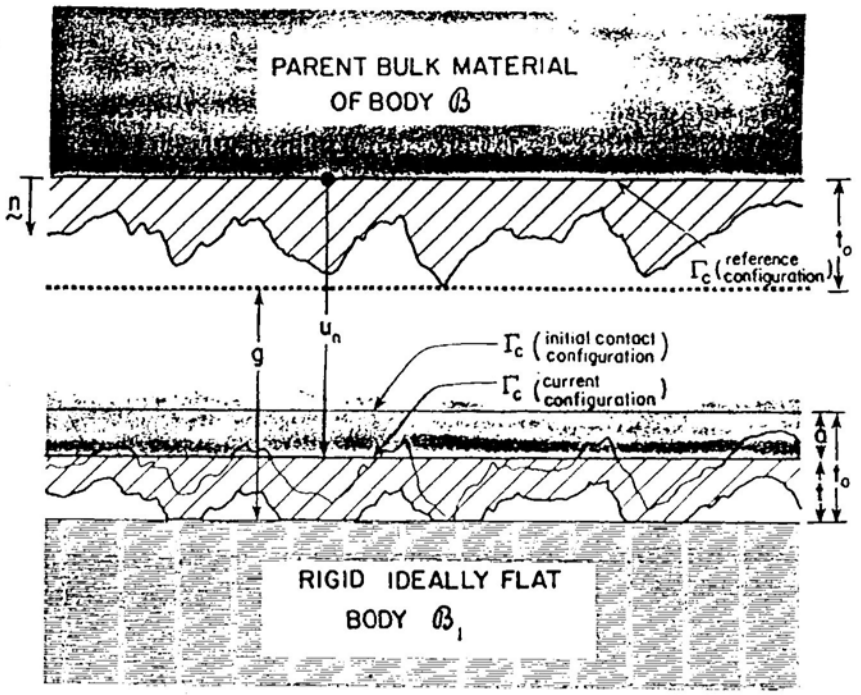

Fig. 47. Initial gap, normal displacement and penetrating approach at the contact surface Γ_C.

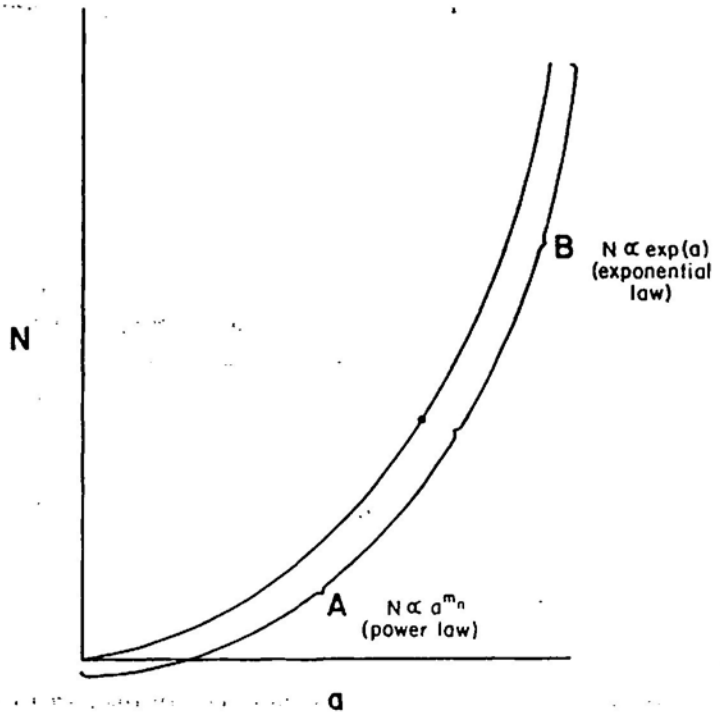

Fig. 48. Normal force versus approach relationship suggested by experimental and statistical theoretic results. Portion A, 'light' normal loads characteristic of sliding interfaces. Portion B, 'heavy' normal loads characteristic of fixed interfaces.

$$-\sigma_n = c_n(u_n - g)_+^{m_n} . \tag{6.3}$$

Here c_n and m_n are material parameters independent of a.

Much of the experimental evidence described earlier indicated that the material parameters c_n and m_n can be easily determined from interface compression experiments. Other effects could be added to this interface law, but it is sufficiently general to model the principal mechanisms of interest here.

REMARK 6.1. The form of the interface constitutive equation (6.4) is consistent with the experimental observations outlined earlier (recall Section 3.1):

(a) $$\left.\frac{d\sigma_n}{da}\right|_{a=0} = 0 \quad (a = (u_n - g)_+),$$

(b) $$-\sigma_n \propto a^{m_n} \quad \text{with } 2 \leq m_n \leq 3.33 .$$

REMARK 6.2. Finite element computations of *static* contact problems using such a normal interface constitutive equation were first done by Back, Burdekin and Cowley [10].

7. A problem in elastodynamics

We shall now formulate a class of initial-value problems in elastodynamics which include sliding friction effects. We begin by considering a linearly elastic body, the interior of which is an open bounded domain Ω in $\mathbf{R}^N$ ($N = 2$ or 3) with boundary Γ consisting of portions Γ_D, Γ_F, Γ_E and Γ_C, as indicated in Fig. 49. Displacements u are prescribed on Γ_D, tractions t are prescribed on Γ_F, the body may be elastically supported by springs of modulus k_{ij} on Γ_E, and Γ_C is the candidate contact surface. We suppose that the body may come in contact with a rough sliding belt (a moving foundation) which slides by the material contact surface Γ_C with a velocity $\dot{U}_T^C$. This foundation is initially (at $t = 0$) at a gap distance g and Γ_C. While strains in the body are small, certain large rigid motions relative to the reference configurations are permitted in our theory. For simplicity, the body is assumed to be composed of a Hookean material characterized by the classical constitutive equation,

$$\sigma_{ij}(u) = E_{ijkl} u_{k,l} , \tag{7.1}$$

where $u_{k,l} = \partial u_k / \partial x_l$, $1 \leq i, j, k, l \leq N$, and the elasticities satisfy

$$E_{ijkl} = E_{jikl} = E_{ijlk} = E_{klij} , \qquad E_{ijkl} \in L^\infty(\Omega) ,$$

$$E_{ijkl} A_{kl} A_{ij} \geq \alpha A_{ij} A_{ij} \quad \begin{array}{l}(\text{a.e. in } \Omega \text{ for every symmetric tensor } A_{ij} ,\\ \alpha \text{ being a positive constant}) ,\end{array}$$

$$\sup_{1 \leq i, j, k, l \leq N} \|E_{ijkl}\|_\infty \leq M . \tag{7.2}$$

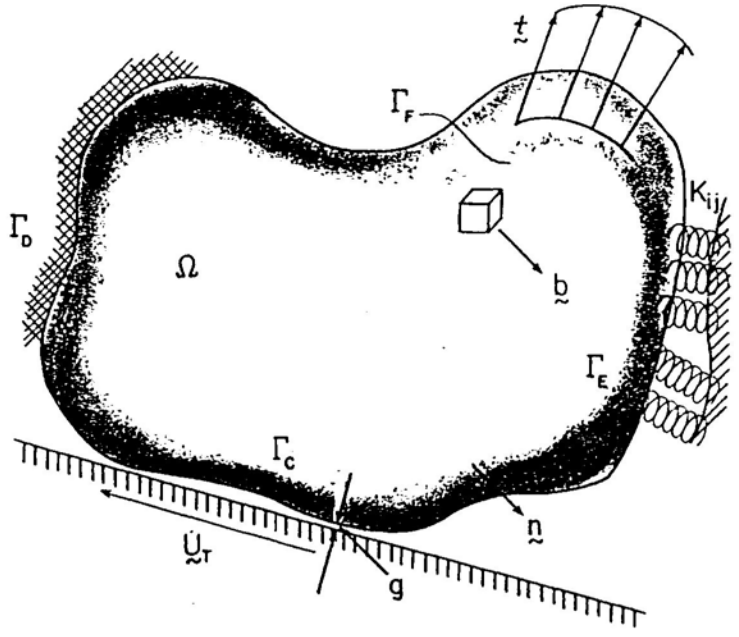

Fig. 49. Geometry and notation used in elastodynamics problem with sliding friction.

For a time interval $[0, T]$, the equations governing this elastodynamics problem are grouped as follows:

Linear momentum (constitutive equations, angular momentum, and mass conservation):

$$\sigma_{ij}(u)_{,j} + b_i = \rho \ddot{u}_i \quad \text{in } \Omega \times (0, T), \tag{7.3}$$

where

b_i = the components of body force per unit volume, assumed to be sufficiently smooth functions of $x = (x_1, x_2, \ldots, x_N)$;

ρ = the mass density,

$$\frac{\partial \rho}{\partial t} = 0, \qquad \rho \in L^\infty(\Omega), \qquad \rho \geq \rho_0 > 0;$$

$\ddot{u}_i$ = particle acceleration $\equiv \partial^2 u_i / \partial t^2$;

$$\sigma_{ij}(u) = E_{ijkl} u_{k,l} \quad (\sigma_{ij} = \sigma_{ji}).$$

Boundary conditions on $\Gamma_D, \Gamma_F, \Gamma_E$;

$$\begin{aligned} u_i &= U_i^D && \text{on } \Gamma_D \times (0, T), \\ \sigma_{ij}(u) n_j &= t_i && \text{on } \Gamma_F \times (0, T), \\ \sigma_{ij}(u) n_j &= -k_{ij}(u_j - U_j^E) && \text{on } \Gamma_E \times (0, T), \end{aligned} \tag{7.4}$$

where U_i^D, t_i and U_j^E are given sufficiently smooth functions.

Initial conditions:

$$u = u_0, \qquad \dot{u} = u_1 \quad \text{in } \Omega \text{ at } t = 0, \tag{7.5}$$

with u_0, u_1 given smooth functions of x.

Normal interface response: Recalling (6.3), we have

$$\sigma_n(u) = -c_n(u_n - g)_+^{m_n} \quad \text{on } \Gamma_C \times (0, T). \tag{7.6}$$

Friction conditions: Let σ_T be the tangential (frictional) stresses developed on the contact surface ($\sigma_{Ti} = \sigma_{ij} n_j - \sigma_n n_i$). Then we shall employ the following friction law:

$$u_n \leqslant g \Rightarrow \sigma_T(u) = 0,$$

$$u_n > g \Rightarrow \begin{cases} |\sigma_T(u)| \leqslant c_T(u_n - g)_+^{m_T}, \\ |\sigma_T(u)| < c_T(u_n - g)^{m_T} \Rightarrow \dot{u}_T = \dot{U}_T^C, \\ |\sigma_T(u)| = c_T(u_n - g)_+^{m_T} \Rightarrow \exists \lambda \geqslant 0,\ \dot{u}_T - \dot{U}_T^C = -\lambda \sigma_T \text{ on } \Gamma_C \times (0, T). \end{cases} \tag{7.7}$$

Here c_T and m_T are material constants depending on interface properties (indeed, characterizing further constitutive properties of the interface), $\dot{u}_T$ is the tangential velocity of material particles on Γ_C, and $\dot{U}_T^C$ is the prescribed tangential velocity of the foundation (adjacent body) with which Γ_C comes in contact.

The friction law (7.7) is a generalization of the Coulomb's friction law, which is recovered if $m_n = m_T$. In such a case, $\mu = c_T/c_n$ is the usual coefficient of friction. The law (7.7) allows for a dependence of the friction coefficient on the normal contact pressure (recall Sections 4.1. and 4.2).

We remark that other possible choices would also have been easy to introduce at this point. The one presented above can be interpreted as allowing for deviations of Amonton's first law due to a variation of the true area of contact with a power of the normal stress level different from unity,

$$\mu = C|\sigma_n|^\alpha, \quad \alpha = \frac{m_T}{m_n} - 1 \text{ and } C = \frac{c_T}{c_n^{m_T/m_n}}. \tag{7.8}$$

8. Variational formulations

8.1. A nonlinear hyperbolic variational inequality

We now consider the formulation of a variational principle corresponding to the elastodynamics problem outlined above. Following steps similar to those of Duvaut and Lions [37], the nonlinear elastodynamics problem can be shown to be formally equivalent to the following variational problem:

Problem 1: Find the function $t \to u(t)$ of $[0, T] \to V$ such that

$$\langle \ddot{u}(t), v - \dot{u}(t) \rangle + a(u(t), v - \dot{u}(t)) + \langle P(u(t)), v - \dot{u}(t) \rangle + j(u(t), v) - j(u(t), \dot{u}(t)) \geq$$
$$\geq \langle f(t), v - \dot{u}(t) \rangle \quad \forall v \in V, \tag{8.1}$$

with the initial conditions

$$u(0) = u_0, \qquad \dot{u}(0) = u_1 . \tag{8.2}$$

We have assumed here, for simplicity, that $\rho \equiv 1$ and that $U_i^D \equiv 0$. The following notations and definitions were also used:

$$V = \text{the space of admissible displacements (velocities)}$$
$$= \{v = (v_1, v_2, \ldots, v_N) | \, v_i \in H^1(\Omega), \gamma(v_i) = 0 \text{ a.e. on } \Gamma_D\} ,$$
$$a : V \times V \to \mathbf{R} , \; a(u, v) = a_0(u, v) + a_1(\gamma u, \gamma v) , \tag{8.3}$$

where

$$a_0(u, v) = \text{virtual work (power) produced by the action of the stresses } \sigma_{ij}(u) \text{ on the strains (strain rates) } \varepsilon_{ij}(v) = \tfrac{1}{2}(v_{i,j} + v_{j,i})$$
$$= \int_\Omega \sigma_{ij}(u) \varepsilon_{ij}(v) \, dx$$
$$= \int_\Omega E_{ijkl} u_{k,l} v_{i,j} \, dx, \quad u, v \in V, \tag{8.4}$$

where u is a displacement and v is a virtual displacement (velocity);

$$a_1(\xi, \eta) = \text{virtual work (power) produced by the deformation of the linear springs on } \Gamma_E$$
$$= \int_{\Gamma_E} K_{ij} \xi_j \eta_i \, ds, \quad \xi, \eta \in (L^2(\Gamma_E))^N . \tag{8.5}$$

$P : V \to V'$,

$\langle P(u), v\rangle$ = virtual work (power) produced by the normal contact pressure on the displacement (velocity) v

$$= \int_{\Gamma_C} c_n (u_n - g)_+^{m_n} v_n \, ds \; ; \tag{8.6}$$

$j : V \times V \to \mathbb{R}$,

$j(u, v)$ = virtual power produced by the frictional force on the velocity v

$$= \int_{\Gamma_C} c_T (u_n - g)^{m_T} | v_T - \dot{U}_T^C | \, ds \; ; \tag{8.7}$$

$f(t) \in V'$,

$\langle f(t), v\rangle$ = virtual work (power) produced by the external forces (body forces, prescribed tractions, initial deflection of the linear springs) on the displacement (velocity) v

$$= \int_\Omega b_i v_i \, dx + \int_{\Gamma_F} t_i \gamma(v_i) \, ds + \int_{\Gamma_E} K_{ij} \dot{U}_j^E \gamma(v_i) \, ds . \tag{8.8}$$

Here $\langle \cdot, \cdot \rangle$ denotes duality pairing on $V' \times V$ where V' is the topological dual of V; γ is the trace operator mapping $(H^1(\Omega))^N$ onto $(H^{1/2}(\Omega))^N$ which may be decomposed into normal components $\gamma_n(v)$ and tangential components $\gamma_T(v)$. For simplicity of notation, the latter are denoted as v_n and v_T, respectively. We also observe that the boundary integrals on Γ_C are well defined for $1 \leqslant m_n$, $m_T \leqslant 3$ if $N = 3$ and for $1 \leqslant m_n$, m_T if $N = 2$, because, for $v_i \in H^1(\Omega)$, $\gamma(v_i) \in L^q(\Gamma)$, with $1 \leqslant q \leqslant 4$ for $N = 3$, and with $1 \leqslant q$ for $N = 2$. We can thus conclude that for the case $N = 2$ all the experimentally observed values of m_n ($m_n \in [2, 3.33]$, recall Section 3.1) can be used in a mathematically consistent way in our formulation. For the case $N = 3$, the mathematical restriction $m_n \leqslant 3$ will be harmless in most of the cases: in [9] only one experimental value of m_n is shown (3.125) which slightly exceeds 3, the most common value for m_n being 2.

Of course, for a complete definition of Problem 1 we would need to make precise the assumed regularity of the displacements, velocity and acceleration relatively to the time variable t, i.e., we would need to specify the spaces of abstract functions to which the mappings $t \to u(t)$, $t \to \dot{u}(t)$ of $[0, T] \to V$ and $t \to \ddot{u}(t)$ of $[0, T] \to V'$ belong. Intimately related to this question is the need for the initial conditions (8.2) to make sense and the need to be precise in what sense the variational inequality (8.1) is satisfied along the time interval $(0, T)$.

These questions will not be addressed here. Instead, *we will proceed formally*, and seek a computational algorithm to obtain approximate solutions for the problem above.

8.2. A regularization of the friction functional

Our first goal is to approximate Problem 1 by a family of regularized problems which lead to the solution of a variational equation instead of a variational inequality (as (8.1)).

Toward this end, we approximate the friction functional $j: V \times V \to \mathbb{R}$ which is nondifferentiable in the second argument (velocity) by a family of functionals j_ε convex and differentiable on the second argument: $j_\varepsilon: V \times V \to \mathbb{R}$,

$$j_\varepsilon(u, v) = \int_{\Gamma_C} c_T(u_n - g)_+^{m_T} \psi_\varepsilon(v_T - \dot{U}_T^C)\, ds, \tag{8.9}$$

where the function $\psi_\varepsilon: (L^q(\Gamma_C))^N \to L^q(\Gamma_C)$ is an approximation of the function $|\cdot|: (L^q(\Gamma_C))^N \to L^q(\Gamma_C)$ and is defined for $\varepsilon > 0$, $\xi \in (L^q(\Gamma_C))^N$ and a.e. $x \in \Gamma_C$, according to

$$\psi_\varepsilon(\xi) \equiv \begin{cases} \varepsilon \left|\frac{\xi}{\varepsilon}\right|^2 \left(1 - \frac{1}{3}\left|\frac{\xi}{\varepsilon}\right|\right) & \text{if } |\xi(x)| \leq \varepsilon, \\ \varepsilon \left(\left|\frac{\xi}{\varepsilon}\right| - \frac{1}{3}\right) & \text{if } |\xi(x)| > \varepsilon. \end{cases} \tag{8.10}$$

REMARK 8.1. Since for a.e. $x \in \Gamma_C$, $|\psi_\varepsilon(\xi(x))| \leq |\xi(x)|$ and since $|\xi| \in L^q(\Gamma_C)$ then $\psi_\varepsilon(\xi) \in L^q(\Gamma_C)$ as stated above and no additional restrictions on m_T are required for the integral on (8.9) to be well defined.

The partial derivative of j_ε relative to the second argument, at (u, w) in the direction of v, is then given by

$$\begin{aligned} \langle J_\varepsilon(u, w), v\rangle &\equiv \langle \partial_2 j_\varepsilon(u, w), v\rangle \\ &= \int_{\Gamma_C} c_T(u_n - g)_+^{m_T} [\phi_\varepsilon(w_T - \dot{U}_T^C)(v_T)]\, ds \quad \forall u, v, w \in V, \end{aligned} \tag{8.11}$$

where, for $\varepsilon > 0$, $\xi, \eta \in (L^q(\Gamma_C))^N$ and a.e. $x \in \Gamma_C$,

$$\phi_\varepsilon(\xi)(\eta) \equiv \psi_\varepsilon'(\xi)(\eta) = \begin{cases} \frac{1}{\varepsilon}\left(2 - \left|\frac{\xi}{\varepsilon}\right|\right)(\xi \cdot \eta) & \text{if } |\xi(x)| \leq \varepsilon, \\ \frac{1}{|\xi|}(\xi \cdot \eta) & \text{if } |\xi(x)| > \varepsilon, \end{cases} \tag{8.12}$$

is the directional derivative of ψ_ε at ξ in the direction of η.

REMARK 8.2. From the definition it is easy to see that for a.e. $x \in \Gamma_C$, $|[\phi_\varepsilon(\xi)(\eta)](x)| \leq 2|\eta(x)|$ and consequently $[\phi_\varepsilon(\xi)(\eta)] \in L^q(\Gamma_C)$. The integral in (8.11) is then well defined without any further restrictions on m_T.

We now define the regularized form of Problem 1:

Problem 1_ε: Find the function $t \to u_\varepsilon(t)$ of $[0, T] \to V$ s.t.

$$\langle \ddot{u}_\varepsilon(t), v\rangle + a(u_\varepsilon(t), v) + \langle P(u_\varepsilon(t)), v\rangle + \langle J_\varepsilon(u_\varepsilon(t), \dot{u}_\varepsilon(t)), v\rangle = \\ = \langle f(t), v\rangle, \quad \forall v \in V, \tag{8.13}$$

with the initial conditions

$$u_\varepsilon(0) = u_0, \qquad \dot{u}_\varepsilon(0) = u_1 . \tag{8.14}$$

We observe that now we have a variational equation instead of a variational inequality. We also observe that this problem is formally equivalent to the problem defined by a system of equations analogous to (7.3)–(7.6) with u_ε replacing u and again $\rho \equiv 1$, $U^D \equiv 0$. However, the friction conditions on Γ_C are now of the form:

Regularized friction conditions:

$$\sigma_T(u) = -c_T(u_n - g)_+^{m_T} \begin{cases} \left(2 - \left|\dfrac{\dot{u}_T - \dot{U}_T^C}{\varepsilon}\right|\right)\dfrac{\dot{u}_T - \dot{U}_T^C}{\varepsilon} & \text{if } |\dot{u}_T - \dot{U}_T^C| \leq \varepsilon , \\ \dfrac{\dot{u}_T - \dot{U}_T^C}{|\dot{u}_T - \dot{U}_T^C|} & \text{if } |\dot{u}_T - \dot{U}_T^C| > \varepsilon . \end{cases} \tag{8.15}$$

In order to visualize the regularization procedure used above, we consider now its particularization for the case of a two-dimensional ($N = 2$) domain Ω with a boundary Γ_C sufficiently smooth that we can define a unit vector i_T tangent to Γ_C. In this case each vector ξ tangent to Γ_C is determined by the real number ξ such that $\xi = \xi i_T$. The functions ψ_ε and $\phi_\varepsilon \equiv \psi_\varepsilon'$ are then, essentially, real-valued functions of a real variable, defined by

$$\psi_\varepsilon(\xi) = \begin{cases} \varepsilon \left|\dfrac{\xi}{\varepsilon}\right|^2 \left(1 - \tfrac{1}{3}\left|\dfrac{\xi}{\varepsilon}\right|\right) & \text{if } |\xi| \leq \varepsilon , \\ \varepsilon \left(\left|\dfrac{\xi}{\varepsilon}\right| - \tfrac{1}{3}\right) & \text{if } |\xi| > \varepsilon ; \end{cases}$$

$$\phi_\varepsilon(\xi) = \begin{cases} \left(2 - \left|\dfrac{\xi}{\varepsilon}\right|\right)\dfrac{\xi}{\varepsilon} & \text{if } |\xi| \leq \varepsilon , \\ \operatorname{sgn}(\xi) & \text{if } |\xi| > \varepsilon . \end{cases} \tag{8.16}$$

The graphs of these functions are depicted in Fig. 50 together with the graphs of the functions which they approximate: the function $|\cdot|$ and its derivative in $\mathbb{R} - \{0\}$, $\operatorname{sgn}(\cdot)$.

Finally we observe that a physical interpretation might be attributed to the above regularization procedure. The increasing branch of the $\phi_\varepsilon(\xi)$ curve is essentially of the same nature as those experimentally observed during creep sliding (recall Section 5.1.2). However, we prefer to regard it exclusively as a mathematical procedure to obtain an approximate problem which corresponds to a variation equation. We do so because the values of ε which

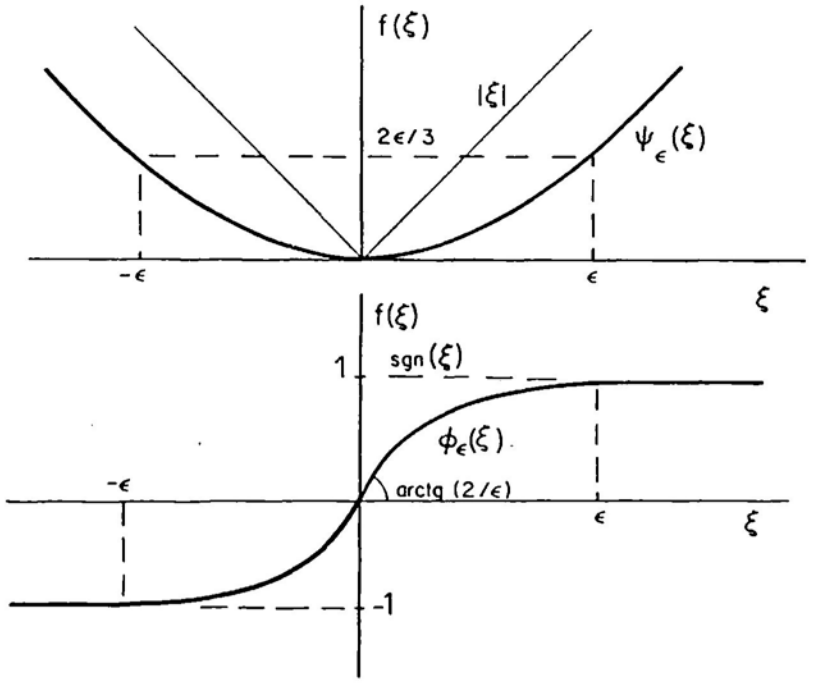

Fig. 50. Graphs of the function ψ_ϵ and ϕ_ϵ for the case of unidimensional Γ_C.

will be used in actual computations will not be so small as those required for the above physical interpretation to be valid in the case of hard metals with which we will be considering. The choice of ε will be dictated only by the desired proximity of the solutions of Problems 1 and 1_ϵ and the corresponding computational costs associated.

Many examples of similar regularization procedures in dynamic friction problems can be found in the literature. Among them we refer to [37] for mathematical aspects; to [101] and [81] for computational applications to Theory of Mechanisms and to [62] for a finite element analysis of a simplified friction problem.

We are aware of some of the difficulties associated with these regularization procedures: a perfect zero relative velocity between the contacting surfaces is not possible – when 'stuck' the contact surfaces will creep with a relative velocity smaller than ε; trying to impose a very small ε will imply the need to reduce substantially the steps of the time integration scheme, particularly in unloading situations – transitions from 'slip' to 'stick'.

Part III. Finite element models and numerical analysis

9. Finite element approximations of the regularized problem

Using standard finite element procedures, approximate versions of Problem 1_ϵ can be constructed in finite-dimensional subspaces V_h ($\subset V \subset V'$). For a certain mesh (h) the approximate displacements, velocities and accelerations at each time t are elements of V_h,

$$v^h(t), \dot{v}^h(t), \ddot{v}^h(t) \in V_h .$$

Within each element $\bar{\Omega}_e^h$ $(e = 1, 2, \ldots, E_h)$ the components of the displacements, velocities and accelerations are expressed in the form

$$v_j^h(x, t) = \sum_{I=1}^{N_e} v_j^I(t) N_I(x), \qquad \dot{v}_j^h(x, t) = \sum_{I=1}^{N_e} \dot{v}_j^I(t) N_I(x), \qquad \ddot{v}_j^h(x, t) = \sum_{I=1}^{N_e} \ddot{v}_j^I(t) N_I(x),$$

where $j = 1, 2, \ldots, N$; N_e = number of nodes of the element; $v_j^I(t)$, $\dot{v}_j^I(t)$, $\ddot{v}_j^I(t)$ are the nodal values of the displacements, etc., at time t and N_I is the element shape function associated with the node I.

The finite element version of Problem 1_ε is then:

Problem 1_ε^h: Find the function $t \to u_\varepsilon^h(t)$ of $[0, T] \to V_h$ s.t.

$$\begin{aligned}&(\ddot{u}_\varepsilon^h(t), v^h) + a(u_\varepsilon^h(t), v^h) + \langle P(u_\varepsilon^h(t)), v^h \rangle \\ &\quad + \langle J_\varepsilon(u_\varepsilon^h(t), \dot{u}_\varepsilon^h(t)), v^h \rangle = \langle f(t), v^h \rangle \quad \forall v^h \in V^h ,\end{aligned} \tag{9.1}$$

with the initial conditions

$$(\dot{u}_\varepsilon^h(0), v^h) = (u_0, v^h), \qquad (\dot{u}_\varepsilon^h(0), v^h) = (u_1, v^h), \quad \forall v^h \in V^h . \tag{9.2}$$

If N_h is the number of nodes of the finite element mesh, then this problem is equivalent to the following:

Find the function $t \to r(t)$ of $[0, T] \to \mathbb{R}^{N \times N_h}$, s.t.

$$M\ddot{r}(t) + Kr(t) - P(r(t)) + J(r(t), \dot{r}(t)) = F(t) , \tag{9.3}$$

with the initial conditions

$$r(0) = p_0, \qquad \dot{r}(0) = p_1 . \tag{9.4}$$

Here we have introduced the following matrix notations:

$r(t)$, $\dot{r}(t)$, $\ddot{r}(t)$: the column vectors of nodal displacements, velocities and accelerations, respectively;

M: standard mass matrix;

K: standard stiffness matrix;

$F(t)$: consistent nodal force vector;

$P(r(t))$: vector of consistent nodal normal forces on Γ_C;

$J(r(t), \dot{r}(t))$: vector of consistent nodal friction forces on Γ_C;

$p_0(p_1)$: initial nodal displacement (velocity).

The components of the element vector ${}^{(e)}P$ are of the form

$$ {}^{(e)}P_{I_j} = -\int_{(e)\Gamma_C} \sigma_n n_j N_i \, ds , \tag{9.5} $$

and the components of the element vector ${}^{(e)}J$ are of the form

$$ {}^{(e)}J_{I_j} = -\int_{(e)\Gamma_C} \sigma_{T_j} N_I \, ds . \tag{9.6} $$

10. Algorithms for nonlinear dynamical systems

The algorithms that we shall use for solving the discrete dynamical system involve variants of standard schemes in use in nonlinear structural dynamics calculations. An outline of these computational procedures follows.

10.1. A Newmark-type algorithm

We begin with the presentation of an implicit Newmark-type algorithm that has proved to be effective for many problems in the general class under study.

Let P denote a partition of the time domain $[0, T]$ into M intervals of length Δt such that $0 = t_0, t_1, \ldots, t_K, \ldots, t_M = T$ with $t_{K+1} - t_K = \Delta t$. We shall approximate the velocities and accelerations at time t_K by expressing them as functions of the displacements velocities and accelerations at time t_{K-1} and of the displacements at time t_K, by the following relations:

$$ \begin{aligned} \dot{u}_K &= \frac{\gamma}{\beta \Delta t}(u_K - u_{K-1}) + \left(1 - \frac{\gamma}{\beta}\right) \dot{u}_{K-1} + \Delta t \left(1 - \frac{\gamma}{2\beta}\right) \ddot{u}_{K-1} , \\ \ddot{u}_K &= \frac{1}{\beta \Delta t^2}(u_K - u_{K-1}) - \frac{1}{\beta \Delta t} \dot{u}_{K-1} - \left(\frac{1}{2\beta} - 1\right) \ddot{u}_{K-1} , \end{aligned} \tag{10.1} $$

where γ and β are the so-called Newmark parameters and $u_K \equiv u_\epsilon^h(t_K)$, etc. are used in the foregoing, if no confusion is likely to arise.

Introducing the above relations into the variational equation (9.1), we obtain the following variation equation at time t_K:

$$ \frac{1}{\beta \Delta t^2}(u_K, v) + a(u_K, v) + \langle P(u_K), v \rangle + \langle \bar{J}(u_K), v \rangle = \langle \hat{f}_K, v \rangle, \quad \forall v \in V^h . \tag{10.2} $$

Here

$$ \begin{aligned} \langle \bar{J}(u_K), v \rangle &\equiv \langle J_\epsilon(\bar{u_K}, \dot{u}_K), v \rangle \\ &= \left\langle J_\epsilon\left(u_K, \frac{\gamma}{\beta \Delta t}(u_K - u_{K-1}) + \left(1 - \frac{\gamma}{\beta}\right) \dot{u}_{K-1} + \Delta t \left(1 - \frac{\gamma}{2\beta}\right) \ddot{u}_{K-1}\right), v \right\rangle , \end{aligned} $$

$$ \langle \hat{f}_K, v \rangle = \langle f_K, v \rangle + \left(\frac{1}{\beta \Delta t^2} u_{K-1} + \frac{1}{\beta \Delta t} \dot{u}_{K-1} + \left(\frac{1}{2\beta} - 1\right) \ddot{u}_{K-1}, v\right) . $$

The above variational equation can be put in the operator form

$$R_K(u_K) = 0 \quad \text{in } V_h', \tag{10.3}$$

with $R_K : V_h \to V_h'$ being the nonlinear operator defined by

$$\langle R_K(u_K), v\rangle_{V_h \times V_h'} = \frac{1}{\beta \Delta t^2}(u_K, v) + a(u_K, v) + \langle P(u_K), v\rangle + \langle \bar{J}(u_K), v\rangle - \langle \hat{f}_K, v\rangle, \quad \forall u_K, v \in V_h. \tag{10.4}$$

Let $\tilde{K}_K(u_K) = DR_K(u_K) \in \mathcal{L}(V_h, V_h')$ be the derivative of the map R_K at $u_K \in V_h$. Then the Newton–Raphson iteration technique for solving (10.3) is as follows: Given a starting value $u_K^{(0)} \in V^h$, obtain successive approximations of the solution u_K by using the recurrence formula

$$u_K^{(i+1)} = u_K^{(i)} - [\tilde{K}_K(u_K^{(i)})]^{-1} R_K(u_K^{(i)}), \tag{10.5}$$

where $i = 0, 1, \ldots$ is the iteration counter. Thus, at each iteration i, the following variational equation has to be solved:

$$\langle \tilde{K}_K(u_K^{(i)})(\Delta U_K^{(i)}), v\rangle_{V_h \times V_h'} = -\langle R_K(u_K^{(i)}), V\rangle_{V_h \times V_h'}, \quad \forall v \in V_h, \tag{10.6}$$

with $\Delta u_K^{(i)} = u_K^{(i+1)} - u_K^{(i)}$.

In the present problem we have, for $u_K, w, v \in V_h$,

$$\langle \tilde{K}_K(u_K)(w), v\rangle_{V_h \times V_h'} = a(w, v) + \frac{1}{\beta \Delta t^2}(w, v) + \langle DP(u_K)(w), v\rangle + \langle D\bar{J}(u_K)(w), v\rangle,$$

where

$$\langle DP(u_K)(w), v\rangle = \int_{\Gamma_C} c_n m_n (u_n - g)_+^{m_n - 1} w_n v_n \, ds,$$

$$\langle D\bar{J}(u_K)(w), v\rangle = \langle \partial_1 J_\epsilon(u_K, \dot{u}_K)(w), v\rangle + \frac{\gamma}{\beta \Delta t}\langle \partial_2 J_\epsilon(u_K, \dot{u}_K)(w), v\rangle$$

$$= \int_{\Gamma_C} c_T m_T (u_{nK} - g)_+^{m_T - 1} [\phi_\epsilon(\dot{u}_{TK} - \dot{U}_T^C)(v_T)] w_n \, ds$$

$$+ \frac{\gamma}{\beta \Delta t} \int_{\Gamma_C} c_T (u_{nK} - g)_+^{m_T} [\pi_\epsilon(\dot{u}_{TK} - \dot{U}_T^C)(w_T, v_T)] \, ds,$$

where, for $\varepsilon > 0$, ξ, η, ζ traces on Γ_C of V_h functions, and $x \in \Gamma_C$,

$$\pi_\varepsilon(\xi)(\eta,\zeta)=\begin{cases}-\dfrac{1}{\varepsilon^2|\xi|}(\xi\cdot\eta)(\xi\cdot\zeta)+\dfrac{1}{\varepsilon}\left(2-\left|\dfrac{\xi}{\varepsilon}\right|\right)(\eta\cdot\zeta) & \text{if } |\xi(x)|\leqslant\varepsilon\,,\\ -\dfrac{1}{|\xi|^3}(\xi\cdot\eta)(\xi\cdot\zeta)+\dfrac{1}{|\xi|}(\eta\cdot\zeta) & \text{if } |\xi(x)|>\varepsilon\,.\end{cases}\tag{10.7}$$

REMARK 10.1. If $N=2$ the above definition reduces to

$$\pi_\varepsilon(\xi)(\eta,\zeta)=\begin{cases}\dfrac{2}{\varepsilon}\left(1-\left|\dfrac{\xi}{\varepsilon}\right|\right)(\eta\cdot\zeta) & \text{if } |\xi(x)|\leqslant\varepsilon\,,\\ 0 & \text{if } |\xi(x)|>\varepsilon\,.\end{cases}$$

We next recast (10.6) in matrix form:

$$\bar{\boldsymbol{K}}_K^{(i)}\Delta\boldsymbol{r}_K^{(i)}=-\boldsymbol{R}_K^{(i)}\,,$$

where

$$\bar{\boldsymbol{K}}_K^{(i)}=\boldsymbol{K}+\frac{1}{\beta\Delta t^2}\boldsymbol{M}+\boldsymbol{K}_K^{n(i)}+\boldsymbol{K}_K^{Tn(i)}+\frac{\gamma}{\beta\Delta t}\boldsymbol{C}_K^{T(i)},$$

$$\Delta\boldsymbol{r}_K^{(i)}=\boldsymbol{r}_K^{(i+1)}-\boldsymbol{r}_K^{(i)}\,,$$

$$\boldsymbol{R}_K^{(i)}=\left[\frac{1}{\beta\Delta t^2}\boldsymbol{M}+\boldsymbol{K}\right]\boldsymbol{r}_K^{(i)}+\boldsymbol{P}_K^{(i)}+\boldsymbol{J}_K^{(i)}-\hat{\boldsymbol{F}}_K$$

and

$$\hat{\boldsymbol{F}}_K=\boldsymbol{F}_K+\boldsymbol{M}\left[\frac{1}{\beta\Delta t^2}\boldsymbol{r}_{K-1}+\frac{1}{\beta\Delta t}\dot{\boldsymbol{r}}_{K-1}+\left(\frac{1}{2\beta}-1\right)\ddot{\boldsymbol{r}}_{K-1}\right].$$

The element components of the matrices $\boldsymbol{K}^n$, $\boldsymbol{K}^{Tn}$ and $\boldsymbol{C}^T$ for the case $N=2$ are of the form

$${}^{(e)}K^n_{M_iN_j}=\int_{(e)\Gamma_C}c_n m_n(u_n-g)_+^{m_n-1}n_i n_j N_M N_N\,ds\,,$$

where ${}^{(e)}\Gamma_C$ is the part of Γ_C belonging to element e;

$$
{}^{(e)}K^{\mathrm{Tn}}_{M_i N_j} = \int_{{}^{(e)}\Gamma_C} c_T m_T (u_n - g)_+^{m_T - 1} \begin{cases} \dfrac{1}{\varepsilon}\left(2 - \dfrac{|\dot{u}_T - \dot{U}^C_T|}{\varepsilon}\right)(\dot{u}_{Ti} - \dot{U}^C_{Ti}) n_j N_M N_N \, \mathrm{d}s \\ \quad \text{if } |\dot{u}_T - \dot{U}^C_T| \leqslant \varepsilon\,, \\ \dfrac{1}{|\dot{u}_T - \dot{U}^C_T|}(\dot{u}_{Ti} - \dot{U}^C_{Ti}) n_j N_M N_N \, \mathrm{d}s \\ \quad \text{if } |\dot{u}_T - \dot{U}^C_T| > \varepsilon\,, \end{cases}
$$

$$
{}^{(e)}C^{T}_{M_i N_j} = \int_{{}^{(e)}\Gamma_C(\leqslant)} c_T (u_n - g)_+^{m_T} \frac{2}{\varepsilon}\left(1 - \frac{|\dot{u}_T - \dot{U}^C_T|}{\varepsilon}\right)(\delta_{ij} - n_i n_j) N_M N_N \, \mathrm{d}s\,.
$$

where ${}^{(e)}\Gamma_C(\leqslant)$ is the part of ${}^{(e)}\Gamma_C$ where $|\dot{u}_T - \dot{U}^C_T| \leqslant \varepsilon$.

Physically, the matrix $\boldsymbol{K}^{n}$ produces a variation of the normal nodal forces due to a variation of the nodal normal displacements; the matrix $\boldsymbol{K}^{Tn}$ produces a variation of the nodal friction forces due to a variation of the nodal normal displacements; finally, the matrix $\boldsymbol{C}^{T}$ produces a variation of the nodal friction forces due to a variation of the nodal sliding velocities.

Both $\boldsymbol{K}^{n}$ and $\boldsymbol{C}^{T}$ are symmetric matrices because both are associated with terms of $\langle \tilde{K}_K(u_K)(w), v\rangle$ which can be considered as second derivatives of functionals. In fact,

$$
\langle \mathrm{D}P(u)(w), v\rangle = \langle \mathrm{D}^2 p(u)(w), v\rangle
$$

for $u, v, w \in V$, with $p: V \to \mathbb{R}$ being the deformation energy associated with the nonlinear springs on Γ_C,

$$
p(u) = \int_{\Gamma_C} \frac{c_n}{m_n + 1}(u_n - g)_+^{m_n + 1} \, \mathrm{d}s\,.
$$

We also have that

$$
\langle \partial_2 \boldsymbol{J}_\varepsilon(u, \dot{u})(w), v\rangle = \langle \partial_2^2 j_\varepsilon(u, \dot{u})(w), v\rangle
$$

is the second partial derivative of the friction functional j_ε relative to the second variable (velocity). We also observe that, in the two-dimensional case ($N = 2$) $\boldsymbol{C}^{T}$ is the incremental damping matrix associated with the region of Γ_C which is 'stuck' at some instant (the modulus of the sliding velocity is smaller than ε). Finally, we observe that the matrix $\boldsymbol{K}^{Tn}$ is not symmetric. This results from the fact that, according to the normal contact behavior, the normal stresses on Γ_C depend only on the penetration $(u_n - g)_+$. A change on the sliding velocity does not produce any change on the normal contact forces.

10.2. Semi-explicit, central-difference scheme

It is well known that the central-difference technique is equivalent to the Newmark method for $\beta = 0$, $\gamma = \frac{1}{2}$. This special case of the algorithm described above is now outlined. The

accelerations and the displacements at time t_K are related with the displacements, velocities and accelerations at time t_{K-1} and with the velocities at time t_K, according to

$$\ddot{u}_K = -\ddot{u}_{K-1} + \frac{2}{\Delta t}(\dot{u}_K - \dot{u}_{K-1}), \qquad u_K = u_{K-1} + \Delta t \dot{u}_{K-1} + \tfrac{1}{2}\Delta t^2 \ddot{u}_{K-1}. \tag{10.8}$$

Introducing these relations into (9.1), the following variational equation is obtained at time t_K:

$$\frac{2}{\Delta t}(\dot{u}_K, v) + \langle \bar{J}(\dot{u}_K), v\rangle = \langle \hat{f}_K, v\rangle, \quad \forall v \in V^h, \tag{10.9}$$

where, now

$$\langle \bar{J}(\dot{u}_K), v\rangle \equiv \langle J_\varepsilon(u_K, \dot{u}_K), v\rangle$$
$$= \langle J_\varepsilon(u_{K-1} + \Delta t u_{K-1} + \tfrac{1}{2}\Delta t^2 \ddot{u}_{K-1}, \dot{u}_K), v\rangle, \tag{10.10}$$

$$\langle \hat{f}_K, v\rangle = \langle f_K, v\rangle - \langle P(u_{K-1} + \Delta t \dot{u}_{K-1} + \tfrac{1}{2}\Delta t^2 \ddot{u}_{K-1}), v\rangle$$
$$+\left(\ddot{u}_{K-1} + \frac{2}{\Delta t}\dot{u}_{K-1}, v\right) - a(u_{K-1} + \Delta t \dot{u}_{K-1} + \tfrac{1}{2}\Delta t^2 \ddot{u}_{K-1}, v). \tag{10.11}$$

It is important to observe that the second equation in (10.8) determines uniquely the displacement at time t_K from the values of the velocity and acceleration at the previous time t_{K-1}. The nonlinearity involved in (10.9) results only from the nonlinear dependence of the frictional forces on the tangential velocities. In the iterative process required to solve (10.9), the displacements (and consequently the normal stresses) will thus remain constant.

Using again the Newton–Raphson method to solve (10.9) for the unknown velocities $\dot{u}_K$, the following linear equation is obtained at each iteration:

$$\langle \tilde{K}_K(\dot{u}_K^{(i)})(\Delta \dot{u}_K^{(i)}), v\rangle = -\langle R_K(\dot{u}_K^{(i)}), v\rangle, \quad \forall v \in V_h. \tag{10.12}$$

In this case,

$$\Delta \dot{u}_K^{(i)} = \dot{u}_K^{(i+1)} - \dot{u}_K^{(i)},$$
$$\langle \tilde{K}_K(\dot{u}_K)(w), v\rangle = \frac{2}{\Delta t}(w, v) + \langle D\bar{J}(\dot{u}_K)(w), v\rangle, \quad \forall \dot{u}_K, w, v \in V_h,$$
$$\langle R_K(\dot{u}_K), v\rangle = \frac{2}{\Delta t}(\dot{u}_K, v) + \langle \bar{J}(\dot{u}_K), v\rangle - \langle \hat{f}_K, v\rangle, \quad \forall \dot{u}_K, v \in V_h,$$
$$\langle D\bar{J}(\dot{u}_K)(w), v\rangle = \langle \partial_2 J_\varepsilon(u_K, \dot{u}_K)(w), v\rangle. \tag{10.13}$$

The discrete variational equation leads to the following system of algebraic linear equations to be solved at each iteration:

$$\bar{K}_K^{(i)} \Delta \dot{r}_K^{(i)} = -R_K^{(i)}, \tag{10.14}$$

where

$$\tilde{K}_K^{(i)} = \frac{2}{\Delta t} M + C_K^{T(i)}, \qquad \Delta \dot{r}_K^{(i)} = \dot{r}_K^{(i+1)} - \dot{r}_K^{(i)},$$

$$R_K^{(i)} = \frac{2}{\Delta t} M \dot{r}_K^{(i)} + J_K^{(i)} - \hat{F}_K, \tag{10.15}$$

$$\hat{F}_K = F_K + M\left[\ddot{r}_{K-1} + \frac{2}{\Delta t}\dot{r}_{K-1}\right] - K\left[r_{K-1} + \Delta t\,\dot{r}_{K-1} + \tfrac{1}{2}\Delta t^2\,\ddot{r}_{K-1}\right]$$
$$- P(r_{K-1} + \Delta t\,\dot{r}_{K-1} + \tfrac{1}{2}\Delta t^2\,\ddot{r}_{K-1}).$$

Some computational advantages of this algorithm over the Newmark scheme described earlier are the following:

(i) Both M and $C_K^{T(i)}$ (hence $K_K^{(i)}$) are *symmetric* matrices.

(ii) If a *diagonalized mass* matrix M is used, the only nondiagonal entries of $\tilde{K}_K^{(i)}$ result from the points on Γ_C which are 'stuck'. The structure of $\tilde{K}_K^{(i)}$ for an appropriate numbering of the nodes of the mesh on Γ_C suggests that the use of a symmetric skyline solver for the solution of (10.14) may prove to be very efficient.

(iii) If, in addition to the diagonalization of the mass matrix:

(a) a *rotation of the degrees of freedom* on Γ_C is performed in such a way that the final degrees of freedom have the direction of the normal and the tangent to Γ_C at each contact node;

(b) the element contributions to C^T are computed with a quadrature rule which uses the nodes as integration points (e.g., *trapezoidal rule for linear elements* and *Simpson's rule for quadratic elements*);

then the matrix $C_K^{T(i)}$ is also diagonal and the solution of (10.14) becomes very simple.

REMARK 10.2. The discontinuity of the Coulomb's friction law at zero sliding velocity is a major source of computational difficulties in friction problems. Even though, in the algorithms described in this and the previous section, a regularized form of that law is used, those difficulties cannot be completely avoided. The situation which may arise when using the methods described here with a constant time step is the following: in unloading situations (passage from sliding to adhesion) the Newton–Raphson iterative techniques may fail to converge if ε is very small and the time step too large. This situation does not seem to be dependent on the specific iterative technique used or on the type of regularization of Coulomb's law adopted. In a previous paper [62] we found similar problems though we used a different iterative scheme (successive approximations) and a different regularization (piecewise linear ϕ_ϵ). Our numerical results suggest that for small values of ε the radius of convergence of the iterative scheme used is very small due to the steep changes in ϕ_ϵ on the interval $[-\varepsilon, \varepsilon]$.

The critical situations arise in transitions from sliding to adhesion because it is then that the most important changes in the solution occur. We observe that, for the nonregularized problem, a discontinuity of the tangential acceleration arises when a point on the contact surface ceases to be sliding and a period of adhesion is initiated.

One simple remedy for these difficulties is to decrease the time step until two successive solutions are not too far apart. Obviously this increases the computational costs and other

more sophisticated and less expensive remedies are desirable. We feel, however, that radical improvements in efficiency should not be expected.

In the computer code that we have developed, reduction of the time step Δt_{max} is only performed if the Newton–Raphson iteration fails to converge in a prescribed number MAXITE of iterations. In that situation, successively smaller time steps Δt are tried until a convergent solution is obtained. This smaller time step is then kept for a prescribed number of steps KSTEPR during which the most drastic changes in the solution are expected to occur. After this time interval, the time step is gradually increased again to Δt_{max}.

It was found that for the smaller time steps, a reduction below $0.1\Delta t_{max}$ was rarely needed if a Δt_{max} was used which provided simultaneously for accurate computation of dynamic response and for the stability of the central difference technique and if the values of ε used were not too small. The parameter MAXITE has been set usually to 5 and KSTEPR to a number in the range 10–20. An indication of the extra computational work resulting from the reduced time steps is given by the quotient T'/T, where T is the total physical time spanned by our analysis (with the time step reductions) with some total number of time steps and T' is the total physical time that would be possible to span with the same total number of time steps if no reduction of time steps were needed. In most of the computations, values of this ratio of order 1.2–1.5 were experienced. If more restrictive values of ε are used, this value will increase significatively: for example, for $\varepsilon = 0.02\,\mathrm{cm\,s^{-1}}$ in the example of the next section, $T'/T = 4.2$.

11. Numerical studies

In this section, we discuss several applications of the models and methods discussed earlier to representative problems.

11.1. An elastic slab subjected to periodic loading

Our first example is designed more to test the performance and robustness of the algorithms described in the preceding section than as a model of complex dynamic friction phenomena. We begin with the analyses of motion of the elastic slab shown in Fig. 51. The dimensions of the slab are $16\,\mathrm{cm} \times 2\,\mathrm{cm}$, as indicated, and it is assumed to be of unit thickness and to be constructed of a linearly elastic material with properties close to those of cast iron. Young's modulus was assumed to be $E = 1.4 \times 10^6$ ($10^3\,\mathrm{Kg\,cm^{-1}\,s^{-2}}$), Poisson's ratio $\nu = 0.25$ and the mass density $\rho = 7 \times 10^{-6}$ ($10^3\,\mathrm{Kg\,cm^{-3}}$). The slab is assumed to be in a state of plane strain; it is simply supported on the portion Γ_D of its boundary and is compressed along a frictional interface Γ_C by a flat 'rigid' surface, the vertical downward displacement of which is prescribed. This corresponds to prescribing an initial uniformly distributed gap $g = -5 \times 10^{-4}\,\mathrm{cm}$. The prescribed tangential velocity of the 'rigid' surface is zero ($\dot{U}_T^C = 0$). The normal contact properties of the interface were taken from Table 1 of [9], assuming that both surfaces in contact are of cast iron hand-scraped with a surface finish (peak to valley distance) in the range 6–8 μm. The coefficient m_n is then equal to 2 and, after a change of units, $c_n = 10^8$ ($10^3\,\mathrm{Kg\,cm^{-3}\,s^{-2}}$). The friction coefficient along Γ_C was arbitrarily assumed to be $\mu = 0.3$ and independent of the normal load. Consequently, $m_T = 2$ and $c_T = 0.3 \times 10^8$ ($10^3\,\mathrm{Kg\,cm^{-3}\,s^{-2}}$).

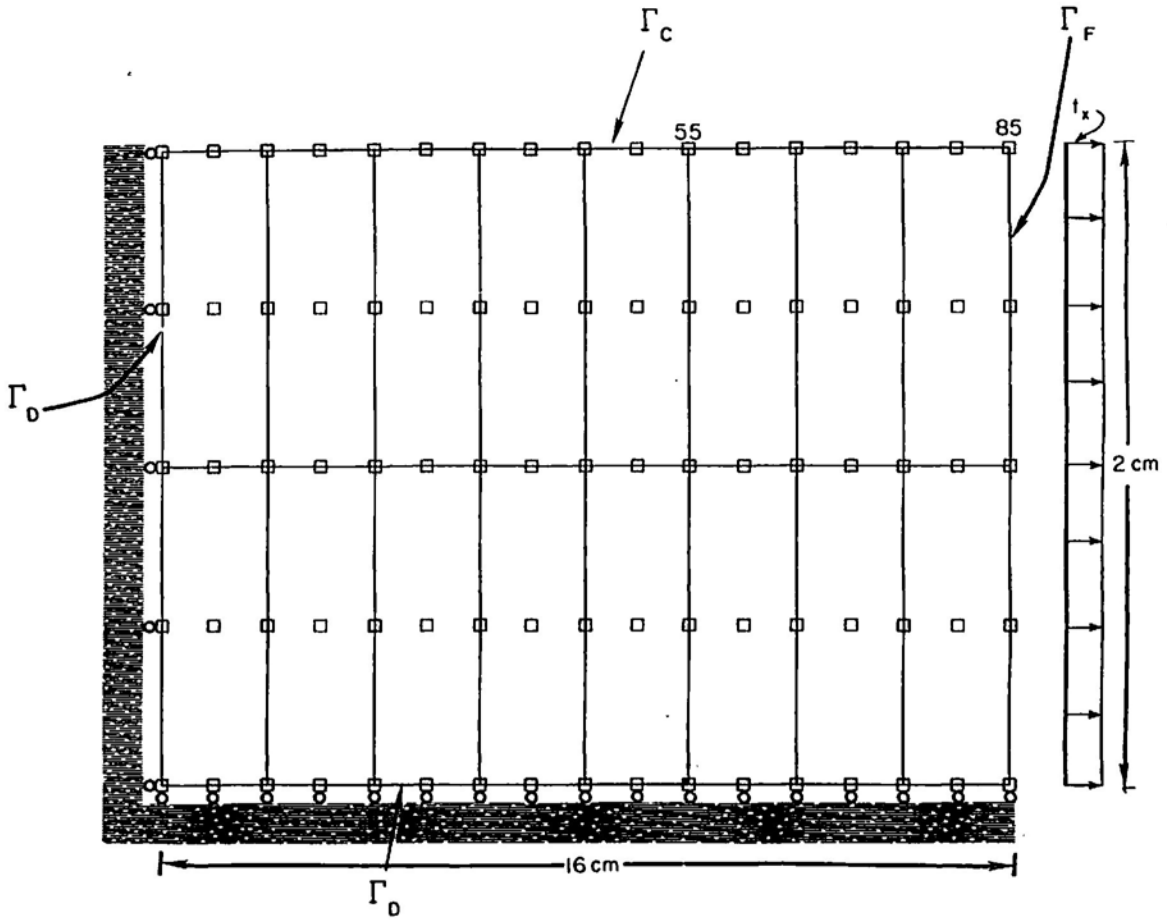

Fig. 51. Dimensions and finite element discretization of an elastic slab.

On one of its ends (Γ_F), the slab is subjected to a time-dependent uniformly distributed force

$$t_x = \bar{t} \sin \bar{\omega} t,$$

where $\bar{t} = 30$ (10^3 Kg cm^{-1} s^{-2}) and $\bar{\omega} = 3 \times 10^4$ rad s^{-1}.

The prescribed initial conditions are as follows: the initial velocities in all the slab are zero ($\dot{r}(0) = 0$) and the initial displacements are the static equilibrium displacements of the slab due to the normal compression exerted by the flat surface on Γ_C alone (no friction on Γ_C and no applied tractions on Γ_F).

We observe that, due to the normal deformation of the interface, the equilibrium normal displacements and normal pressure on Γ_C are not known a priori. The initial equilibrium displacements solution is obtained by solving the following system of nonlinear algebraic equations:

$$\boldsymbol{K}\boldsymbol{r}(0) + \boldsymbol{P}\boldsymbol{r}(0) = \boldsymbol{0}. \tag{11.1}$$

The numerical solution of this frictionless unilateral contact problem is obtained by using a standard Newton–Raphson algorithm analogous to that discussed in Section 10.1.

The finite elements mesh used in this analysis consists of 16 nine-node isoparametric quadratic elements, as illustrated in Fig. 51. The regularization parameter ε for the Coulomb's friction law was taken, successively, to be equal to 1, 0.1 and 0.02 cm s^{-1}. The dynamical equations of this discrete model were integrated using Newmark's method, as discussed earlier, with parameters $\beta = 0.25$, $\gamma = 0.5$ and a maximum time step of $\Delta t_{max} = 10^{-6}$ s.

The distributions of normal stresses at several time instants obtained with $\varepsilon = 0.1$ cm s^{-1}, are shown in Fig. 52.

The distributions of friction stresses on Γ_C at several time instants are shown in Fig. 53. The travelling wave type evolution of these stresses can be clearly observed in that figure as can the sharp transition between the sliding and adhesion regions on Γ_C.

The effect of the regularization parameter ε on the evolution of the displacements, velocities, and friction stresses at the contact nodes 55 and 85 are shown in Figs. 54–59. As might be expected, smaller values of ε lead to sharper transitions between sliding and adhesion states; large values of ε smooth out the fronts in these solutions. It can be also observed that the major discrepancies between results obtained for different values of ε occur in the tangential displacements and velocities, not on the friction stresses. This results from the fact that when sliding occurs, the value of the friction stress is necessarily μ times the normal

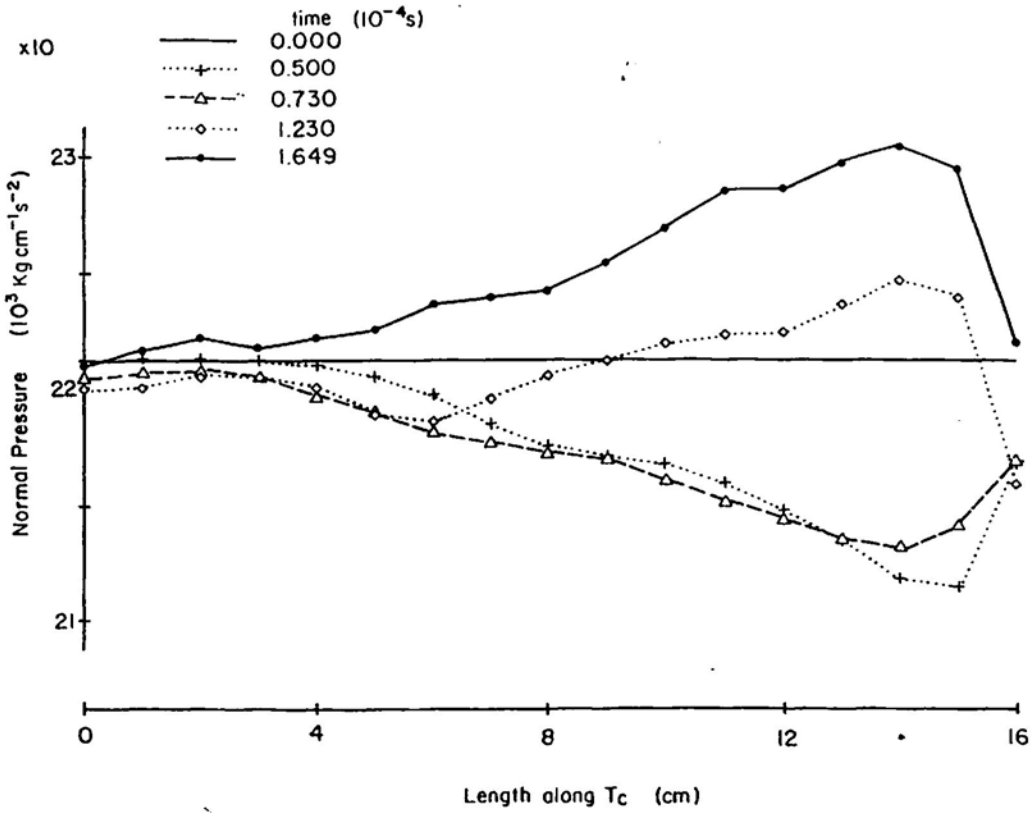

Fig. 52. Distribution of normal stresses on Γ_C at several time instants due to periodic loading on Γ_F.

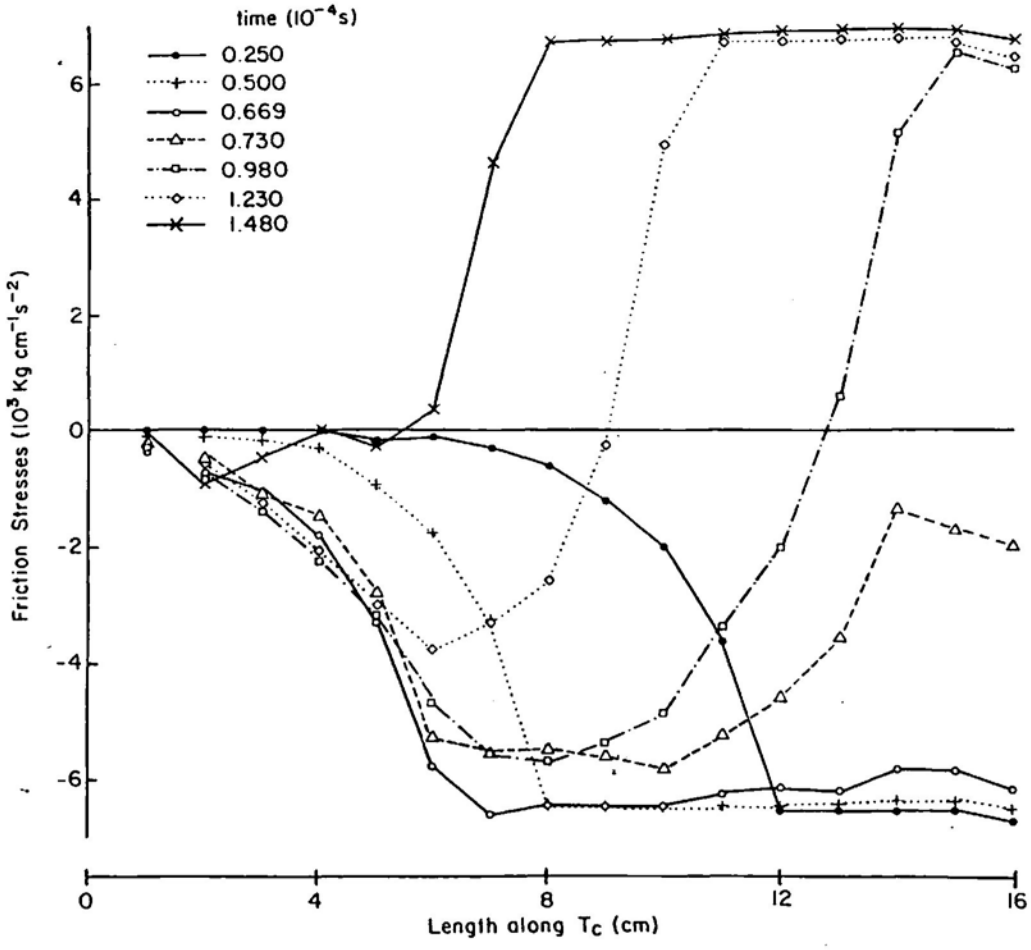

Fig. 53. Distribution of tangential stresses on Γ_C at several time instants due to periodic loading on Γ_F.

pressure. Consequently, the only possible discrepancy is in the relative duration of stick and slip states and in values of the friction stress during the stick state. Since, in the present case, the alternating stick and slip states are closely conditioned by the variation of the periodic forcing function, it is not surprising that the discrepancies are small. It is likely that for other situations the use of large values for ε could produce friction stress solutions much less accurate than in the present example.

An examination of the computed variation in the tangential displacements and velocities leads us to the conclusion that the essential effect of the reduction of ε is to produce more accurate adhesion states. High values of ε (e.g. $\varepsilon = 1$) lead to solutions which only vaguely resemble those obtained with smaller values of ε, no meaningful conclusion relative to stick or slip being possible. From a practical point of view it appears reasonable to choose values of ε, that are sufficiently small relative to the order of magnitude of the tangential velocities that occur during the sliding states. In this manner, sliding and adhesion will be essentially relative and not absolute concepts. We observe that for tangential velocities on the order of 1 cm s^{-1},

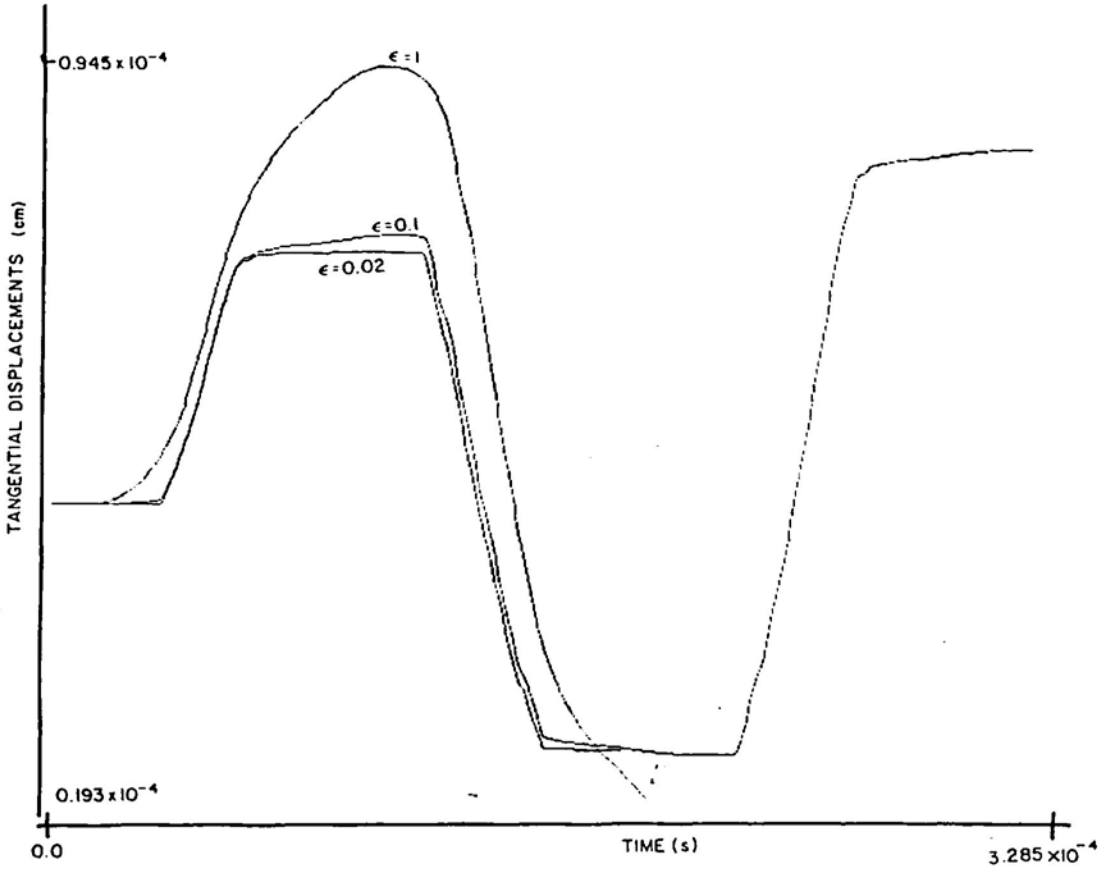

Fig. 54. Tangential displacements at Node 55 using different values of ε.

the value of $\varepsilon = 1\,\mathrm{cm\,s^{-1}}$ is obviously inadequate while results obtained with $\varepsilon = 0.1$, $0.02\,\mathrm{cm\,s^{-1}}$ seem to be physically reasonable.

11.2. Steady sliding and dynamic stability of a rigid block

As a prelude to examples dealing with nonlinear dynamics of a model of a continuous body, we shall now consider applications of the algorithms developed in Section 10 to some very simple dynamical systems. Our mission here is to construct very simple models of stick-slip motion, consistent with the continuum models discussed previously, that have sufficient degrees of freedom to capture qualitatively dynamic friction phenomena of the type observed experimentally by Tolstoi [103] and others: in stick-slip motions of sliding bodies, tangential jumps occur in strict synchronization with jumps normal to the sliding surfaces.

For this purpose, a minimum of three degrees-of-freedom seems to be necessary; two (normal and tangential) is inadequate since this would not provide the coupling between tangential and normal motions observed in Part I. A simple mechanical system, not unlike many seen in friction experiments, that can capture this coupling is a simple rigid body in plane motion, the rotational degree-of-freedom providing the coupling mechanism. Such a

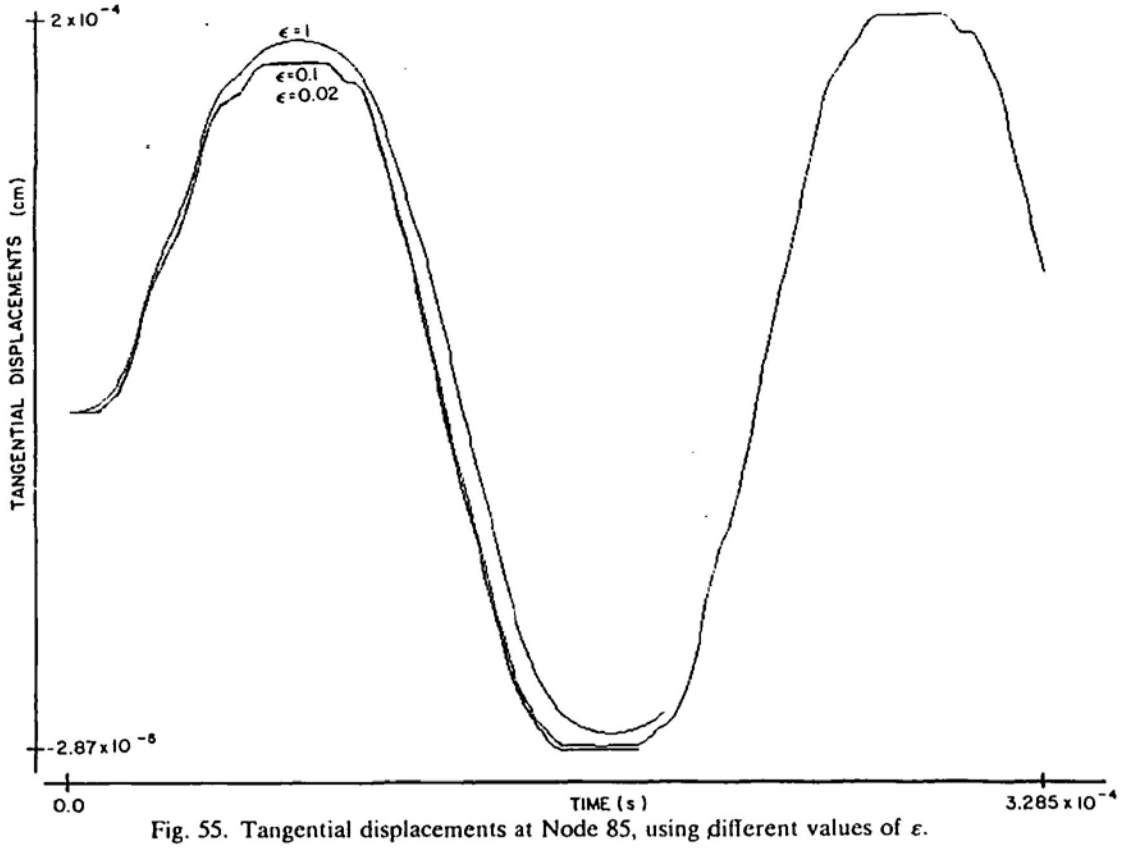

Fig. 55. Tangential displacements at Node 85, using different values of ε.

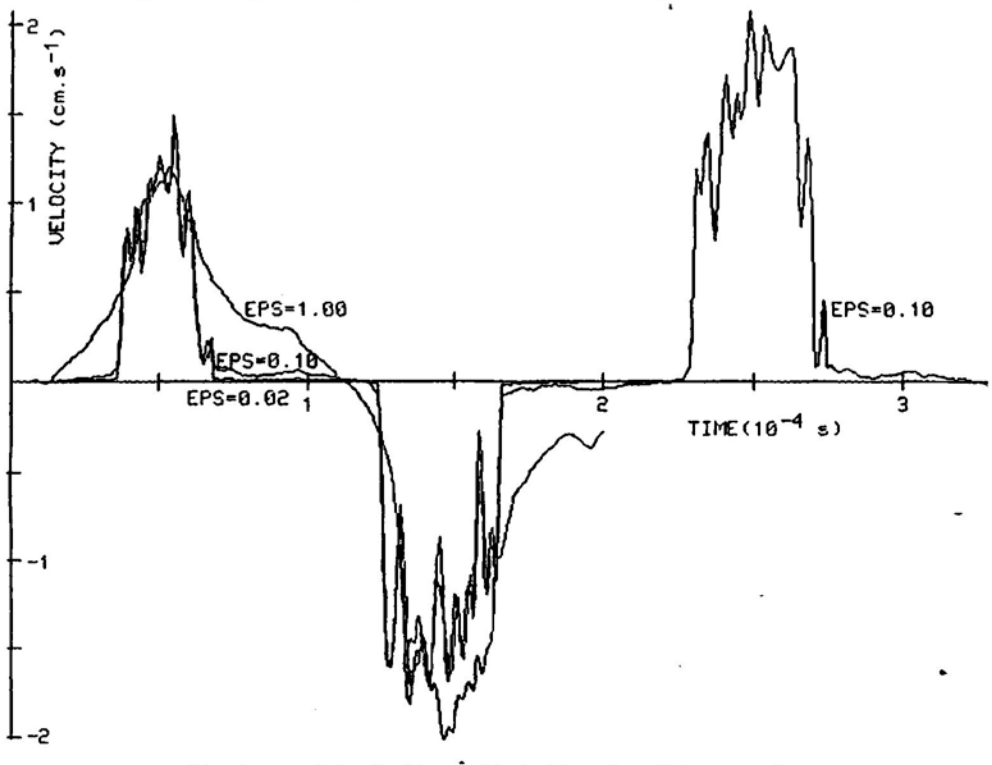

Fig. 56. Tangential velocities at Node 55, using different values of ε.

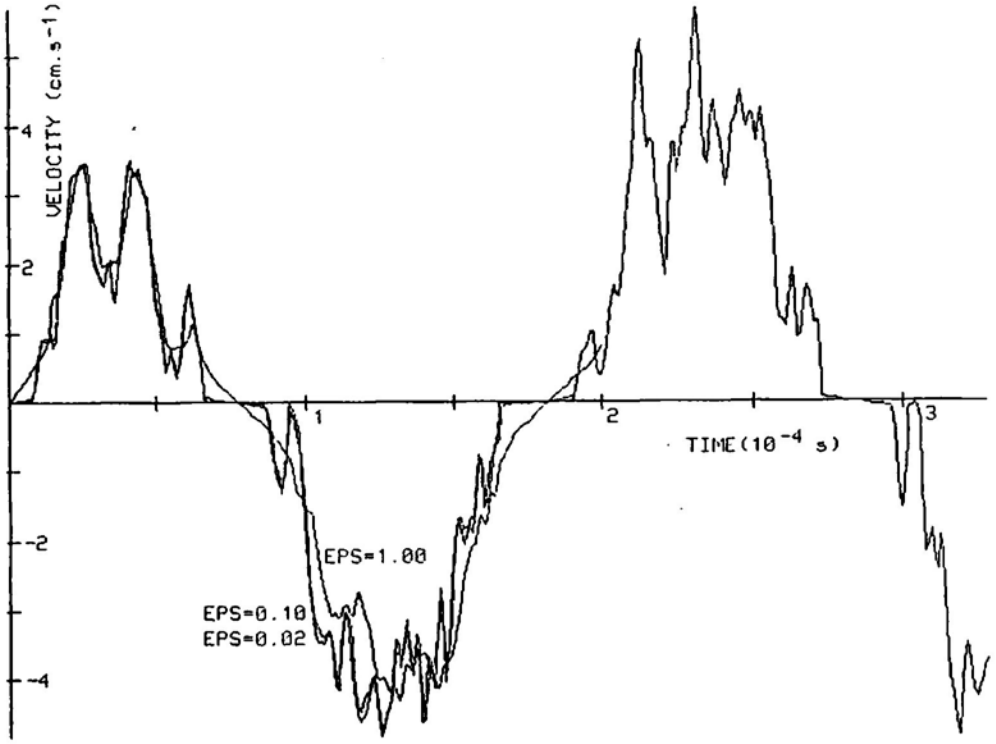

Fig. 57. Tangential velocities at Node 85, using different values of ε.

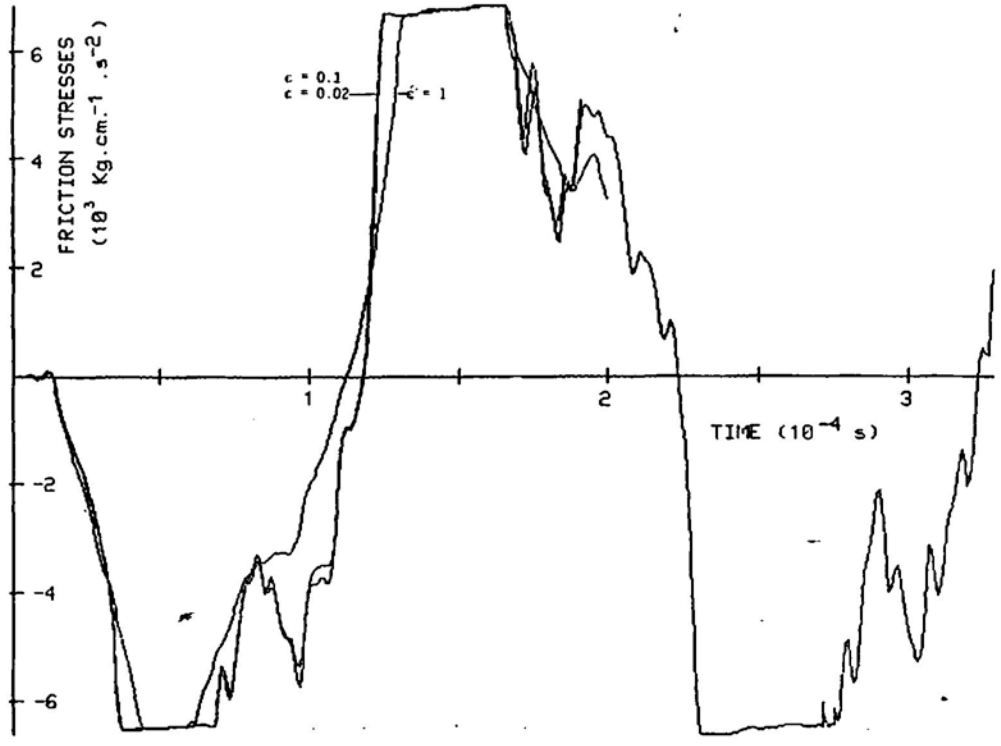

Fig. 58. Friction stress at Node 55 using different values of ε.

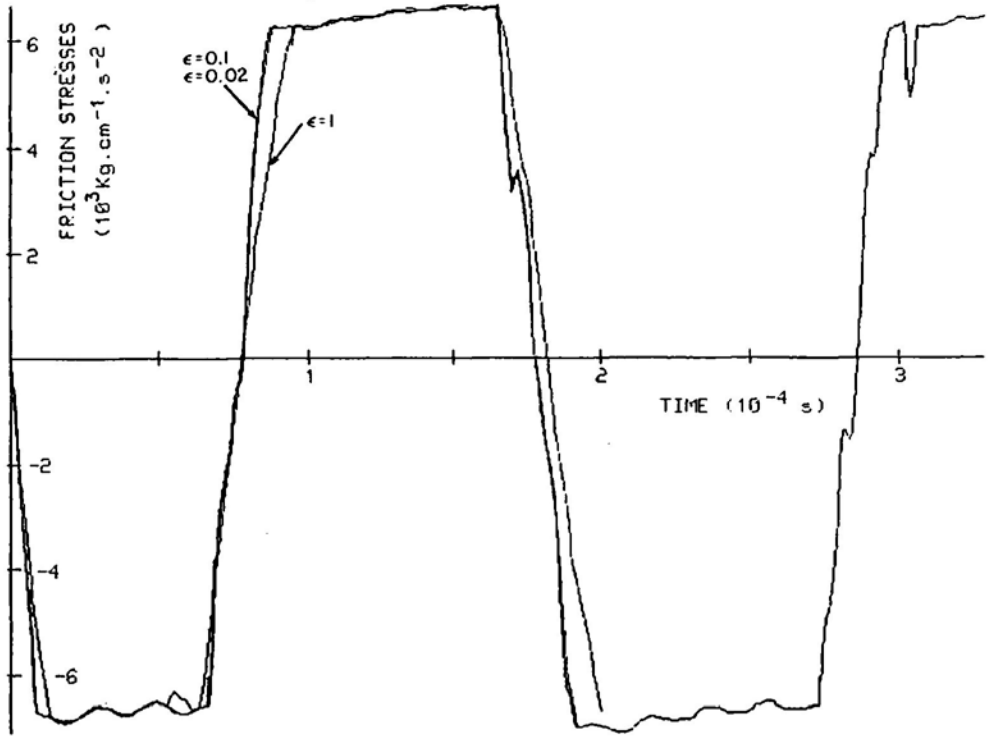

Fig. 59. Friction stresses at Node 85, using different values of ε.

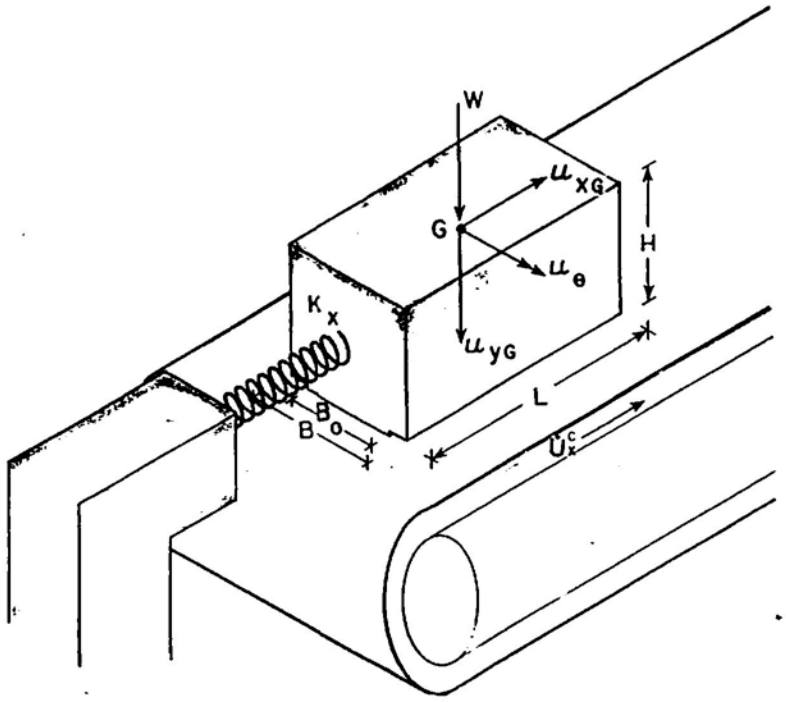

Fig. 60. A block sliding with friction on a moving belt.

system is shown in Figs. 60 and 61 where we have indicated as degrees-of-freedom the sliding and penetrating (normal) displacements u_{xG} and u_{yG} and the rotation u_θ.

Assuming small rotations and applying the same contact-interface laws used in our continuum interface model, we arrive at a (regularized) system of equations for this model which is again of the form

$$\boldsymbol{M}\ddot{\boldsymbol{r}}(t)+\boldsymbol{C}\dot{\boldsymbol{r}}(t)+\boldsymbol{K}\boldsymbol{r}(t)+\boldsymbol{P}(\boldsymbol{r}(t))+\boldsymbol{J}(\boldsymbol{r}(t),\dot{\boldsymbol{r}}(t))=\boldsymbol{F}, \tag{11.2}$$

where

$$\boldsymbol{M}=\begin{bmatrix} M & 0 & 0\\ 0 & M & 0\\ 0 & 0 & I\end{bmatrix},\quad \boldsymbol{C}=\begin{bmatrix} C_x & 0 & 0\\ 0 & C_y & 0\\ 0 & 0 & C_\theta\end{bmatrix},\quad \boldsymbol{K}=\begin{bmatrix} K_x & 0 & 0\\ 0 & 0 & 0\\ 0 & 0 & 0\end{bmatrix},\quad \boldsymbol{F}=\begin{Bmatrix} 0\\ W\\ 0\end{Bmatrix}.$$

$$\boldsymbol{P}=\begin{Bmatrix} 0\\ P_y\\ P_\theta\end{Bmatrix}=B_0c_n\int_{-L/2}^{L/2}[a(s)]^{m_n}\begin{Bmatrix} 0\\ 1\\ -s\end{Bmatrix}\mathrm{d}s$$

$$=B_0c_n\int_{-L/2}^{L/2}(u_{yG}-su_\theta)_+^{m_n}\begin{Bmatrix} 0\\ 1\\ -s\end{Bmatrix}\mathrm{d}s, \tag{11.3}$$

$$\boldsymbol{J}=\begin{Bmatrix} J_x\\ 0\\ J_\theta\end{Bmatrix}=B_0c_T\phi_\epsilon(\dot{u}_{xG}+\tfrac{1}{2}H\dot{u}_\theta-\dot{U}_x^C)\begin{Bmatrix} 1\\ 0\\ \frac{1}{2}H\end{Bmatrix}\int_{-L/2}^{L/2}(u_{yG}-su_\theta)_+^{m_T}\,\mathrm{d}s.$$

Here M is the mass of the body, W its weight, I its moment of inertia relative to the mass center, C_x, C_y, C_θ are damping coefficients introduced to model dissipation effects if needed, K_x the (tangential) spring stiffness, B_0 is the transverse width of the contact surfaces, L is the length of the sliding surface in the direction of sliding, $\frac{1}{2}H$ the height of the center of mass

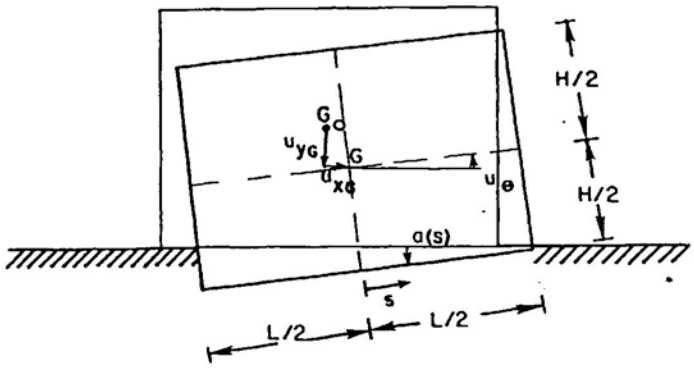

Fig. 61. The degrees of freedom and the contact penetration of a rigid block with plane motion.

above Γ_C, and the remaining terms are recognizable from our discussions in Sections 6–10. The penetrating approach at a point s on the contact surface is $a(s) = (u_{yG} - su_\theta)_+$.

We now use this to study the dynamic stability of steady sliding. By steady sliding we mean, with reference to Fig. 60, the static equilibrium position of the body in frictional contact with the moving belt. The equilibrium position is characterized by the equilibrium equation (set $\ddot{r} = \dot{r} = 0$ in (11.2))

$$\boldsymbol{K}\boldsymbol{r}_0 + \boldsymbol{P}(\boldsymbol{r}_0) + \boldsymbol{J}(\boldsymbol{r}_0, 0) = \boldsymbol{F}. \tag{11.4}$$

During stick-slip oscillations, the body does not stay in this equilibrium position, although at the conclusion of the 'stick part' of a cycle, one would expect the body to be in a state very close to such an equilibrium position. The questions that then arise are the following: does a solution for (11.4) exist?; is it unique?; how can it be computed?; is it dynamically stable? We will address here only the last two questions. While we hope to consider some questions of existence and uniqueness of the general problem in a later paper, our numerical results are physically reasonable and were obtained without computational difficulty.

In order to compute solutions of (11.4) for a certain range $[0, \bar{c}_T]$ of values of the parameter c_T, we subdivide the interval $[0, \bar{c}_T]$ into a prescribed number NINCT of increments $\Delta c_T = \bar{c}_T/\text{NINCT}$ and, for each increment, $K = 1, \ldots, \text{NINCT}$, we again solve the nonlinear system of equations (11.4) by the Newton–Raphson method. For the Newton process, starting values for the equilibrium solutions at the end of the Kth increment are taken to be the (converged) solution for the $(K-1)$th increment. The initial solution at $c_T = 0$ obviously corresponds to a frictionless unilateral contact problem of the type in (11.1).

Having computed the steady sliding equilibrium position for each value of c_T, we now explore the sensitivity of these equilibrium states to small perturbations. If in (11.2) we let

$$\boldsymbol{r}(t) = \boldsymbol{r}_0 + \boldsymbol{w}(t)$$

and subtract the equilibrium equation (11.4) from the resulting equation, we obtain

$$\boldsymbol{M}\ddot{\boldsymbol{w}} + \boldsymbol{C}\dot{\boldsymbol{w}} + \boldsymbol{K}\boldsymbol{w} + [\boldsymbol{P}(\boldsymbol{r}_0 + \boldsymbol{w}) - \boldsymbol{P}(\boldsymbol{r}_0)] + [\boldsymbol{J}(\boldsymbol{r}_0 + \boldsymbol{w}, \dot{\boldsymbol{w}}) - \boldsymbol{J}(\boldsymbol{r}_0, 0)] = \boldsymbol{0}. \tag{11.5}$$

Assuming that the perturbation $\boldsymbol{w}(t)$ is small, we consider only the linear contributions for the terms in brackets in the above equation:

$$\begin{aligned} &\boldsymbol{P}(\boldsymbol{r}_0 + \boldsymbol{w}) - \boldsymbol{P}(\boldsymbol{r}_0) \simeq \left.\frac{\partial \boldsymbol{P}}{\partial \boldsymbol{r}}\right|_{\boldsymbol{r}=\boldsymbol{r}_0} \boldsymbol{w} \overset{\text{df}}{=} \boldsymbol{K}^{\text{n}}(\boldsymbol{r}_0)\boldsymbol{w}, \\ &\boldsymbol{J}(\boldsymbol{r}_0 + \boldsymbol{w}, \dot{\boldsymbol{w}}) - \boldsymbol{J}(\boldsymbol{r}_0, 0) \simeq \left.\frac{\partial \boldsymbol{J}}{\partial \boldsymbol{r}}\right|_{\boldsymbol{r}=\boldsymbol{r}_0,\, \dot{\boldsymbol{r}}=0} \boldsymbol{w} + \left.\frac{\partial \boldsymbol{J}}{\partial \dot{\boldsymbol{r}}}\right|_{\boldsymbol{r}=\boldsymbol{r}_0,\, \dot{\boldsymbol{r}}=0} \dot{\boldsymbol{w}} \overset{\text{df}}{=} \boldsymbol{K}^{\text{Tn}}(\boldsymbol{r}_0, 0)\boldsymbol{w} + \boldsymbol{C}^{\text{T}}(\boldsymbol{r}_0, 0)\dot{\boldsymbol{w}}. \end{aligned} \tag{11.6}$$

The matrices $\boldsymbol{K}^{\text{n}}$, $\boldsymbol{K}^{\text{Tn}}$ and $\boldsymbol{C}^{\text{T}}$ are precisely the three-degrees-of-freedom analogs of the finite element matrices derived in Section 10. It also turns out that the matrix $\boldsymbol{C}^{\text{T}}(\boldsymbol{r}_0, 0)$ is null because, in the equilibrium positions of the body, the velocity of the body is zero but the

prescribed velocity of the moving belt is different from zero, $|\dot{U}_x^s| > \varepsilon > 0$. This means that the equilibrium points correspond to velocities on the horizontal branches of the friction law depicted in Fig. 50 and consequently the derivative of the friction stresses with respect to the sliding velocity is zero. This also means that the linearization of the equations of motion about the equilibrium position is independent of the regularization approximation used: we are outside neighborhoods of the discontinuity of Coulomb's friction law.

The final system of linearized equations for the small oscillations about the equilibrium position is then

$$\boldsymbol{M}\ddot{\boldsymbol{w}} + \boldsymbol{C}\dot{\boldsymbol{w}} + [\boldsymbol{K} + \boldsymbol{K}^{n} + \boldsymbol{K}^{Tn}]\boldsymbol{w} = \boldsymbol{0}\,. \tag{11.7}$$

The behavior of this linear system is determined by the solutions of the following quadratic eigenvalue problem:

$$[\lambda^2\boldsymbol{M} + \lambda\boldsymbol{C} + [\boldsymbol{K} + \boldsymbol{K}^{n} + \boldsymbol{K}^{Tn}]]\boldsymbol{W} = \boldsymbol{0}\,. \tag{11.8}$$

This system differs from standard structural dynamics eigenvalue problems because of the absence of symmetry due to friction effects entering the non-symmetric structure of the matrix $\boldsymbol{K}^{Tn}$. To illustrate numerically what can happen due to this lack of symmetry, we compute the equilibrium positions (11.4) of a block sliding on a moving surface, as shown in Fig. 60, for different values of c_T and for each of these positions we compute the corresponding eigenvalues for (11.8).

The data used are close to the experimental setting devised by Bell and Burdekin [13]. This does not mean that we will be trying to reproduce any experimental results: several geometrical features are distinct and other data (m_T, c_T, μ, I) are arbitrarily assumed or approximated from tables provided by other authors (e.g. c_n, m_n). For the time being, we are primarily concerned with qualitative behaviors of this simple system. The data used for our numerical experiments are the following:

$$\begin{aligned}
&K_x = 2388\ 10^3\ \text{Kg s}^{-2}, \qquad M = 450\ \text{Kg},\\
&I = \tfrac{1}{12}M(L^2 + H^2) = 124.2\ 10^3\ \text{Kg cm}^2\,,\\
&C_x = 0.0 \qquad C_y = 0.0;\ 57.16;\ 571.6;\ 5716\ 10^3\ \text{Kg s}^{-1}\,,\\
&C_\theta = 0.0;\ 1.388\times 10^4;\ 1.388\times 10^5;\ 1.388\times 10^6\ 10^3\ \text{Kg cm}^2\,\text{s}^{-1}\,,\\
&c_n = 10^{10}\ 10^3\ \text{Kg cm}^{-3.5}\,\text{s}^{-2}, \qquad m_n = m_T = 2.5, \qquad c_T = \mu c_n, \quad \mu \in [0, 1.6)\,,\\
&L = 48.8\ \text{cm}, \qquad H = 30.5\ \text{cm}, \qquad B_0 = 30.5\ \text{cm}\,,\\
&W = 450\ 10^3\ \text{Kg cm s}^{-2}\,.
\end{aligned} \tag{11.9}$$

We observe that the geometry of the problem and the conditions of support of the body imply that a necessary condition for equilibrium is that $\mu < L/H = 1.6$.

The values of the equilibrium displacements u_{xG}, u_{yG} and u_θ for the different values of μ are plotted in Fig. 62. It can be seen that u_{xG} increases linearly with μ and that u_{yG} and u_θ increase indefinitely as μ approaches 1.6.

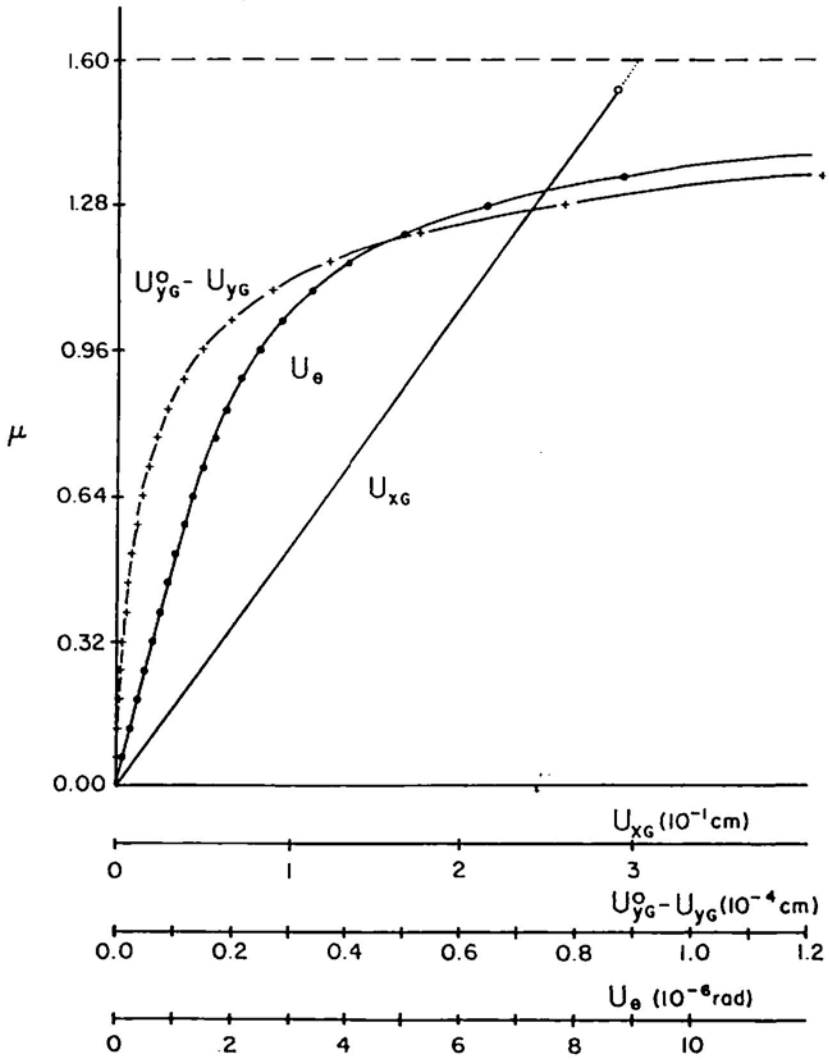

Fig. 62. Equilibrium displacements of a rigid block in steady sliding on a moving belt for the admissible values of the coefficient of friction.

Fig. 63 is a plot of the computed evolution in the complex plane of the eigenvalues associated with the normal and rotational degrees of freedom for the successive equilibrium positions obtained with increasing values of μ. In the absence of normal and rotational damping, these eigenvalues are found to be pure imaginary and distinct for $\mu = 0$. As μ is increased, at some value of μ they coalesce and start having real components symmetric with respect to the imaginary axis. At a larger value of μ they become pure imaginary again and a conjugate pair of the eigenvalues approaches the point $(0, 0)$ along the imaginary axis as $\mu \to 1.6$. This behavior as $\mu \to 1.6$ is exactly what should be expected since for $\mu = 1.6$ the equilibrium of the body cannot be sustained and the body acquires a free rigid body mode (tumbling). We also observe that for the geometric and stiffness properties of this problem the

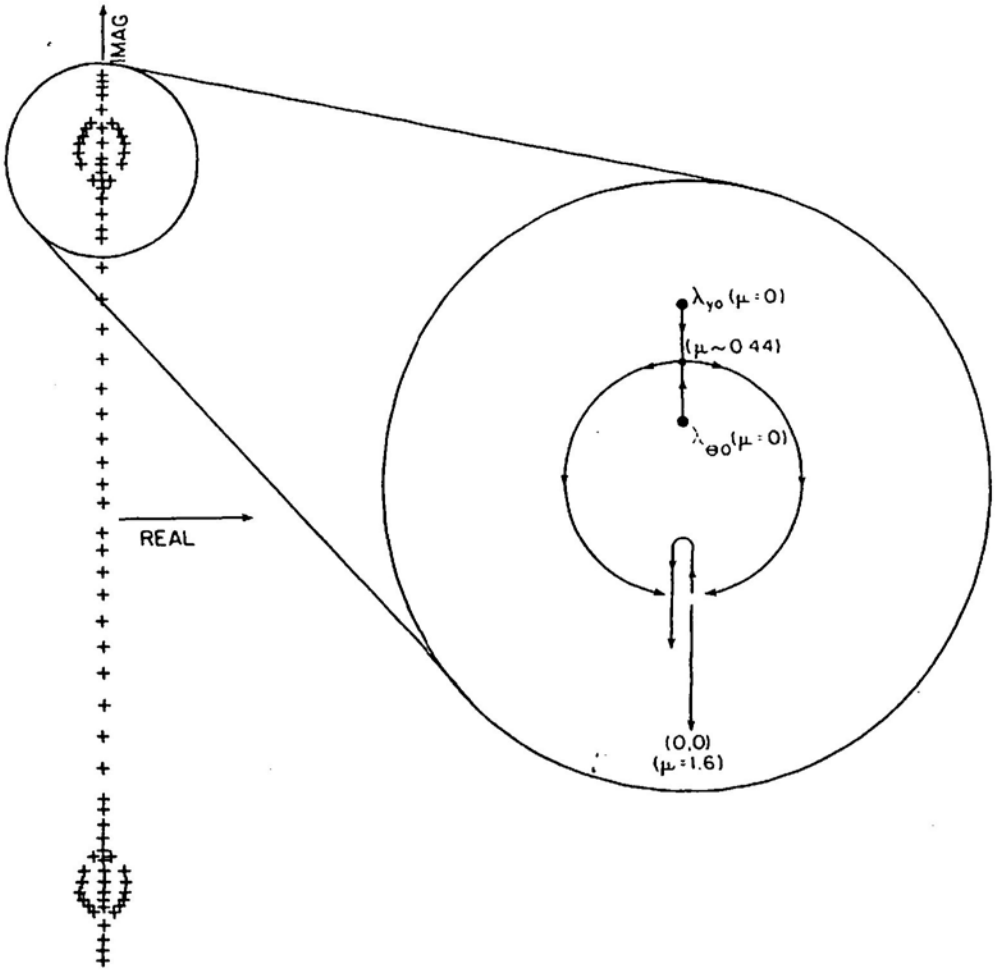

Fig. 63. Evolution of the eigenvalues on the complex plane for the successive equilibrium positions obtained with increasing coefficient of friction (no damping).

eigenvalues associated with the tangential degree of freedom are uncoupled with the normal and rotational freedoms and remain constant for all the values of μ.

However, the essential fact to be gained from this analysis is that *the non-symmetry of the frictional contact laws can produce, for sufficiently large values of the coefficient of friction, eigenvalues with positive real part which determine the dynamic instability of the steady sliding.* It can also be shown that, due to the uncoupling of the tangential mode *the introduction of external tangential damping* (C_x) *would not stabilize the system*; for viscous stabilization an external normal (C_y) and rotational (C_θ) damping are required. This behavior is made clear in the complex plane diagram of Fig. 64. The essential effect of such viscous damping is to shift the eigenvalues towards the negative real axis. For sufficiently high damping, all the eigenvalues associated with the normal and rotation freedoms, for all admissable values of μ, will have negative real parts.

A short note on the damping factors $\hat{\xi}_y$ and $\hat{\xi}_\theta$ in Fig. 64 is needed: these are merely indicators of the amount of damping introduced. They are defined using the natural frequen-

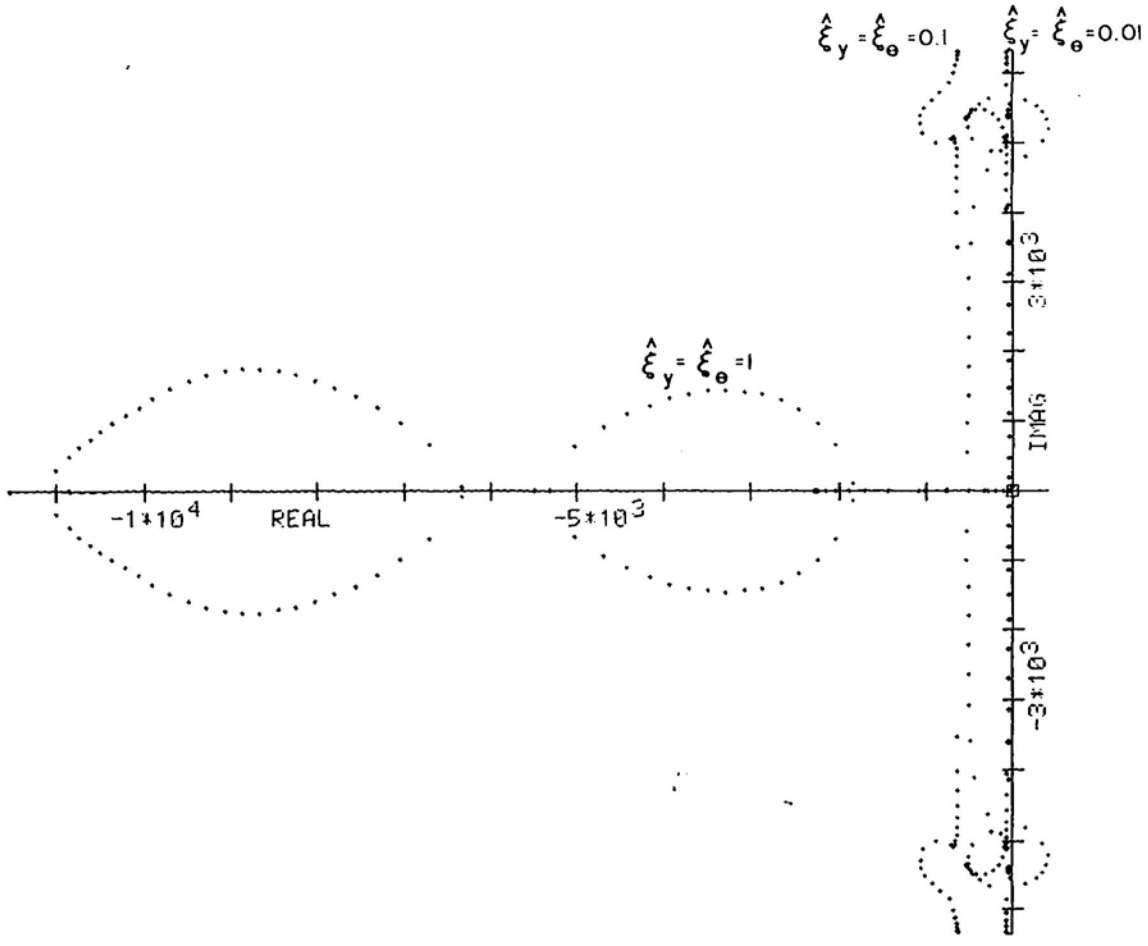

Fig. 64. Influence of the normal and rotational damping on the eigenvalues.

cies ω_{y0} and $\omega_{\theta 0}$ of the linearized system for the equilibrium position at $\mu = 0$: $\hat{\xi}_y = C_y/2M\omega_{y0}$; $\hat{\xi}_\theta = C_\theta/2I\omega_{\theta 0}$.

We will now show the effects of the eigenvalues structure of (11.8) on the motion of the rigid body. For each set of data, we perform a transient analysis of the motion of the body assuming that the initial conditions are the following: the displacements corresponding to the steady sliding equilibrium and a small perturbation on the velocities – an upwards translational velocity, i.e.,

$$\dot{r}(0) = \{0.0, -0.01\ \text{cm s}^{-1}, 0.0\}^t . \tag{11.10}$$

We first consider a case in which μ is smaller than the value at which some eigenvalues start to have real components. The data used are

$$\begin{aligned} &M, I, c_n, m_T, L, H, B_0, W \ \text{ as in (11.9)}, \\ &K_x = 11100\ 10^3\ \text{Kg s}^{-2}, \\ &c_T = \mu c_n, \quad \mu = 0.15, \qquad \dot{U}_x^c = 0.080\ \text{cm s}^{-1}, \end{aligned} \tag{11.11}$$

$$\Delta t_{max} = 1 \times 10^{-5}\,\text{s}, \qquad \varepsilon = 0.002\,\text{cm s}^{-1}. \tag{11.12}$$

In Figs. 65, 66 and 67 we show phase plane plots for the tangential (u_{xG}), normal (u_{yG}) and rotational (u_θ) displacements. It is clear that the resulting motion is a small-amplitude stable oscillation. Obviously, if we had considered some damping this oscillation would be damped out and the steady sliding would be essentially attained after a period of time.

A more interesting situation arises when μ is such that some eigenvalues have positive real parts. Starting from a basic data set and modifying, one at a time, several physical parameters, it was possible to assess the influence of these parameters on the dynamic responses obtained in this case. The data used are the following (when more than one value is given for some parameter, the first belongs to the basic data set):

$$L, H, c_n, m_n, m_T \text{ as in (11.9)},$$

$$K_x = 2388, 11100, 44410\ 10^3\,\text{Kg s}^{-2},$$

$$\begin{Bmatrix} M \\ I \end{Bmatrix} = \begin{Bmatrix} 450 \\ 70 \end{Bmatrix}, \begin{Bmatrix} 225 \\ 35 \end{Bmatrix}, \begin{Bmatrix} 900 \\ 140 \end{Bmatrix} \begin{matrix} \text{Kg} \\ 10^3\,\text{Kg cm}^2 \end{matrix},$$

$$\xi_x = C_x/2M\omega_x = 0.005, 0.05, 0.5, 1.6, 5,$$

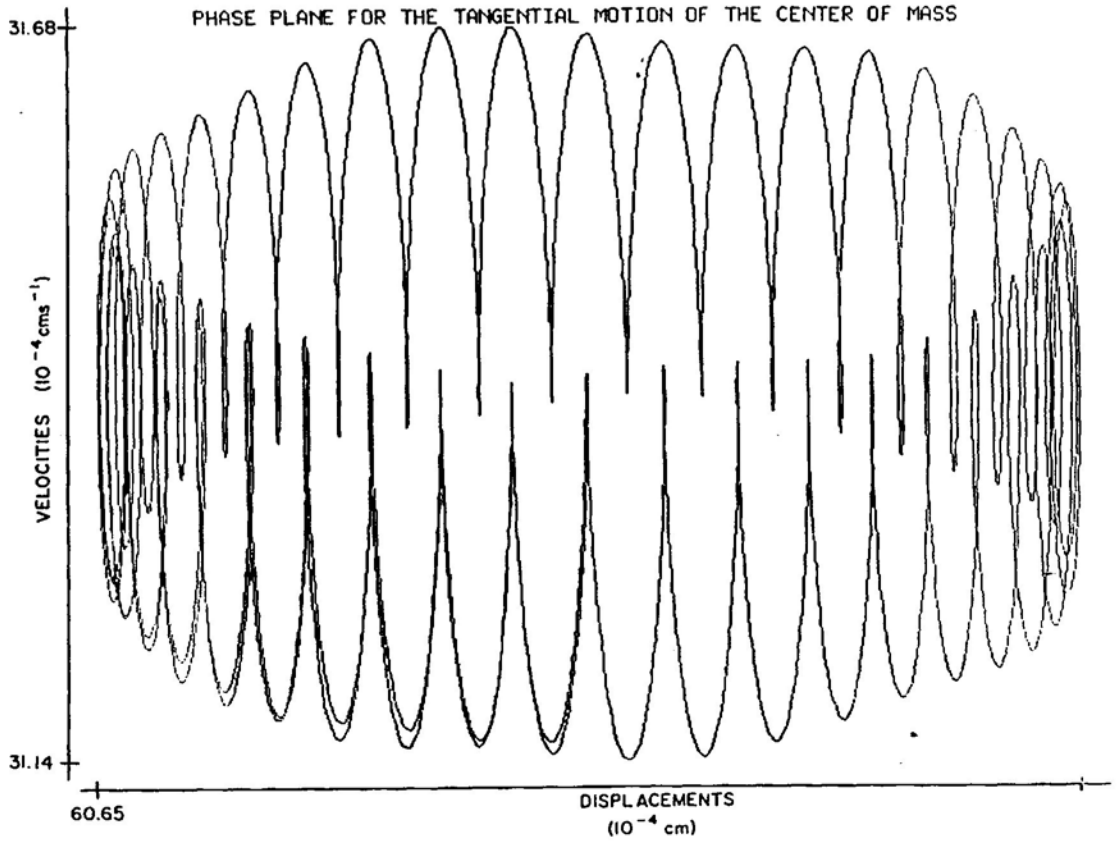

Fig. 65. Phase plane plot for the tangential motion of the center of mass ($\mu = 0.15$).

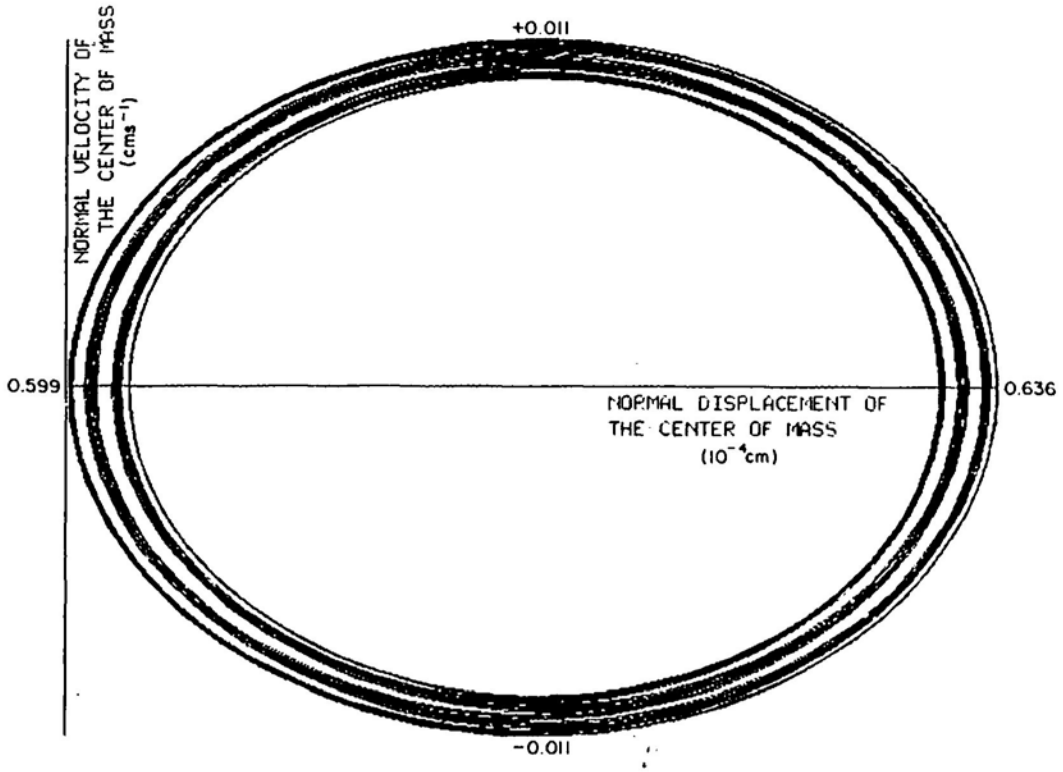

Fig. 66. Phase plane plot for the normal motion of the center of mass ($\mu = 0.15$).

$$\hat{\xi}_y = C_y/2M\omega_{y0} = 0.04, \qquad \hat{\xi}_\theta = c_\theta/2I\omega_{\theta 0} = 0.04,$$

$$B_0 = 14\,\text{cm}, \qquad c_T = \mu c_n, \quad \mu = 1,$$

$$\dot{U}_x^c = 0.127, 0.060, 0.220, 0.287\,\text{cm s}^{-1},$$

$$\Delta t_{\max} = 1 \times 10^{-5}\,\text{s}, \qquad \varepsilon/\dot{U}_x^c \in [0.07, 0.25].$$

The following remarks summarize our interpretation of the numerical results:

(i) Due to the instability of the normal and rotational modes, the normal and rotational oscillations grow (see Fig. 68).

(ii) The variation of the normal force on the contact produces changes in the sliding friction force which in turn produce a tangential oscillation.

(iii) The tangential oscillation may then become sufficiently large that, for small values of the velocity of the belt $\dot{U}_x^c$ the points of the body on the contact surface attain the velocity $\dot{U}_x^c$ and the body sticks for short intervals of time (see Fig. 69).

(iv) With the growing of the normal oscillation actual normal jumps of the body may occur (see Fig. 68).

(v) The repeated periods of adhesion have the result of decreasing the average value of the friction force on the contact and, due to the absence of equilibrium with the restoring force on

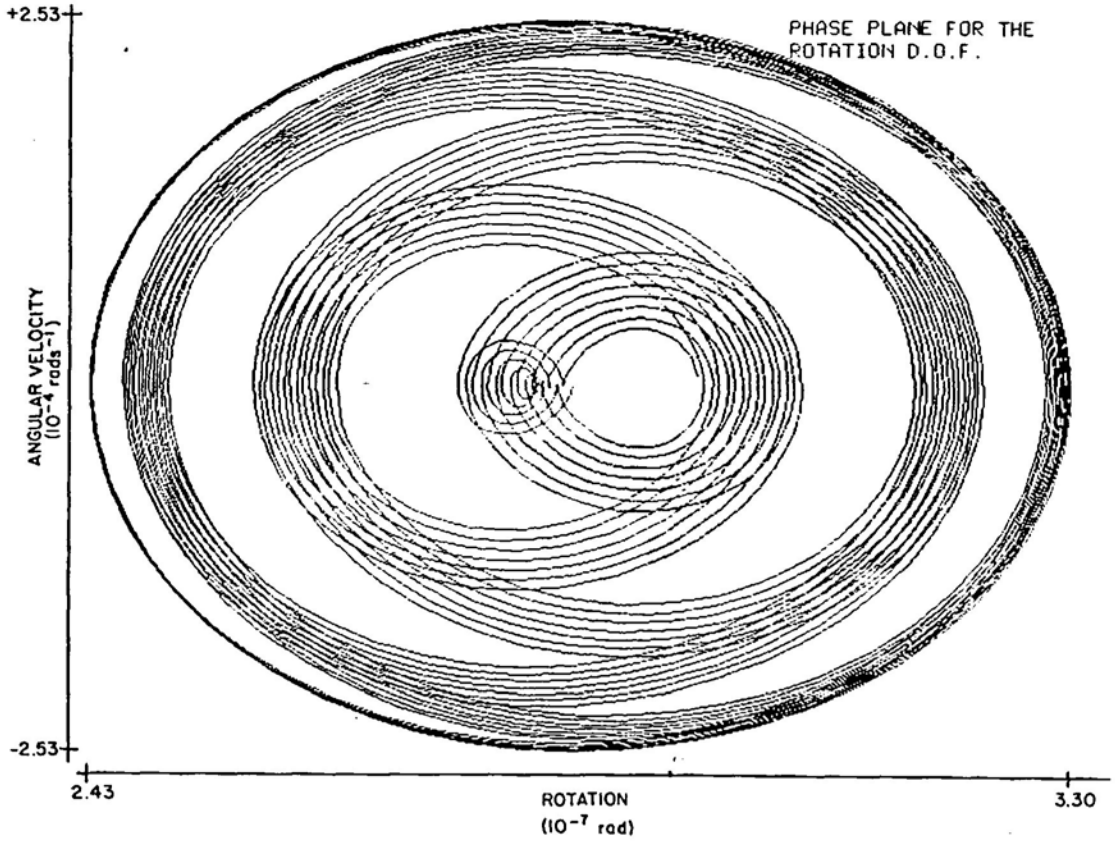

Fig. 67. Phase plane plot for the rotation of the center of mass ($\mu = 0.15$).

the tangential spring, the tangential displacement of the center of mass decreases (see Figs. 70–73).

(vi) Then, one of the two following situations may occur:

(a) the normal, rotational and tangential oscillations evolve to what appears to be a steady oscillation (see Fig. 74) with successive periods of adhesion and sliding, the average values of the friction force and of the spring elongation being smaller than those corresponding to the steady sliding equilibrium position (see Fig. 70, $\dot{U}_x^C = 0.287\,\text{cm s}^{-1}$);

(b) at a sufficiently small value of the spring elongation the normal and rotational damping are able to damp out the corresponding oscillations and the body sticks (see e.g. Fig. 72) since the restoring force of the spring is then smaller than the maximum available friction force.

Thus monitoring the spring elongations as is usually done in friction experiments, case (a) *would be perceived as an apparently smooth sliding with a coefficient of kinetic friction smaller than the coefficient of static friction and case* (b) *would be perceived as stick-slip motion.*

Fig. 70 shows that, as observed experimentally, an increase on the velocity $\dot{U}_x^C$ produces an increase of the frequency of the stick-slip motion and a decrease of the tangential displacement amplitude (for our data this decrease is small). It also shows that, as expected, the transition from stick-slip motion to an apparently smooth sliding occurs abruptly at some critical velocity

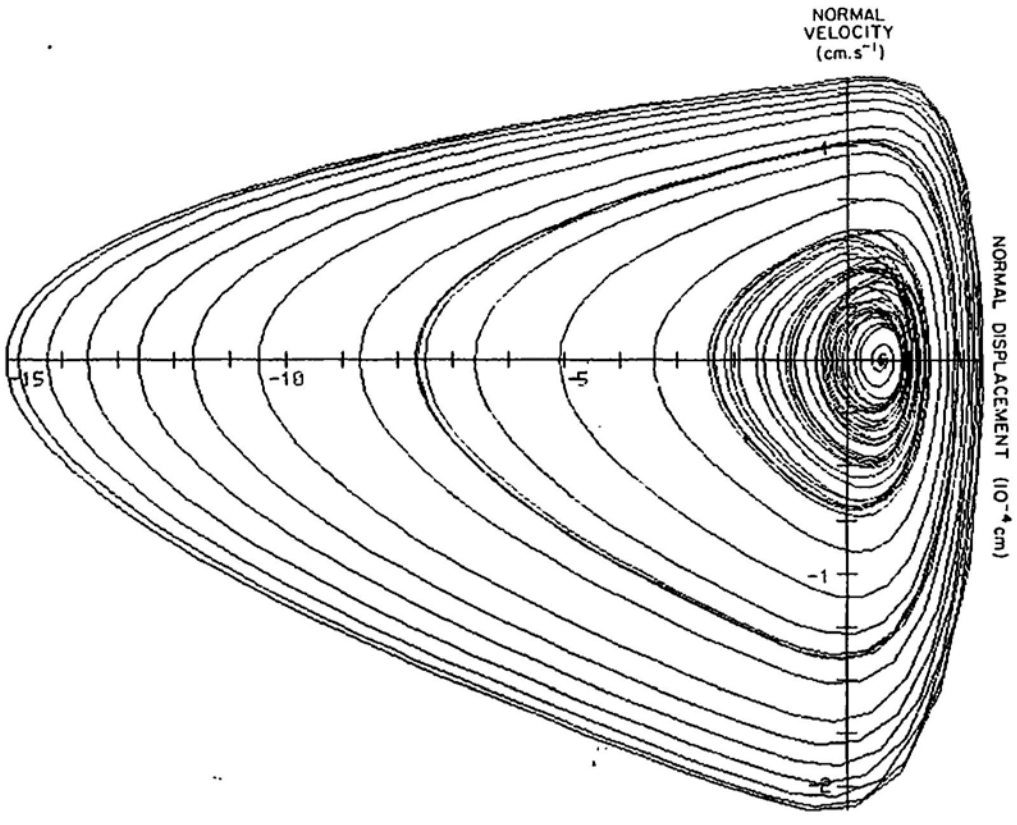

Fig. 68. Phase plane plot of the initial part of the normal oscillation of the center of mass ($\mu = 1$).

($\dot{U}_x^{cr} \simeq 0.240$ cm s^{-1}). However, for the data that we have used, that transition occurs when the stick-slip frequency ($\sim$1.5 Hz) is excessively small compared with the tangential natural frequency of the body ($\sim$11.6 Hz).

Fig. 71 shows that an increase in tangential damping produces a (small) decrease of the displacement amplitude and that sufficiently large tangential damping produces an apparently smooth sliding with an apparent coefficient of kinetic friction smaller than the coefficient of static friction (in agreement with observations of Tolstoi [103] mentioned earlier).

Figs. 72 and 73 show that, also as expected, decreases of the tangential displacements amplitude can be produced by increasing the tangential stiffness or by decreasing the mass.

11.3. A model for the normal contact dissipation

In Section 6.1, we remarked that if the sliding is not smooth and small ($\sim 10^4$ cm) normal jumps occur, it is possible that some plastic deformation of the asperities will take place. In the numerical experiments presented in the previous section, it appears that damping effects associated with normal and rotational degrees of freedom may play a role in the deceleration phase of the sliding portion of the stick-slip cycles. In the previous section, we assumed arbitrarily that all the damping effects different from dry friction could be simulated by linear

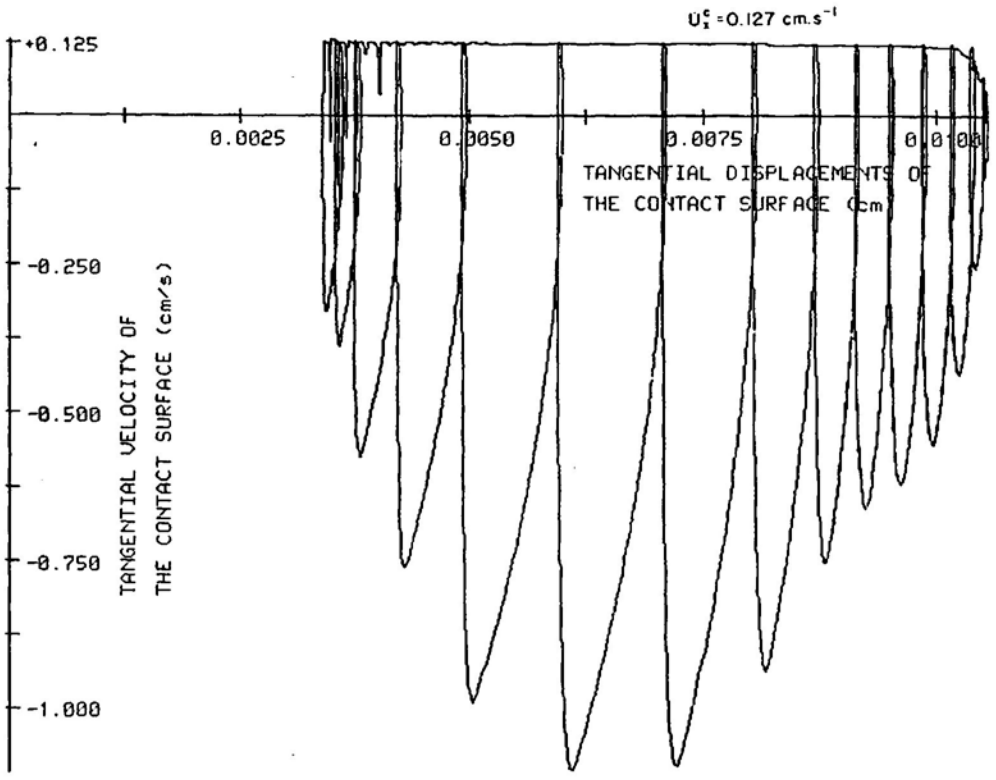

Fig. 69. Phase plane plot of the tangential motion of the points of the block on the contact surface ($\mu = 1$, $K_x = 4.441 \times 10^7\,\mathrm{kg\,s^{-2}}$).

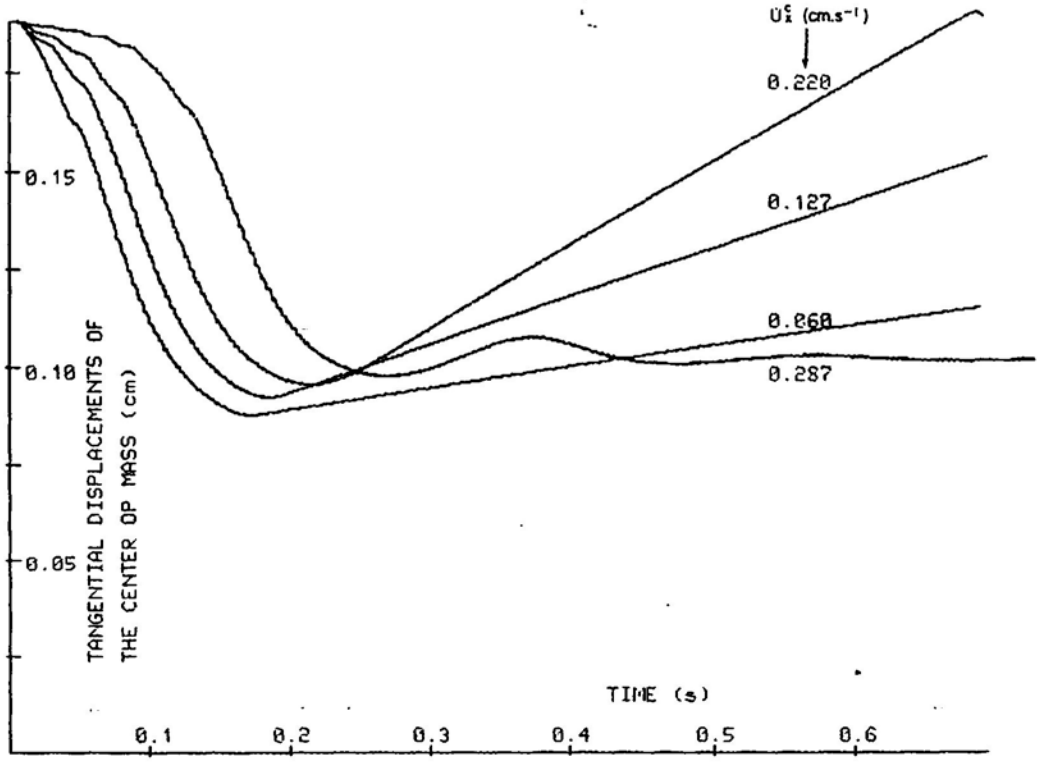

Fig. 70. Influence of the velocity of the support on the tangential motion of the center of mass ($\mu = 1$).

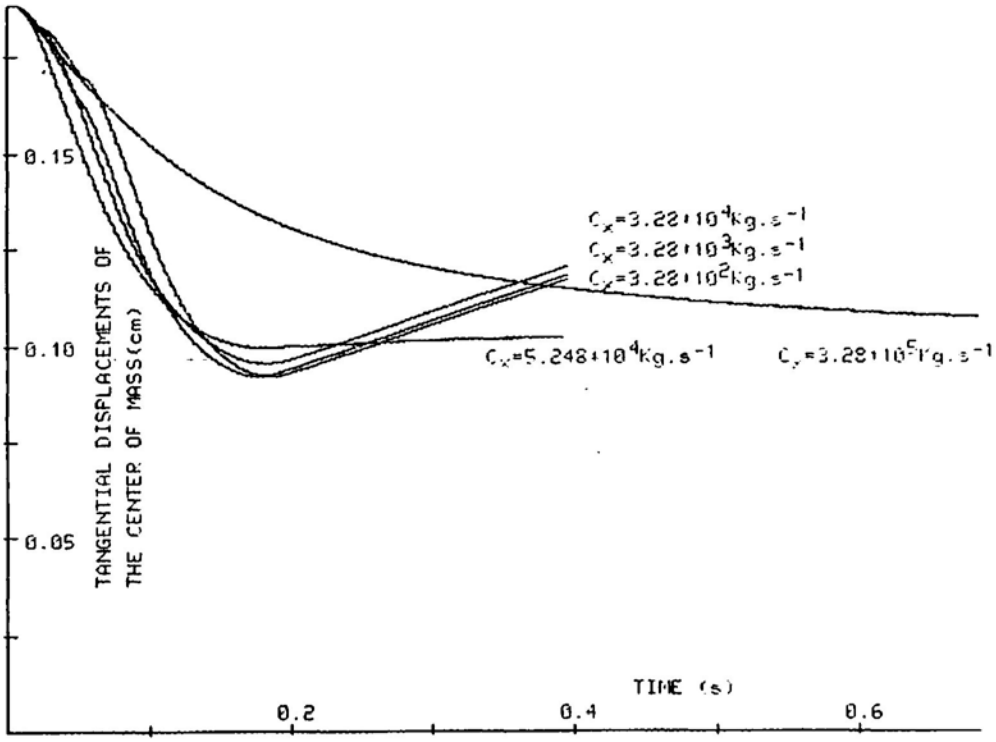

Fig. 71. Influence of the tangential damping on the tangential motion of the center of mass ($\mu = 1$).

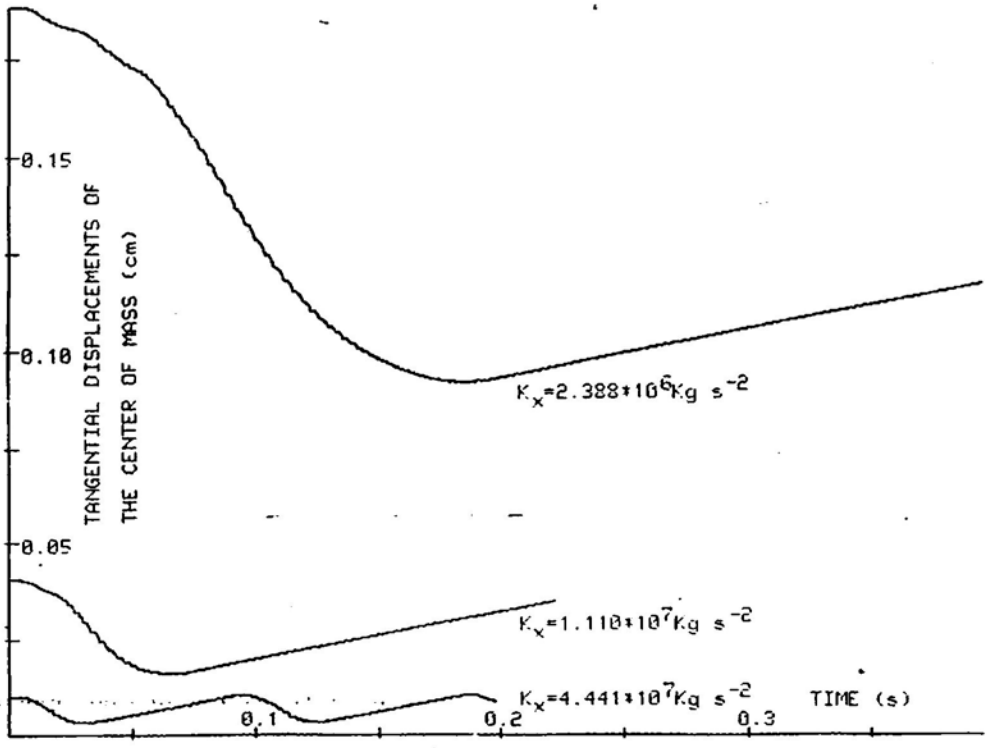

Fig. 72. Influence of the tangential stiffness on the tangential motion of the center of mass ($\mu = 1$).

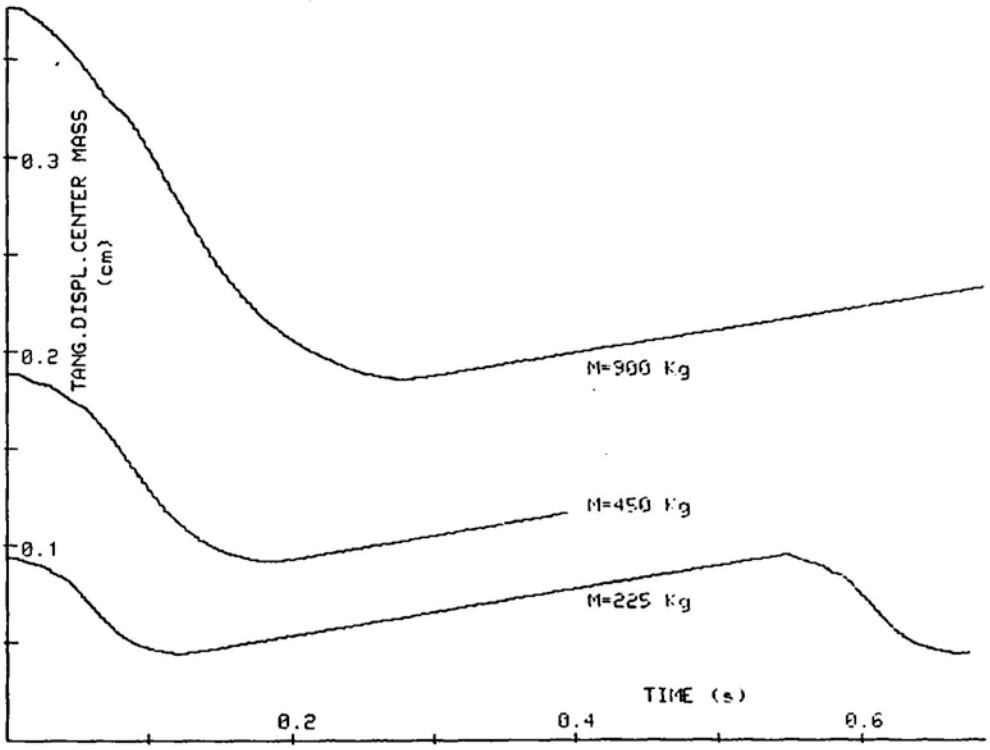

Fig. 73. Influence of the mass of the body on the tangential motion of the center of mass ($\mu = 1$).

viscosity. A consequence of that assumption is the fact, visible e.g. in Fig. 68, that normal and rotational damping act not only during contact but also while the body jumps. On the other hand, trying to formulate a detailed model of the normal elasto-plastic behavior of the asperities to apply in dynamic situations expected to have not too severe dissipative effects does not seem to be worthwhile.

We can borrow one idea for a simple model of such effects from an analysis of vibroimpact phenomena and impact damping by Hunt and Crossley [46]. The key point is to model hysteresis loops of the form presented in Fig. 75(a), which may occur if the surfaces in contact are allowed to unload completely [100], by approximate loops of the form presented in Fig. 75(b).

If the normal elastic pressure-penetration curve is of the power law type ($p = c_n a^{m_n}$) possible additional dissipative terms that can produce loops of the type indicated in Fig. 75(b) can be taken of the form $b_n a^{l_n} \dot{a}$ where a is the penetrating approach and b_n is a nonlinear damping coefficient to be determined experimentally.

Hunt and Crossley [46] do propose for macroscopic Hertzian contacts slight generalizations of the term adopted here and they also show that for the case $l_n = m_n$ and small energy losses the correlation between the energy loss per cycle of contact and the damping coefficient b_n is very simple.

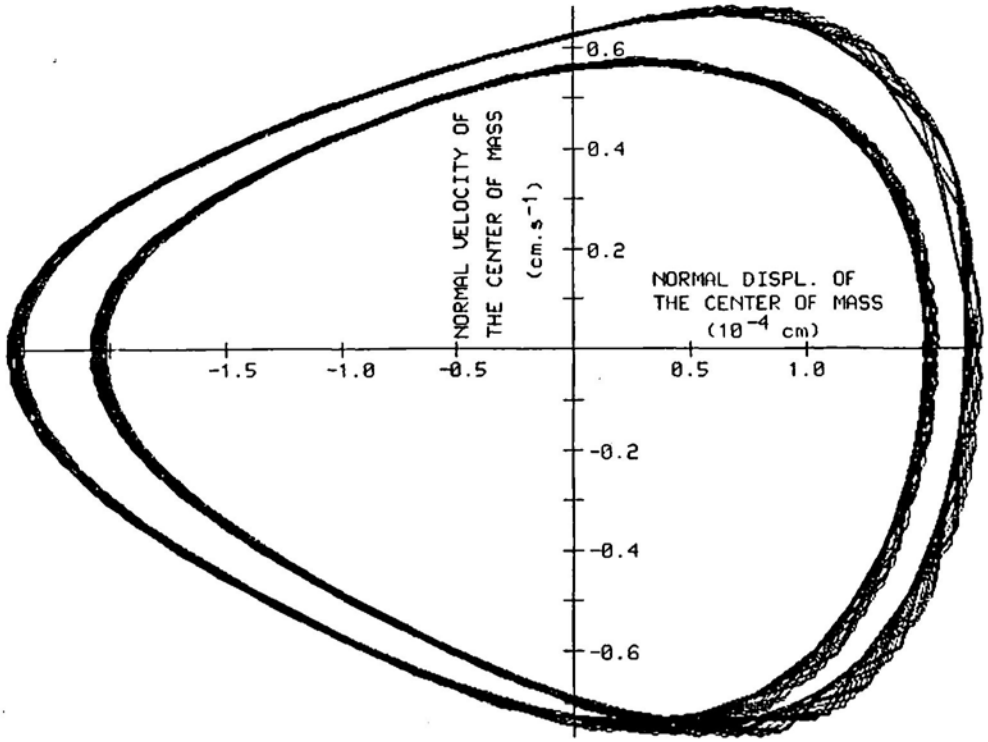

Fig. 74. Phase plane plot of the steady normal oscillation obtained during apparently smooth sliding with an apparent coefficient of kinetic friction lower than the coefficient of static friction ($\mu = 1$, $\dot{U}_x^C = 0.287\,\mathrm{cm\,s^{-1}}$).

With this new term, the normal contact law (6.4) for our continuum model becomes

$$-\sigma_n = c_n(u_n - g)_+^{m_n} + b_n(u_n - g)_+^{l_n}\dot{u}_n\,. \tag{11.13}$$

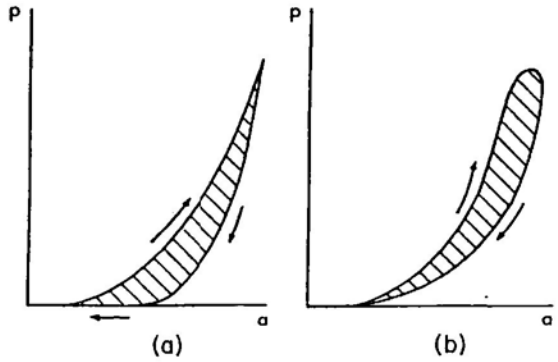

Fig. 75. Hysteresis loops for the normal deformation of the interface (schematic). (a) Experimentally observed loop, under quasi-static loading conditions, if total separation of the surface is allowed during unloadings; (b) Hysteresis loop modelled by the constitutive equation (11.13) under dynamic loading conditions.

Accordingly, a new term must be included on the left-hand side of the variational statements (8.1), (8.13):

$$\langle Q(u, \dot{u}), v\rangle = \int_{\Gamma_C} b_n(u_n - g)_+^{l_n} \dot{u}_n v_n \, ds \,. \tag{11.14}$$

Obviously for the case of the three-dimensional domain, restrictions must be placed upon l_n in order for the integral in the above expression to be well defined.

The above term does not introduce any other complication or restriction on either the finite elements discretization nor on the algorithms described earlier. In Figs. 76, 77 we show the hysteresis loops obtained for the case of the rigid body model with the geometric, mass and contact properties (11.9) used in the previous section, for typical values of the impact velocities $\dot{u}_y^i$, two values for the constant b_n and $l_n = m_n = 2.5$.

We also have checked that complex plane diagrams of the type of Fig. 64 could also be obtained with this type of damping and that the typical stick-slip motion curves of the type of Figs. 70–73 can also be obtained with this more realistic nonlinear damping term.

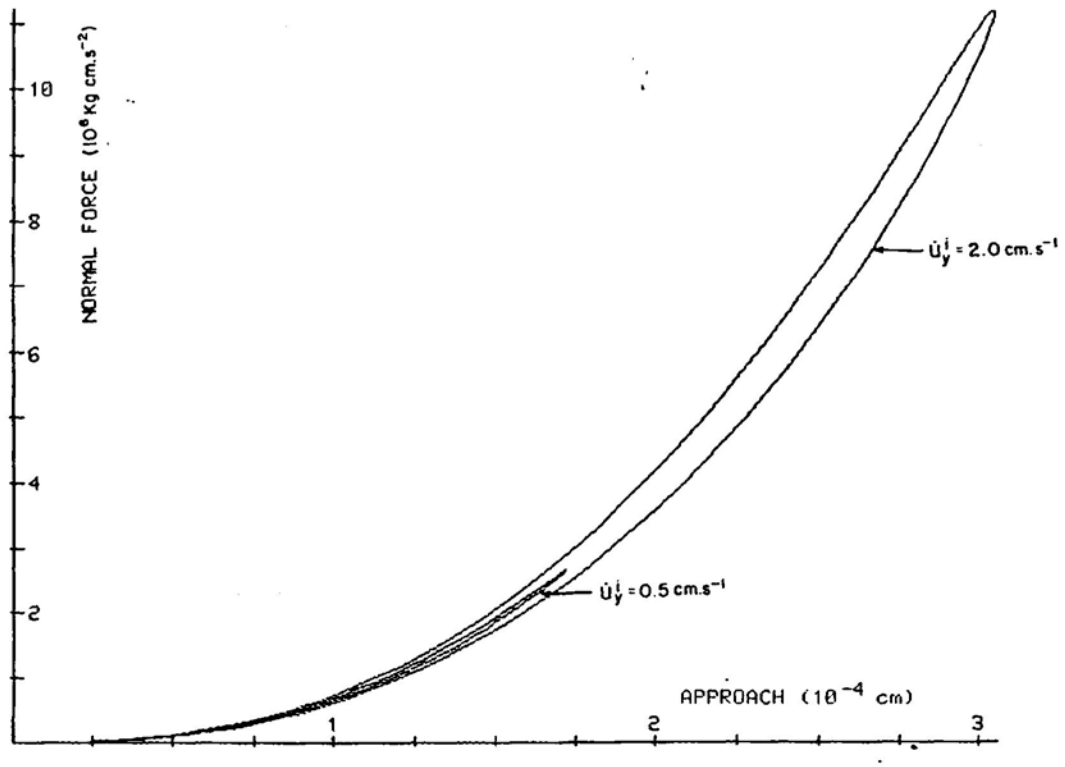

Fig. 76. Hysteresis loops for typical impact velocities $\dot{u}_y^i = 0.5$; 2.0 cm s^{-1} ($b_n = 4.35 \times 10^8$ (10^3 kg cm$^{-4.5}$ s^{-1}); $l_n = 2.5$).

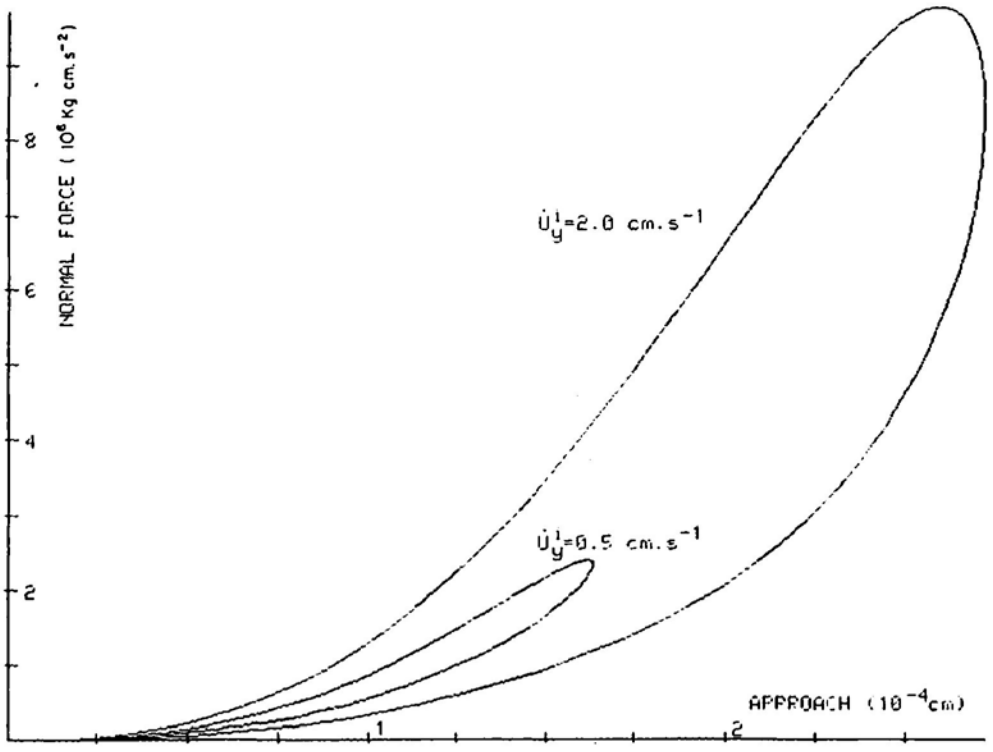

Fig. 77. Hysteresis loops for typical impact velocities $\dot{u}_y^i = 0.5; 2.0\,\mathrm{cm\,s^{-1}}$ ($b = 4.35 \times 10^9$ ($10^3\,\mathrm{kg\,cm^{-4.5}\,s^{-1}}$); $l_n = 2.5$).

11.4. The steady sliding of a linearly elastic body and its dynamic stability

All the computations performed in Section 11.2 with a rigid body can also be done with finite element models of linearly elastic bodies. The essential effects observed there are also observed here.

In order to compare the results of both the computations, we consider the block of Fig. 60 as a linearly elastic body and assume a plane strain state. The geometry, total mass, total tangential stiffness and contact properties are those given by the data (11.9). The Young's modulus is $E = 1.4 \times 10^6$ ($10^3\,\mathrm{Kg\,cm^{-1}\,s^{-2}}$) and the Poisson's ratio is $\nu = 0.25$.

The finite elements mesh used consists of 4×3 nine-node isoparametric elements. In Fig. 78 we show the deformed mesh configurations for the steady sliding equilibrium positions at several values of the coefficient of friction μ. As expected, for the level of forces in presence, the block behaves much like a rigid body.

As in Section 11.2 we have also computed the eigenvalues of (11.8) for the successive equilibrium positions at values of $\mu \in [0, 1.6)$, under the assumption of no damping. In Fig. 79 we compare the rigid body model eigenvalues associated with the normal and rotation displacements with those from the finite elements model which are associated with similar modes. The results are very close, showing that the deformability of the body reduces slightly the imaginary components. All the eigenvalues in the first quadrant of the complex plane are plotted in Fig. 80. It can be observed that in addition to those corresponding to the rigid body normal and rotational displacements, there are other unstable eigenvalues with larger im-

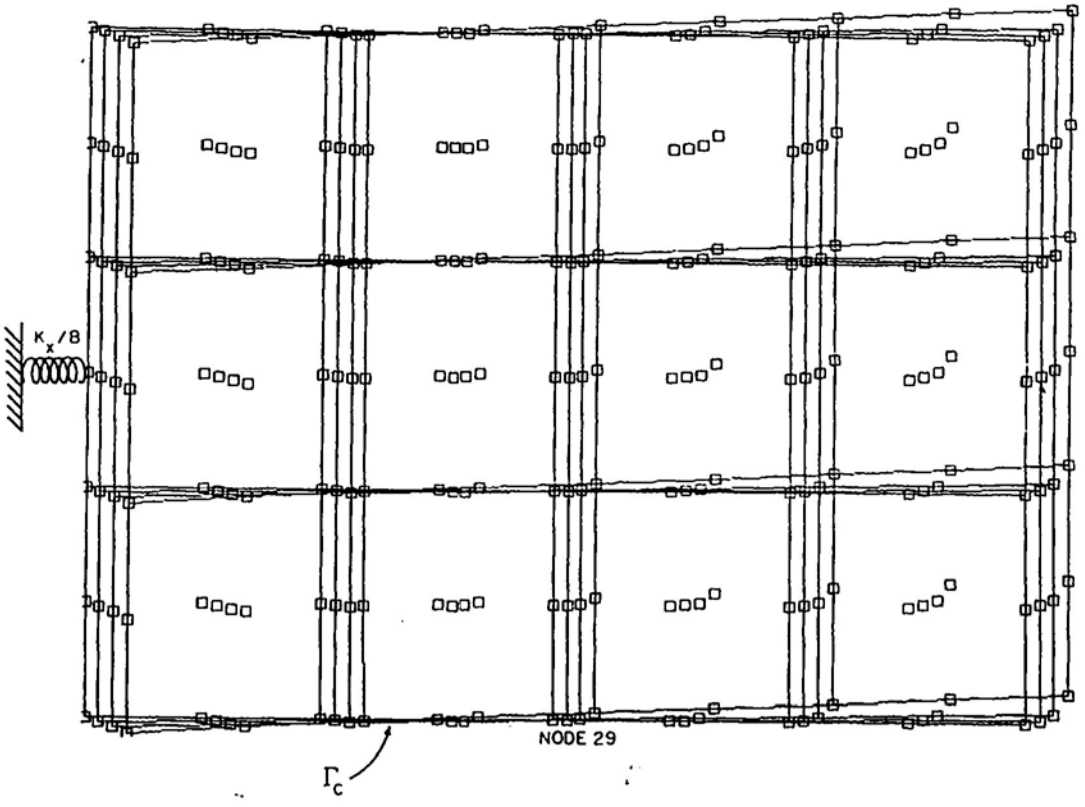

Fig. 78. Deformed configurations of a linearly elastic block for the steady sliding equilibrium configurations at several values of μ. (*Note*: Nodal coordinates and nodal displacements are not to scale – the apparent distortion of the body results from an amplification of the vertical displacements 10^3 larger than the one used for the horizontal displacements; this was needed in order to make visible the rotation of the body.)

aginary components and that one of them does appear for values of μ below the value at which the rigid body instability initiates.

Similar computations were also performed for a case where no rigid body motions of the elastic body could occur. The body is a slab similar to the one presented in Fig. 51. The material and normal contact properties and the boundary conditions on Γ_D are the same as those in Section 11.1. The dimensions are now $16\,\text{cm} \times 1\,\text{cm}$ and the finite elements mesh consists of 9×2 nine-node isoparametric elements. The initial negative normal gap on Γ_C was taken successively to be 5×10^{-4} cm and 1×10^{-3} cm. The 'rigid' flat surface that compresses the body along Γ_C is assumed to have a velocity towards the right. Deformed mesh configurations and distributions of normal stresses on Γ_C are shown in Figs. 81 and 82 for $g = -1 \times 10^{-3}$ cm. The effect of the increase of the compression on the real parts of the eigenvalues is shown in Fig. 83: larger compression produces increased instability.

Our final numerical examples consist of obtaining the dynamic response of the block of Fig. 60 assuming that it is linearly elastic and that it starts from the perturbed equilibrium position considered earlier in Section 11.2.

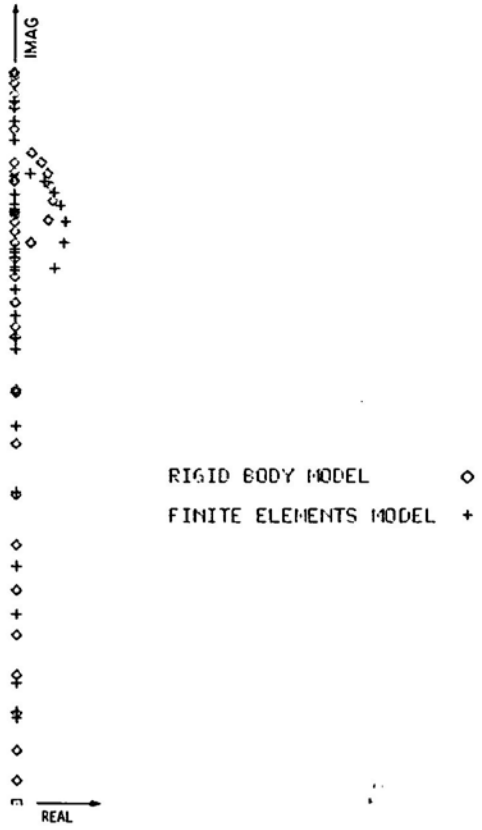

Fig. 79. Comparison of the eigenvalues associated with 'normal and rotational displacements' obtained with the rigid body and the finite elements models.

In these examples we will use the central-difference method with a diagonalized mass matrix. The maximum time step used is $\Delta t_{max} = 3 \times 10^{-6}$ s.

The geometry, normal contact properties and total mass are again as in (11.9). We will now assume the total tangential stiffness K_x equal to 11100 (10^3 Kg s^{-2}), the coefficient of friction μ equal to 0.15 or 0.60 and the velocity $\dot{U}_x^c$ successively equal to 0.01, 0.08, 0.80 cm s^{-1}. No damping effects will be considered when modelling the interior of the linearly elastic body.

We observe that for $\mu = 0.15$ all the eigenvalues are still imaginary (in the absence of any damping). Perturbing the equilibrium position a small stable oscillation is obtained exactly as in the rigid body case. For this reason we do not reproduce here the corresponding plots.

For the case $\mu = 0.6$ (some eigenvalues with positive real parts) we have assumed normal dissipation effects on the contact boundary of the form described in Section 11.3 with $b_n = 0.381 \times 10^{10}$ (10^3 Kg $cm^{-4.5}$ s^{-1}) and $l_n = 2.5$. The description of the motion of the body is essentially the same given for the rigid body case.

The evolution of the elongation of the spring is shown in Fig. 84 for the three velocities $\dot{U}_x^c$ considered. The decrease of the amplitude of the stick-slip motion with the increase of $\dot{U}_x^c$ is again observed. In Fig. 85 we show a phase plane plot of the normal oscillations of the contact

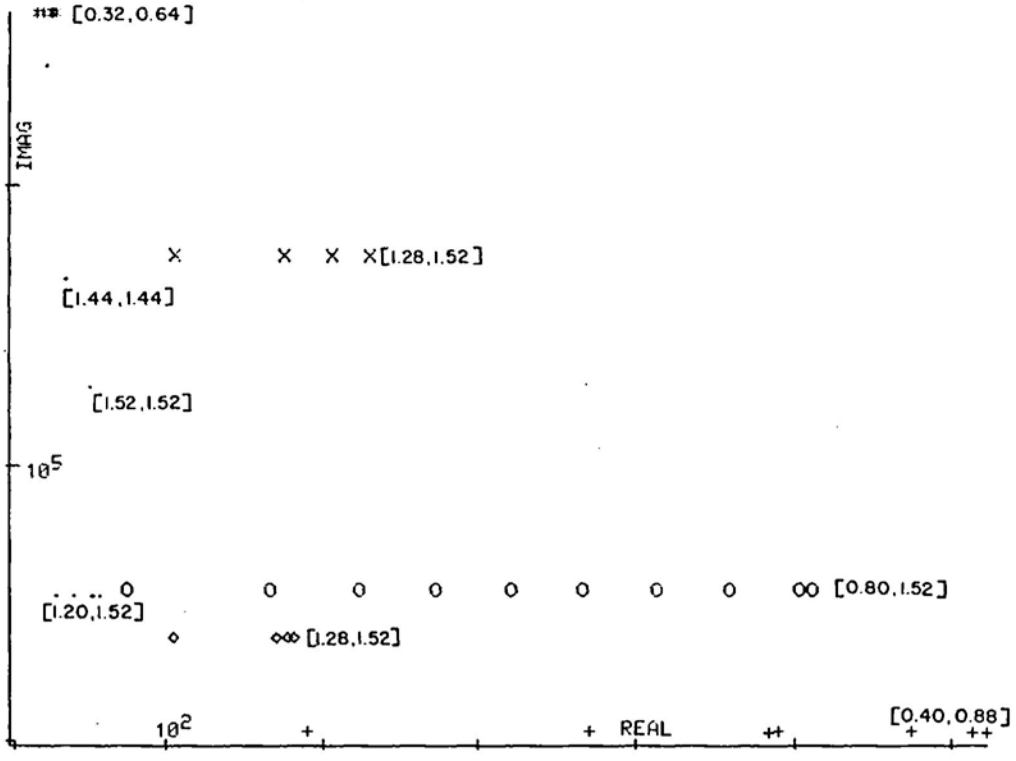

Fig. 80. Eigenvalues with positive real parts for a finite elements discretization of a block in steady sliding on a moving belt. (The ranges of μ for which those eigenvalues were obtained are indicated in the figure between brackets.) NINCT = 20; $\mu \in [0, 1.6)$. Maximum value of μ for which the equilibrium solution was successfully computed: $\bar{\mu} = 1.52$. + Eigenvalues corresponding to the 'rigid body' normal and rotational modes.

Node 29 and in Figs. 86 and 87 we show the evolution of the normal and friction stresses on the same node. In order to assure the reader that the numerous spikes in Figs. 86 and 87 are not erroneous we show in Figs. 88 and 89 what one of those spikes may look like. In Fig. 89 the occurrence at each cycle of contact of periods of adhesion and sliding is indicated. It is also important to observe that having used values for the normal contact properties (c_n, m_n) taken from Table 1 of [9] and having considered a block with dimensions and weight close to those used by Bell and Burdekin [13], it turns out that the frequency of the normal contact oscillations observed in Figs. 85, 86 and 88 is of the order of magnitude indicated by Tolstoi [103] as typical: 10^3 Hz.

For the case of the larger velocity ($\dot{U}_x^C = 0.8\,\mathrm{cm\,s^{-1}}$) that velocity is sufficiently large that the tangential oscillation of the body is not sufficient to produce any stick state. Consequently the average coefficient of friction during sliding is equal to the static coefficient of friction. We note also that the instability of the equilibrium position makes it impossible for the contact damping to damp out the normal oscillation. A steady self-excited oscillation is then attained. That can be observed in Fig. 89 (horizontal oscillation of the node connected to the spring) and in Fig. 90 (normal oscillation of the contact Node 29). In our computations we have

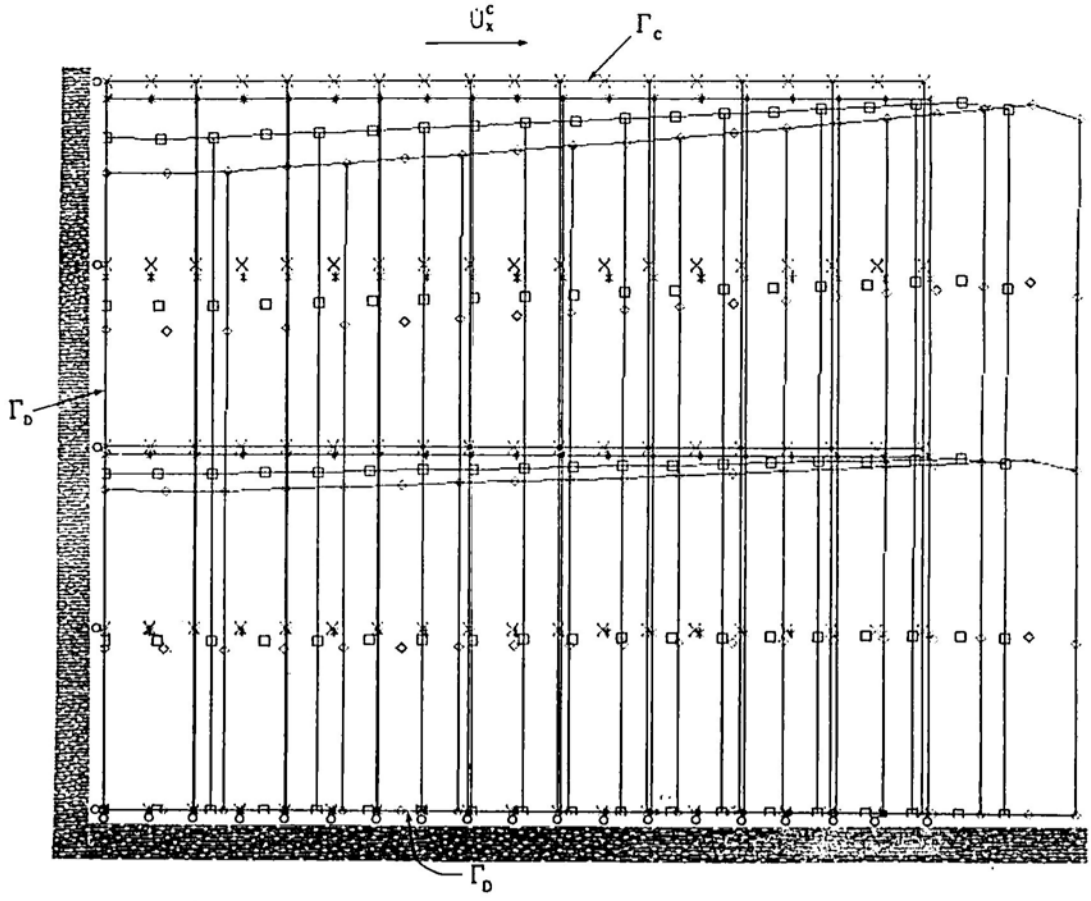

Fig. 81. Undeformed (×), and deformed mesh configurations of a compressed slab in steady sliding equilibrium for $\mu = 0$ (*), $\mu = 0.5$ (□), and $\mu = 1.0$ (◇).

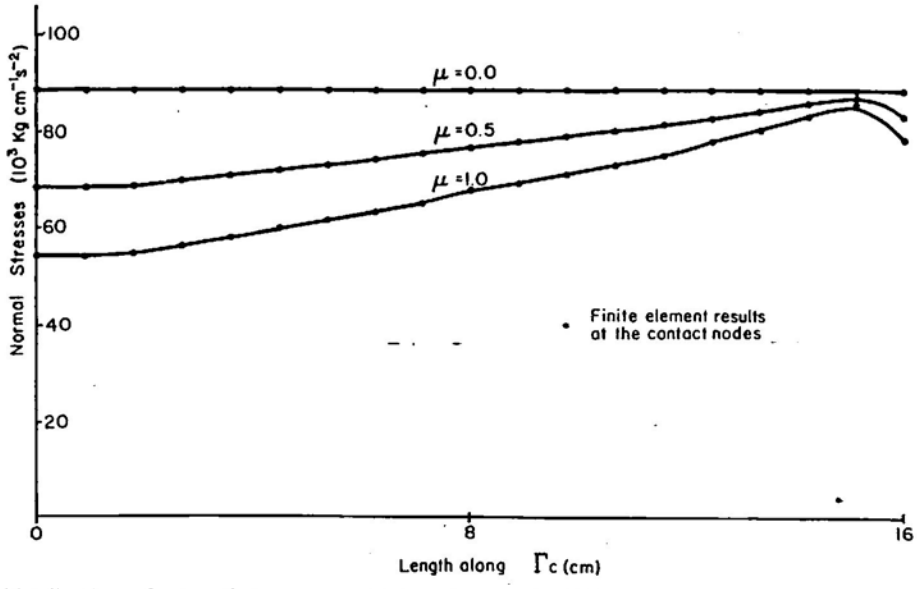

Fig. 82. Distribution of normal stresses on Γ_c for the steady sliding equilibrium at various values of μ.

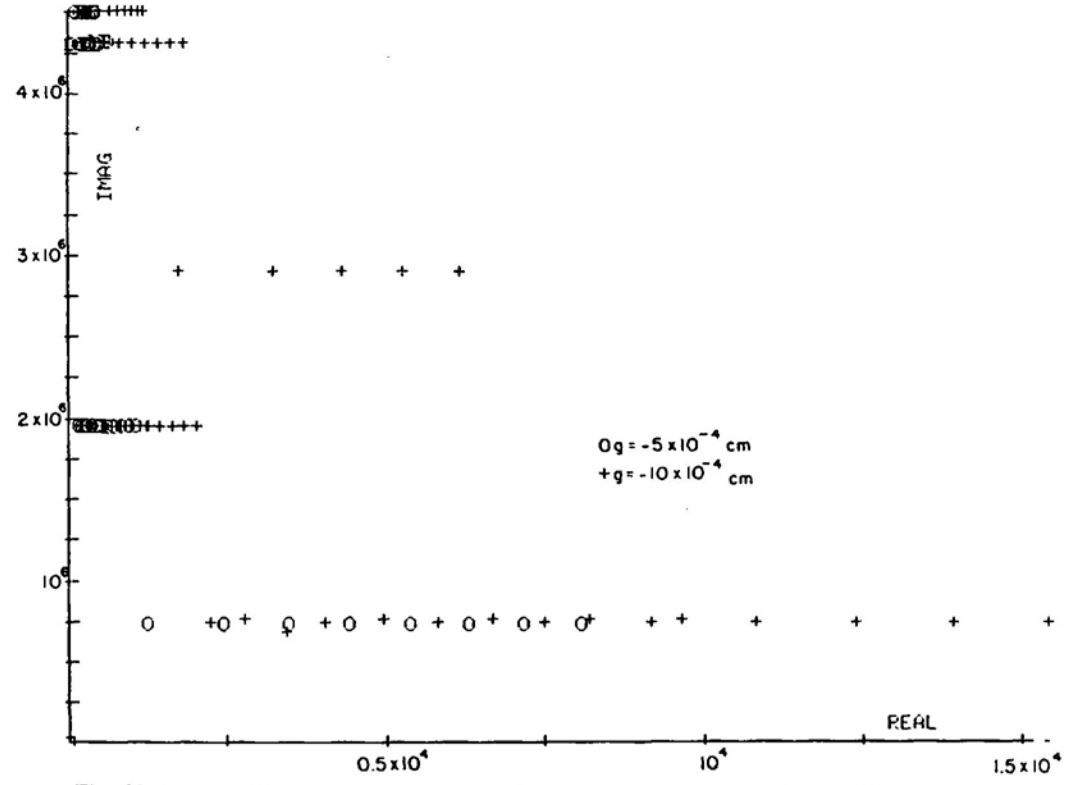

Fig. 83. Effect of increasing the compression on the eigenvalues with positive real part.

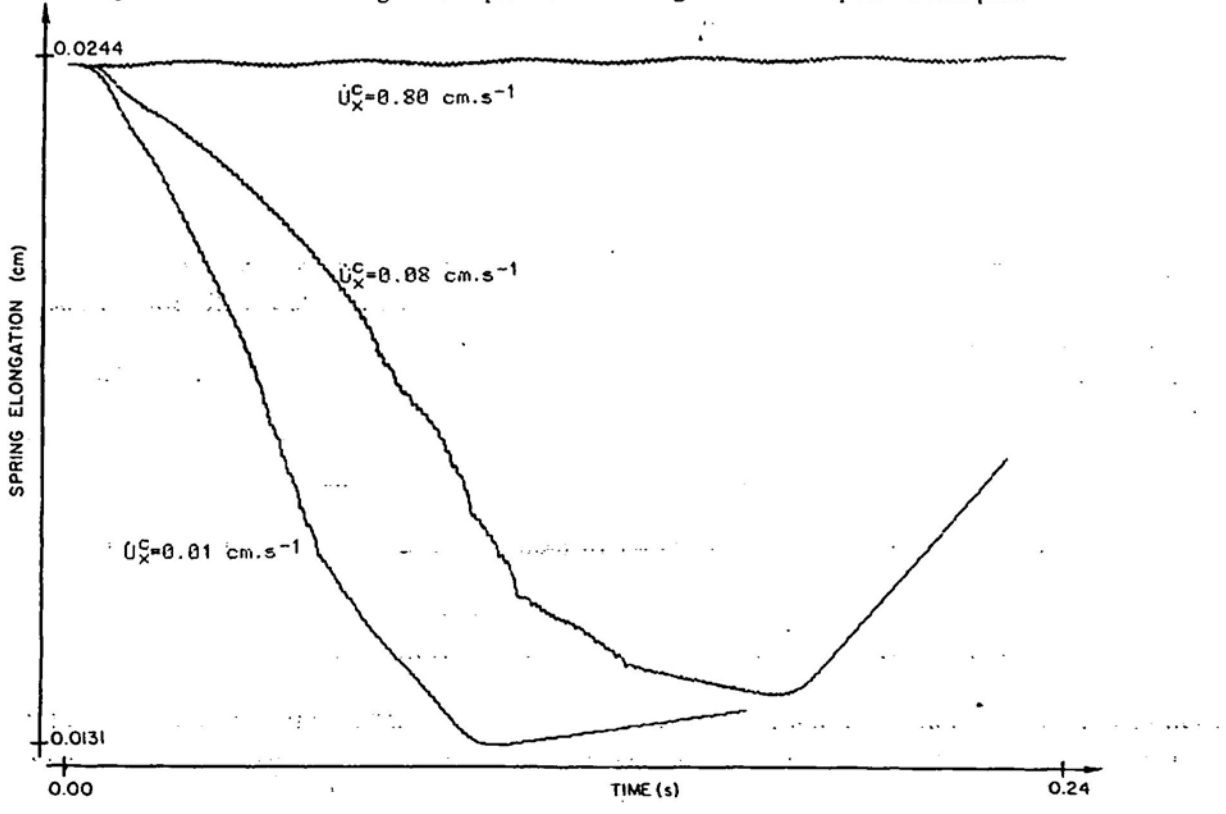

Fig. 84. Evolution of the spring elongation for different velocities $\dot{U}_x^c$.

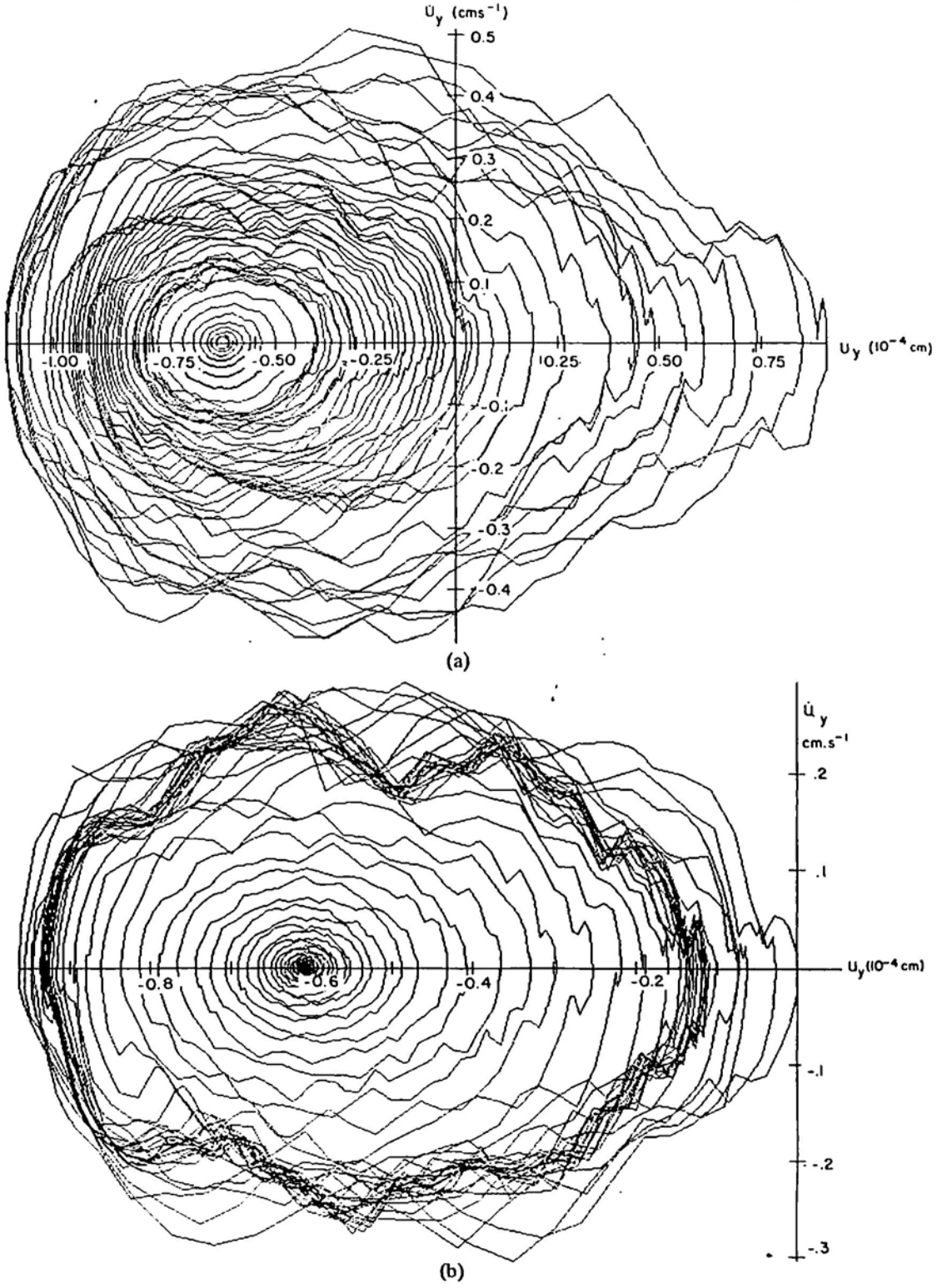

Fig. 85. Phase plane plots of the normal oscillation of the contact Node 29. (a) Initial growing oscillation. (b) Final decreasing oscillation.

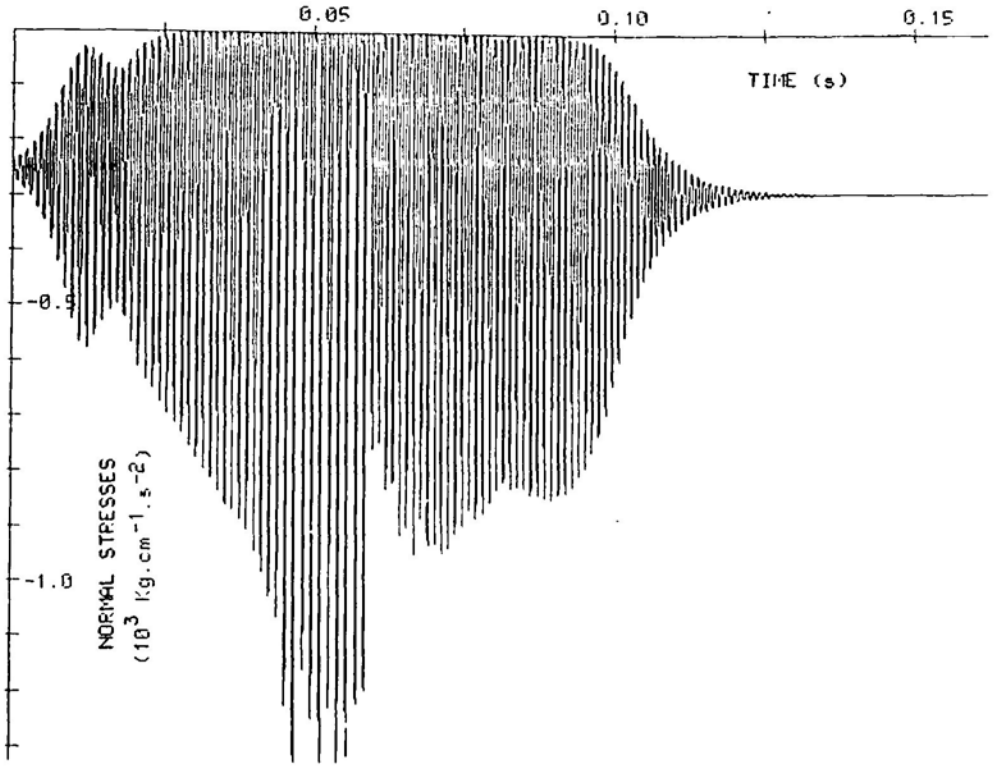

Fig. 86. Evolution of the normal stresses on the contact Node 29 ($\dot{U}_x^C = 0.01$ cm s^{-1}).

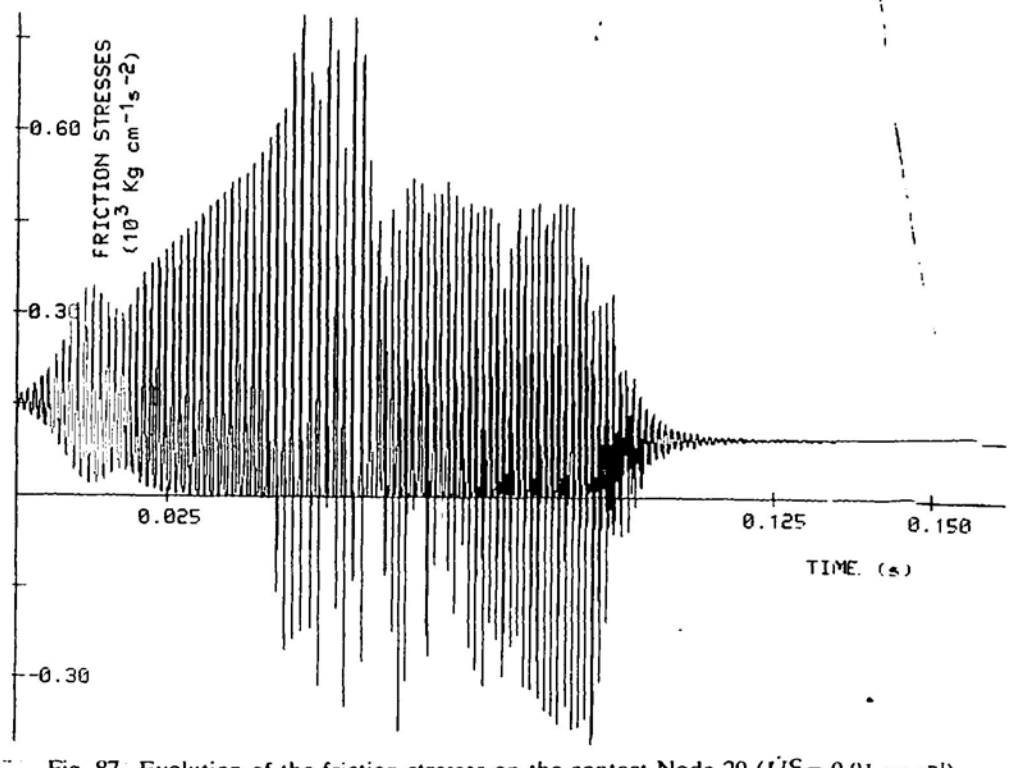

Fig. 87. Evolution of the friction stresses on the contact Node 29 ($\dot{U}_x^C = 0.01$ cm s^{-1}).

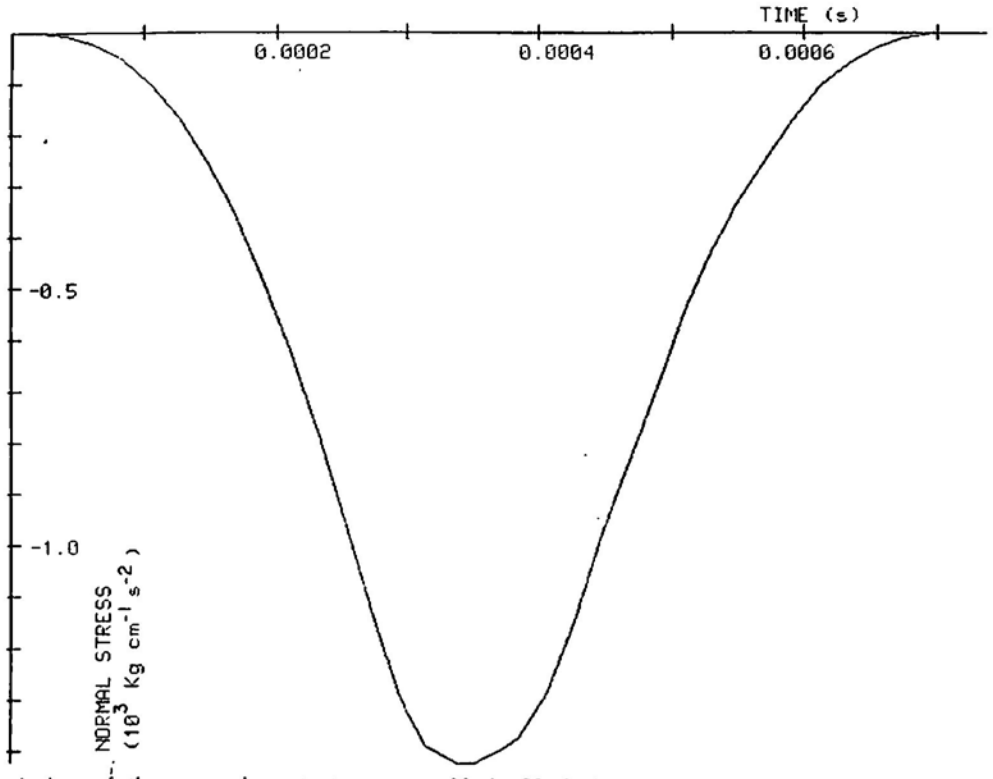

Fig. 88. Evolution of the normal contact stress at Node 29 during the contact portion of a cycle of normal oscillation ($\dot{U}_x^C = 0.08\,\mathrm{cm\,s^{-1}}$).

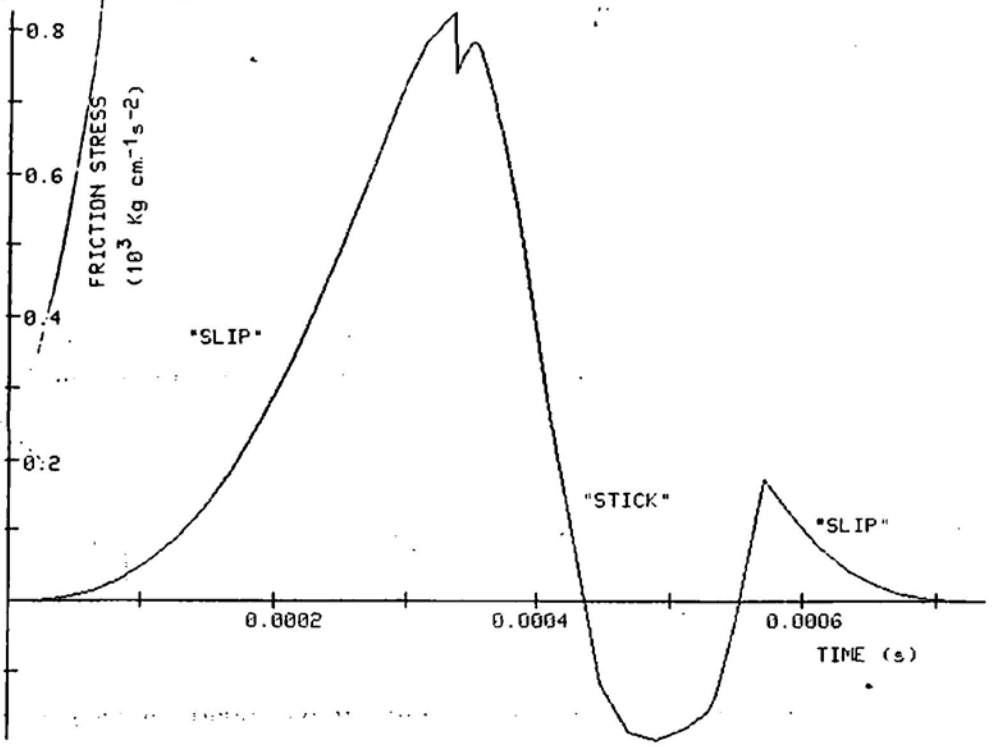

Fig. 89. Evolution of the friction stress at Node 29 during the contact portion of a cycle of normal oscillation ($\dot{U}_x^C = 0.08\,\mathrm{cm\,s^{-1}}$).

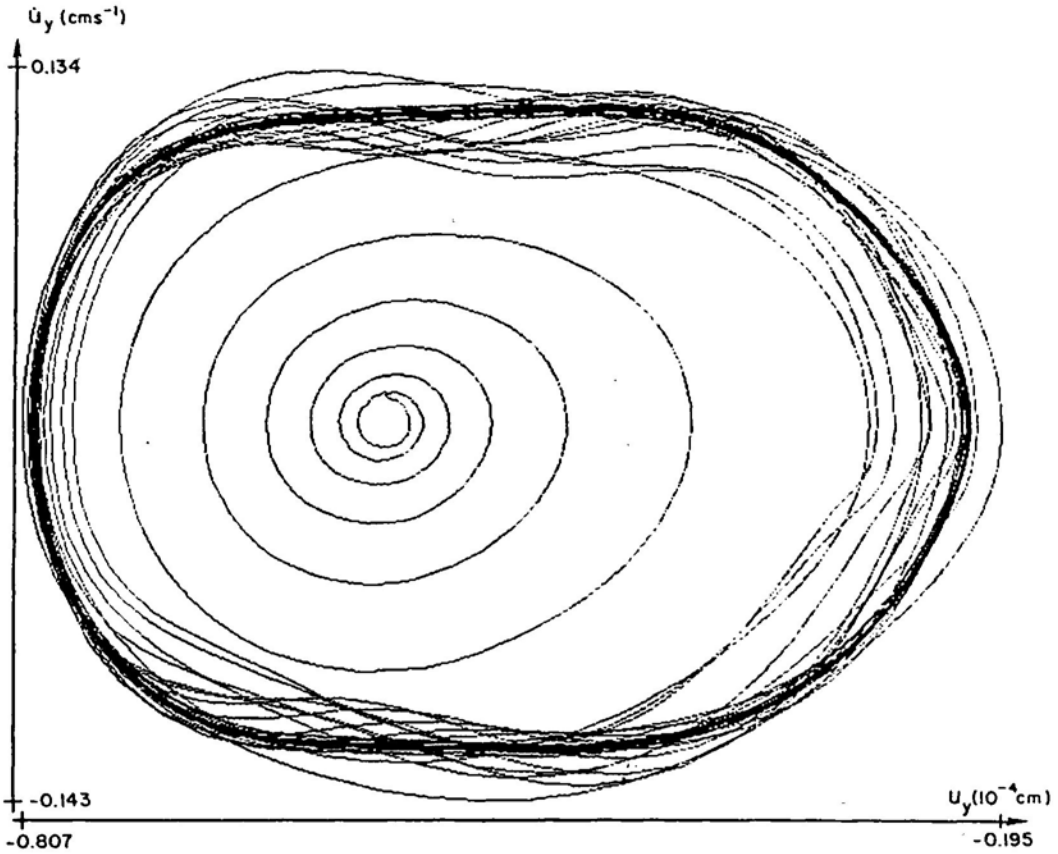

Fig. 90. Phase plane plot of the normal oscillation of Node 29 for $\dot{U}_x^C = 0.80\,\mathrm{cm\,s^{-1}}$.

observed these self-excited oscillations (also in the rigid body case) whenever the velocity $\dot{U}_x^C$ is sufficiently large compared with the critical velocity at which the transition from (global) stick-slip motion to (apparently) smooth sliding occurs and the coefficient of friction is large enough that the steady sliding equilibrium position is not stable.

12. Summary, conclusions and final comments

In this paper a large body of literature on the frictional contact of metallic surfaces was reviewed. Particular emphasis was given to the normal deformability of rough interfaces, the transition between static and kinetic friction, the occurrence of stick-slip motion and the fundamental role played by normal contact oscillations on the frictional behavior.

To provide some focus for this investigation, we have proposed that dry metallic friction phenomena be divided into (at least) three basic categories which perhaps require different theories for their characterization: Type I, quasi-static plastic deformation of interfaces; Type II, dynamic friction phenomena of materially stable interfaces, and Type III, cases in which plowing and wear are significant. The present investigation focuses on Type II friction.

Simple continuum mechanics models for normal and tangential interface response which reflect essential experimental observations were formulated. Variational principles which govern a large class of frictional contact problems in elastodynamics were also presented.

Numerical algorithms for the analysis of finite element approximations of the continuum problems formulated earlier were also proposed. Several numerical experiments show the feasibility of the techniques proposed.

The dynamic stability of steady sliding and its consequences on the behavior of sliding bodies ('rigid' or linearly elastic) was numerically studied. Occurrence of apparently smooth sliding with an apparent coefficient of kinetic friction smaller than the static one and occurrence of stick-slip oscillations were numerically demonstrated. These were shown to be a consequence of dynamic instabilities which occur for sufficiently large values of the coefficient of (static) friction and appropriate values of the other physical parameters involved. Those instabilities were shown to be the consequence of the inherent non-symmetry of frictional contact problems and they may occur even if the coefficient of kinetic friction is assumed to be equal to the coefficient of static friction.

Preliminary numerical results on the effect of the variation of several physical parameters on the qualitative behavior of the sliding at small velocities give evidence that our models are very promising simulators of these classes of dynamic response.

The experimental facts summarized in this paper and the numerical results obtained here do have implications for both the experimental and numerical study of frictional dynamic problems.

Experimental results on the normal deformability of metallic interfaces at low contact pressures for all the combinations of materials and surface finishes of interest in practical applications are desperately needed. A thorough test of the models proposed here will only be possible with close cooperation between experimentalists and numerical analysts.

The dispersion of the values reported in the literature for the coefficient of friction is not too surprising in view of our results. Our results and the experiments of several authors (e.g. Tolstoi [103]) strongly suggest that the (apparently) smooth sliding motion and the corresponding apparent value of the coefficient of kinetic friction are highly dependent on the geometric and dynamic properties of the apparatus used (stiffness, mass, damping). The following observations of Madakson [61] are easily understandable in the above context: "It has been demonstrated that the friction of a given material depends also on the test system. Samples of an identical material were distributed to different laboratories to measure the friction at given conditions. Using different measuring systems each laboratory reported a different value of the friction."

The normal deformability of the interface is an essential feature of dynamic contact problems involving metallic bodies. Not taking into account this deformability in finite elements models of these phenomena (even if frictional effects are negligible) leads to some serious physical inconsistencies. For example, the absence of normal deformability leads to models which can provide oscillations, depending on the mesh used, with frequencies as high as 10^6 Hz but these models may be incapable of delivering experimentally observed contact oscillations of frequencies of the order of 10^3 Hz.

We believe that some difficulties encountered in practical finite element calculations of dynamic friction problems (rapidly alternating contact-release and stick-slip situations) have the same origin as the oscillations observed in our numerical computations – inherent non-symmetry of contact friction contributions to the governing dynamical equations and consequent dynamic instabilities.

These effects are certainly unrealistically exaggerated by the use of an infinitely rigid normal

contact interface response and a programmed (artificial) discontinuous drop of the friction coefficient from a static value to a lower kinetic value upon sliding.

Acknowledgment

We are grateful to the authors and publishers mentioned in the figure captions for giving us permission to reproduce these figures from papers and books.

We also wish to express special thanks to Dr. Anthony Amos for his enthusiastic support.

References

[1] G. Amontons, De la résistance causée dans les machines, Mémoires de l'Académie Royale A (1699) 275–282.
[2] C. Andrew, J.A. Cockburn and A.E. Waring, Metal surfaces in contact under normal forces: Some dynamic stiffness and damping characteristics, Proc. Inst. Mech. Engrs. 182 (3K) (1967–68) 92–100.
[3] H.T. Angus, The significance of hardness, Wear 54 (1979) 33–78.
[4] S.S. Antoniou, A. Cameron and C.R. Gentle, The friction-speed relation from stick-slip data, Wear 36 (1976) 235–254.
[5] J.F. Archard, Elastic deformation and the laws of friction, Proc. Roy. Soc. London A 243 (1957) 190–205.
[6] J.F. Archard, Surface topography and tribology, Tribology Internat. 7 (1974) 213–220.
[7] V. Aronov, A.F. D'Souza, S. Kalpakjian and I. Shareef, Experimental investigation on the effect of system rigidity on wear and friction-induced vibrations, J. Lubr. Technol. 105 (1983) 206–211.
[8] V. Aronov, A.F. D'Souza, S. Kalpakjian and I. Shareef, Interactions among friction, wear and system stiffness – Part 1: Effect of normal load and system stiffness; Part 2: Vibrations induced by dry friction; Part 3: Wear model, J. Lubr. Technol. 106 (1984) 54–69.
[9] N. Back, M. Burdekin and A. Cowley, Review of the research on fixed and sliding joints, in: S.A. Tobias and F. Koenigsberger, eds., Proc. 13th Internat. Machine Tool Design and Research Conference (MacMillan, London, 1973) 87–97.
[10] N. Back, M. Burdekin and A. Cowley, Analysis of machine tool joints by the finite element method, in: S.A. Tobias and F. Koenigsberger, eds., Proc. 14th Internat. Machine Tool Design and Research Conference (MacMillan, London, 1974) 529–537.
[11] A.K. Banerjee, Influence of kinetic friction on the critical velocity of stick-slip motion, Wear 12 (1968) 107–116.
[12] N. Bay and T. Wanheim, Real area of contact and friction stresses at high pressure sliding contact, Wear 38 (1976) 201–209.
[13] R. Bell and M. Burdekin, A study of the stick-slip motion of machine tool feed drives, Proc. Inst. Mech. Engrs. 184(1) (1969–70) 543–557.
[14] J.J. Bikerman, Adhesion in friction, Wear 39 (1976) 1–13.
[15] H. Blok, Fundamental mechanical aspects of boundary lubrication, S.A.E. J. 46(2) (1940) 54–68.
[16] L.C. Bo and D. Pavelescu, The friction-speed relation and its influence on the critical velocity of stick-slip motion, Wear 82 (1982) 277–289.
[17] P.I. Bobrik, Effect of the surface finish of metals on loaded joints, Thesis, Moscow Inst. Aircraft Technol. (MATI), 1947.
[18] C.A. Brockley, R. Cameron and A.F. Potter, Friction-induced vibration, J. Lubr. Technol. 89 (1967) 101–108.
[19] C.A. Brockley and H.R. Davis, The time dependence of static friction, J. Lubr. Technol. 90 (1968) 35–41.
[20] F.P. Bowden and L. Leben, The nature of sliding and the analysis of friction, Proc. Roy. Soc. London A 169 (1939) 371–391.
[21] F.P. Bowden and D. Tabor, The area of contact between stationary and between moving surfaces, Proc. Roy. Soc. London A 169 (1939) 391–413.
[22] F.P. Bowden and D. Tabor, The Friction and Lubrication of Solids (Clarendon Press, Oxford, 1950).

[23] F.P. Bowden and D. Tabor, The Friction and Lubrication of Solids, Part II (Clarendon Press, Oxford, 1964).
[24] B.V. Budanov, V.A. Kudinov and D.M. Tolstoi, Interaction of friction and vibration, Trenie i Iznos 1 (1) (1980) 79–89.
[25] J.T. Burwell and E. Rabinowicz, The nature of the coefficient of friction, J. Appl. Phys. 24(2) (1953) 136–139.
[26] A.W. Bush, R.D. Gibson and T.R. Thomas, The elastic contact of a rough surface, Wear 35 (1975) 87–111.
[27] L.T. Campos, J.T. Oden and N. Kikuchi, A numerical analysis of a class of contact problems with friction in elastostatics, Comput. Meths. Appl. Mech. Engrg. 34 (1982) 821–845.
[28] R. Connoly and R.H. Thornley, The significance of joints on the overall deflection of machine tool structures, in: S.A. Tobias and F. Koenigsberger, eds., Advances in Machine Tool Design and Research, Proc. 6th Internat. M.T.D.R. Conf., The Manchester College of Science & Technology (Pergamon Press, Oxford, 1965) 139–156.
[29] R. Connoly, R.E. Schofield and R.H. Thornley, The approach of machined surfaces with particular reference to their hardness, in: S.A. Tobias and F. Koenigsberger eds., Advances in Machine Tool Design and Research, Proc. 8th Internat. M.T.D.R. Conf., University of Manchester, Part 2 (Pergamon Press, Oxford, 1967) 759–775.
[30] C.A. Coulomb, Théorie des machines simples, Mémoire de Mathématique et de Physique de l'Académie Royale (1785) 161–342.
[31] J.S. Courtney-Pratt and E. Eisner, The effect of a tangential force on the contact of metallic bodies, Proc. Roy. Soc. London A 238 (1957) 529–550.
[32] B.V. Derjaguin, V.E. Push and D.M. Tolstoi, A theory of stick-slip sliding of solids, Proc. Conf. on Lubrication and Wear, Inst. Mech. Engrg., London (1957) 257–268.
[33] S.J. Dokos, Sliding friction under extreme pressures – 1, J. Appl. Mech. 68 (1946) A148–156.
[34] M.P. Dolbey and R. Bell, The contact stiffness of joints at low apparent interface pressures, Ann. C.I.R.P. XVIV (1971) 67–79.
[35] D. Dowson, History of Tribology (Longman, London, 1978).
[36] D.C. Drucker, Coulomb friction, plasticity and limit loads, J. Appl. Mech., Trans. ASME 21 (1954) 71–74.
[37] G. Duvaut and J.L. Lions, Inequalities in Mechanics and Physics (Springer, Berlin, 1976).
[38] L. Euler, Histoire de l'Académie Royale à Berlin iv (1748) 313.
[39] H.A. Francis, Application of spherical indentation mechanics to reversible and irreversible contact between rough surfaces, Wear 45 (1977) 221–269.
[40] B. Fredricksson, Finite element solution of surface nonlinearities in structural mechanics with special emphasis to contact and fracture mechanics problems, Comput. & Structures 6 (1976) 281–290.
[41] D. Godfrey, Vibration reduces metal to metal contact and causes an apparent reduction in friction, ASLE Trans. 10 (1967) 183–192.
[42] J.A. Greenwood and J.B.P. Williamson, Contact of nominally flat surfaces, Proc. Roy. Soc. London A 295 (1966) 300–319.
[43] J.-C. Gu, J.R. Rice, A.L. Ruina and S.T. Tse, Slip motion and stability of a single degree of freedom elastic system with rate and state dependent friction, J. Mech. Phys. Solids (1983).
[44] J. Halling and K.A. Nuri, in: A.D. de Pater and J.J. Kalker, eds., Proc. Symp. IUTAM (Delft Univ. Press, Delft, 1974) 330–341.
[45] P.G. Howe, D.P. Benton and I.E. Puddington, London–Van der Waals attractive forces between glass surfaces, Canad. J. Chem. 33 (1955) 1375–1383.
[46] K.H. Hunt and F.R.E. Crossley, Coefficient of restitution interpreted as damping in vibroimpact, J. Appl. Mech. (1975) 440–445.
[47] S.C. Hunter, Energy absorbed by elastic waves during impact, J. Mech. Phys. Solids 5 (1957) 162–171.
[48] H. Ishigaki, I. Kawaguchi and S. Mizuta, A simple estimation of the elastic-plastic deformation of contacting asperities, Wear 54 (1979) 157–164.
[49] E. Jenckel and E. Klein, Die Bestimmung von Relaxationszeiten aus der Rückparallelastizität, Z. Naturf. 7a (1952) 619–630.
[50] V.I. Johannes, M.A. Green and C.A. Brockley, The role of the rate of application of the tangential force in determining the static friction coefficient, Wear 24 (1973) 384–385.
[51] S. Kato and T. Matsubayashi, On the dynamic behavior of machine-tool slideway – 1st report, Bull. J.S.M.E. 13(55) (1970) 170–179.

[52] S. Kato, N. Sato and T. Matsubayashi, Some considerations on characteristics of static friction of machine tool slideway, J. Lubr. Technol. 94 (1972) 234–247.
[53] S. Kato, K. Yamaguchi and T. Matsubayashi, On the dynamic behavior of machine tool slideway – 2nd report, Bull. J.S.M.E. 13(55) (1970) 180–188.
[54] A. Klabring, Contact problems with friction – Using a finite-dimensional description and the theory of linear complementarity, Thesis, Linköping Studies in Science and Technology, No. 20, Linköping University, Linköping, Sweden, 1984.
[55] I.V. Kragelskii, Friction and Wear (Butterworths, Washington, DC, 1965).
[56] I.V. Kragelskii, M.N. Dobychin and V.S. Kombalov, Friction and Wear: Calculation Methods (Pergamon Press, Oxford, 1982).
[57] D. Kuhlman-Wilsdorf, Dislocation concepts in friction and wear, Fundamentals of Friction and Wear of Materials (American Society for Metals, Ohio, 1981).
[58] J. Leslie, An Experimental Inquiry into the Nature and Propagation of Heat, printed for J. Newman, No. 22 (Poultry, London, 1804).
[59] J.M. Lifshitz and K. Kolsky, Some experiments on anelastic rebound, J. Mech. Phys. Solids 12 (1964) 35–43.
[60] A.E.H. Love, A Treatise on the Mathematical Theory of Elasticity (Dover, New York, 1944).
[61] P.B. Madakson, The frictional behavior of materials, Wear 87 (1983) 191–206.
[62] J.A.C. Martins and J.T. Oden, A numerical analysis of a class of problems in elastodynamics with friction, Comput. Meths. Appl. Mech. Engrg. 40 (1983) 327–360.
[63] D. Maugis, Adherence of solids, in: J.M. Georges ed., Microscopic Aspects of Adhesion and Lubrication (Elsevier, Amsterdam, 1982).
[64] R. Michalowski and Z. Mroz, Associated and non-associated sliding rules in contact friction problems, Archiv. Mech. 30 (1978) 259–276.
[65] B.B. Mikic, Thermal contact conductance; Theoretical considerations, Internat. J. Heat Mass Transfer 17 (1974) 205–214.
[66] R.D. Mindlin, Compliance of elastic bodies in contact, J. Appl. Mech. 16 (1949) 259–268.
[67] D.F. Moore, Principles and Applications of Tribology (Pergamon Press, Oxford, 1975).
[68] P.R. Nayak, Random process model of rough surfaces, J. Lubr. Technol. 93 (1971) 398–407.
[69] M. O'Callaghan and M.A. Cameron, Static contact under load between nominally flat surfaces in which deformation is purely elastic, Wear 36 (1976) 79–97.
[70] J.T. Oden and E.B. Pires, Nonlocal and nonlinear friction laws and variational principles for contact problems in elasticity, J. Appl. Mech. 50(1) (1983) 67–76.
[71] R.A. Onions and J.F. Archard, The contact of surfaces having a random structure, J. Phys. D: Appl. Phys. 6 (1973) 289–304.
[72] P.J. Papenhuyzen, Wrijvingsproeven in verband met het slippen van autobanden, De Ingenieur 53 (1938) 75–81.
[73] E.B. Pires and J.T. Oden, Analysis of contact problems with friction under oscillating loads, Comput. Meths. Appl. Mech. Engrg. 39 (1983) 337–362.
[74] E. Rabinowicz, The nature of the static and kinetic coefficients of friction, J. Appl. Phys. 22(11) (1951) 1373–1379.
[75] E. Rabinowicz, The intrinsic variables affecting the stick-slip process, Proc. Phys. Soc. 71 (1958) 668–675.
[76] E. Rabinowicz, A study of the stick-slip process, in: R. Davies, ed., Symp. on Friction and Wear, Detroit (Elsevier, New York, 1957) 149–161.
[77] E. Rabinowicz, Friction and Wear of Materials (Wiley, New York, 1965).
[78] R.S.H. Richardson and H. Nolle, Surface friction under time-dependent loads, Wear 37 (1976) 87–101.
[79] J.R. Rice and A.L. Ruina, Stability of steady frictional slipping, Paper No. 83-APM-16 ASME Applied Mechanics, Bioengineering, and Fluids Engineering Conference, Houston, TX, 1983.
[80] D.A. Rigney and J.P. Hirth, Plastic deformation and sliding friction of metals, Wear 53 (1979) 345–370.
[81] G.T. Rooney and P. Deravi, Coulomb friction in mechanism sliding joints, Mech. Machine Theory 17 (1982) 207–211.
[82] A.L. Ruina, Friction laws and instabilities: A quasistatic analysis of some dry frictional behavior, Ph.D. Thesis, Brown University, Providence, RI, 1980.
[83] A.L. Ruina, Slip instability and state variable friction laws, J. Geophys. Res. (1983).

[84] J.B. Sampson, F. Morgan, D.W. Reed and M. Muskat, Friction behavior during the slip portion of the stick-slip process, J. Appl. Phys. 14 (1943) 689–700.
[85] E. Sanchez-Palencia and P. Suquet, Friction and homogenization of a boundary, 1983.
[86] A.D. Sarkar, Wear of Materials (Pergamon Press, Oxford, 1976).
[87] T.E. Simkins, The mutuality of static and kinetic friction, Lubr. Engrg. 23 (1967) 26–31.
[88] A.P. Sokolovskii, Rigidity in Mechanical Engineering Technology (Mashgiz, 1946) Ch. 2, p. 60.
[89] A. Soom and C. Kim, Interactions between dynamic normal and friction forces during unlubricated sliding, J. Lubr. Technol. 105 (1983) 221–229.
[90] A. Soom and C. Kim, Roughness-induced dynamic loading at dry and boundary-lubricated sliding contacts, J. Lubr. Technol. 105 (1983) 514–517.
[91] K.J. Stout and T.R. Thomas, eds., Proc. Second Internat. Conf. on Metrology and Properties of Engineering Surfaces, Leicester Polytechnic, U.K., 1982; Wear 83(1, 2) (1982).
[92] N.P. Suh and H.-C. Sin, The genesis of friction, Wear 69 (1981) 91–114.
[93] D. Tabor, The Hardness of Metals (Clarendon Press, Oxford, 1951).
[94] D. Tabor, Friction, lubrication and wear, in: E. Matijević, ed., Surface and Colloid Science, Vol. 5 (Wiley, New York, 1972) 245–312.
[95] D. Tabor, A simplified account of surface topography and the contact between solids, Wear 32 (1975) 269–271.
[96] D. Tabor, Interaction between surfaces: Adhesion and friction, in: J.M. Blakely, ed., Surface Physics of Materials, Vol. II (Academic Press, New York, 1975) Ch. 10.
[97] D. Tabor, Surface forces and surface interactions, J. Coll. Interface Sci. 58(1) (1977) 2–13.
[98] D. Tabor, Friction – The present state of our understanding, J. Lubr. Technol. 183 (1981) 169–179.
[99] T.R. Thomas, Recent advances in the measurement and analysis of surface microgeometry, Wear 33 (1975) 205–233.
[100] R.H. Thornley, R. Connolly, M.M. Barash and F. Koenigsberger, The effect of surface topography upon the static stiffness of machine tool joints, Internat. J. Mach. Tool Des. Res. 5 (1965) 57–74.
[101] D.C. Threlfall, The inclusion of Coulomb friction in mechanisms programs with particular reference to DRAM, Mech. Machine Theory 13 (1978) 475–483.
[102] J.P.A. Tillet, A study on the impact of spheres on plates, Proc. Phys. Soc. B 67 (1954) 677–688.
[103] D.M. Tolstoi, Significance of the normal degree of freedom and natural normal vibrations in contact friction, Wear 10 (1967) 199–213.
[104] D.M. Tolstoi, G.A. Borisova and S.R. Grigorova, Role of intrinsic contact oscillations in normal direction during friction, Nature of the Friction of Solids (Nauka i Tekhnika, Minsk, 1971) 116.
[105] T. Tsukizoe and T. Hisakado, On the mechanism of contact between metal surfaces – the penetrating depth and the average clearance, J. Basic Engrg. 87 (1965) 666–674.
[106] T. Tsukizoe and T. Hisakado, On the mechanism of contact between metal surfaces: Part 2 – the real area and the number of the contact points, J. Lubr. Technol. 90 (1968) 81–88.
[107] A. Tudor and L.C. Bo, The squeeze film under boundary lubrication conditions and its effect on the vertical displacement of sliding bodies, Wear 80 (1982) 115–119.
[108] K.V. Votinov, The Rigidity of Machine Tools (Leningrad Section, Machine Builders Union (LONITOMASH), Leningrad, 1940).
[109] D.J. Whitehouse, Surface topography and quality and its relevance to Wear, in: N.P. Suh and N. Saka, eds., Fund. of Tribology (MIT Press, Cambridge, MA, 1980).
[110] D.J. Whitehouse and J.F. Archard, The properties of random surfaces of significance in their contact, Proc. Roy. Soc. London A316 (1970) 97–121.
[111] D.J. Whitehouse and M.J. Phillips, Discrete properties of random surfaces, Phil. Trans. Roy. Soc. London A 290 (1978) 267–298.
[112] D.J. Whitehouse and M.J. Phillips, Two-dimensional discrete properties of random surfaces, Phil. Trans. Roy. Soc. London A 305 (1982) 441–468.
[113] K.L. Woo and T.R. Thomas, Contact of rough surfaces: A review of experimental work, Wear 58 (1980) 331–340.
[114] N. Kikuchi and J.T. Oden, Contact Problems in Elasticity (1985).